Synthesis and Characterisation of Photoreactive Silanes for the Self-Assembly on Functionalised Silica Surfaces

Dissertation
zur Erlangung des Grades

"Doktor der Naturwissenschaften"

am Fachbereich Chemie und Pharmazie der
Johannes Gutenberg-Universität Mainz
vorgelegt von

Diana R. Boos
geboren in Bad Kreuznach

Mainz 2004

Contents

1 Introduction **1**

2 Principles of Patterned Silane Layers **4**

2.1 Characteristics of Silica Surfaces 6
2.2 Silanisation of SiO_2 Surfaces 6
2.3 Intermolecular and Capillary Forces Acting in Colloidal Assemblies 7
2.4 Photolithography 9
2.5 Colloidal Polymer Particles 12

3 Methods of Characterisation **15**

3.1 Optical Microscopy 15
3.2 Dynamic Light Scattering 16
3.3 Atomic Force Microscopy 17
3.4 Scanning Electron Microscopy 18
3.5 UV-Vis Spectroscopy 20
3.6 Confocal Microscopy 21
3.7 Contact Angle Measurement 22

4 Particle Assembly on Patterned Surfaces **24**

4.1 Formation of Structured Surfaces 24
4.1.1 Solution Phase Deposition 24
4.1.2 Vapour Phase Deposition 25
4.1.3 Combination of Vapour and Solution Phase Deposition 27
4.2 Colloidal Assembly on Patterned Surfaces 28
4.2.1 Assembly of Hydrophobic Aerosil Particles 29
4.2.2 Self-Organisation of Charged Colloidal Particles on Patterned Substrates 32
4.2.2.1 Carboxylated PBA Particles on NR_4^+/SiOH Surfaces . . . 32
4.2.2.2 Carboxylated and Non-Carboxylated Polystyrene Particles on NH_2/SiOH and NH_2/HMDS Patterned Surfaces 34
4.3 Summary 40

5 Photo-Reactive Silane for Chemical Patterning **42**

5.1 Introduction 42
5.2 Azides and Nitrenes 44
5.3 Synthetic Approach 46

5.4 Surface Modification and Characterisation 50
5.4.1 Kinetic Experiments 51
5.4.2 Silane Deposition on Silica Surfaces 51
5.4.3 Dynamic Light Scattering 56
5.4.3.1 Sample Preparation and Experiments 56
5.4.4 UV Irradiation 60
5.5 Site-Selective Patterning of Azidosilanes on Silica Surfaces 64
5.5.1 Experimental Results 66
5.5.1.1 ANTSP Without Particles 67
5.5.1.2 Selective Irradiation Experiments on ANTSP Monolayers with Time-Dependent Colloidal Particle Deposition 67
5.5.1.3 Selective Irradiation Experiments on ANTSP Layers with Charge-Dependent Colloidal Particle Deposition 69
5.5.1.4 Colloidal Assembly After Irradiation 72
5.5.1.5 ANTSP and NR_4^+ Patterns with Polymer Film 74
5.6 Summary 75

6 Wavelength Dependant Patterning of Mixed Silane Layers 76

6.1 Introduction 76
6.2 The Concept of Orthogonal Protecting Groups 79
6.3 Synthetic Details 82
6.4 Surface Modification and Characterisation 85
6.5 Time Dependant Irradiation and UV Measurements 87
6.6 Colloidal Assembly on Site-Selectively Irradiated Wafers 98
6.7 Fluorescence Labelling 99
6.7.1 Fluorescent Dyes 99
6.7.2 Results 100
6.8 Attachment of ODNs on Patterned Surfaces 104
6.8.1 Substrate Preparation 104
6.8.2 Results 106
6.9 Discussion and Summary 110

7 Experimental Section 112

7.1 General 112
7.2 Silane Deposition on Silica Surfaces 114
7.2.1 Solution Phase Silanisation 114
7.2.2 Vapour Phase Silanisation 115
7.2.3 Photolithography 115
7.2.4 Formation of Structured Silane Layers 116
7.3 Colloid Deposition on Silicon Wafers 116
7.3.1 Colloidal Deposition on Patterned Silane layers 117
7.3.2 Colloids Deposition on ANTSP layers 117
7.4 Fluorescence Labelling 117
7.4.1 Buffer Preparation 117
7.4.2 Amine Coupling 118

7.4.3 Carboxylic Acid Coupling 118
7.4.4 Oligonucleotide Immobilisation and Hybrid Capturing 118
7.5 Synthesis of compounds 119
7.5.1 2-Amino-5-nitrobenzoic acid 119
7.5.2 2-Azido-5-nitrobenzonitrile 120
7.5.3 5-Azido-2-nitrobenzoic acid 121
7.5.4 N-Hydroxylsuccinimidyl-5-azido-2-nitrobenzoate 121
7.5.5 (5-Azido-2-nitrobenzoyl)-allylamine 122
7.5.6 (5-Azido-2-nitrobenzyl)triethoxysilylpropylamide (ANTSP) 123
7.5.7 α-(Benzotriazol-1-yl-)arylethyl ether 123
7.5.8 3’,5’-Dimethoxybenzoin 124
7.5.9 But-4-enoic acid-1-(3,5-dimethoxy-phenyl)-2-oxo-2-phenylethyl ester 125
7.5.10 Undec-10-enoic acid-1-(3,5-dimethoxy-phenyl)-2-oxo-2-phenylethyl ester 126
7.5.11 12,12,12-Triethoxsilyl-dodecanoicacid-1-(3,5-dimethoxy-phenyl)-2-oxo-2-phenyl ethyl ester 127
7.5.11.1 Passivation of a Silica Gel Column 128
7.6 Laser Irradiation 128

8 Summary 130

Bibliography 133

Abbreviations and Acronyms

AFM	atomic force microscopy
ANTSP	(5-azido-2-nitrobenzyl)-triethoxysilylpropylbenzamide
APTS	aminopropyltriethoxysilane
aq.	aqueous
Ar	argon
ATP	adenosine triphosphate
Boc	*tert*-butoxycarbonyl
(*t*-Bu)	*tert*-butyl
Bzl	benzyl
Bnz	benzoin
cAMP	caged adenosine monophosphate
CaO	calcium oxide
CCD	charged-coupled device
cf.	confer
CH_2Cl_2	dichloromethane
CO_2	carbondioxide
COOH	carboxylic acid functional group
DCC	dicyclohexylcarbodiimide
DE	diethylether
DIC	differential interference contrast
DMAP	4-dimethylaminopyridine
DNA	deoxynucleic acid
DLS	dynamic light scattering
Et	ethyl
EtOAc	ethylacetate
EtOH	ethanol
Fmoc	9-fluorenylmethoxycarbonyl
HCl	hydrochloric acid
Hex	hexane
Hg	mercury
HMDS	hexamethyldisilazane
H_2O_2	hydrogenperoxide
H_2PtCl_6	hexachloroplatinic acid
$HSi(OEt)_3$	triethoxysilane
H_2SO_4	sulfuric acid
in.	inch
i-PrOH	isopropanol

K_2O	potassiumoxide
LaB6	lanthanumhexaboride
LED	light emitting diode
Milli-Q	deionised water (resistivity=18M Ω*cm)
MMA	methylmethacrylate
NBoc	nitrobenzylcarbonyl
n-BuLi	n-butyl lithium
NMR	nuclear magnetic resonance
NaN_3	sodiumazide
$NaNO_2$	sodiumnitrite
Na_2O	sodiumoxide
NaOH	sodiumhydroxide
NaSS	sodium styrene sulphonate
NHS	N-hydroxysuccinimide
NR_4^+	N-trimethoxysilylpropyl-1-N,N,N-trimethylammoniumchloride
NVoc	nitroveratryloxycarbonyl
ODNs	oligodeoxynucleotides
OTE	octadecyltriethoxysilane
PBA	polybutylacrylate
PBMA	polybutylmethacrylate
PDMS	polymethyldisiloxane
Piranha	solution of conc. H_2SO_4/30% H_2O_2 (7:3 v/v)
PTFE	polytetrafluoroethylene
PS	polystyrene
PS-7/10	polystyrene colloidal particles, bearing charged COOH groups
Rf	retention factor
rpm	rounds per minute
SAM	self-assembled monolayer
Si_3N_4	silicon nitride
SiO_2	silicon dioxide
STM	scanning tunneling microscopy
TMOS	tetramethoxysilane
TFA	trifluoroacetic acid
THF	tetrahydrofuran
TLC	thin layer chromatography
TiO_2	titanium dioxide
vdW	van der Waals
w.r.t.	with respect to

Chapter 1

Introduction

When Richard Feynman postulated in 1959 that 'there was plenty of room at the bottom' he probably did not know that he laid the foundation for nanotechnology and that 40 years later his vision would come true [Feynman 60]. Even though the commercial mass production of nanosystems (*i.e.* "nano"chips) is still far away, the pressure of Moore's law in modern technology is leading to smaller and more complex devices not only in optics and microelectronics, but also in biological area such as biosensors made from DNA fragments, proteins or biomolecules. Fabricating these miniscule devices is taking on nanoscopic dimensions, making the integration of individual objects into these structures a complex task [Sticks 01, Moore 65].

The fabrication of nanosized devices can be approached with "top-down" or "bottom-up" technologies. Top down approaches are based on miniturisation of macroscale components down to the nanometer level. In the last decades great improvements have already been achieved in this field (*e.g.* lithographic patterning of surfaces with the photoresist technology). Nevertheless, top down techniques usually suffer from limitation in the degree of miniturisation, which, in most cases, lies above 100 nm; for example, the minimum feature size in photolithographic techniques is limited by the irradiation wavelength [Xia 98].

The "bottom up technique" is based on assembly concepts that are ubiquitously present in the biological world (*i.e.* base-pairing in DNA strands, molecular recognition between antibodies and antigens, etc.) and mostly rely on interactions at the molecular level between the components involved. Molecular assemblies on the substrate surface, called self-assembled monolayers (SAMs), form the basis for these interactions by defining the chemistry on the surface [Ulman 91]. In a so-called self-organisation process, micro to nanosized objects can spontaneously organise and aggregate into stable, well-defined structures on the SAMs, due to favourable interactions between the chemical groups located at their outmost surface layer [Jonas 02a].

In this context, this thesis presents a strategy for the assembly of nanosized objects (colloidal particles and oligonucleotides) onto predetermined locations on planar surfaces, which have been modified with specific chemical functionalities. The chemical pattern that defines the site-selective adsorption of the colloids is obtained by a photolithographic process using photoreactive silane layers. Upon irradiation of the layer through a mask, a photochemical reaction is induced on selected regions of the surface, where colloidal particles and oligonucleotides can be assembled.

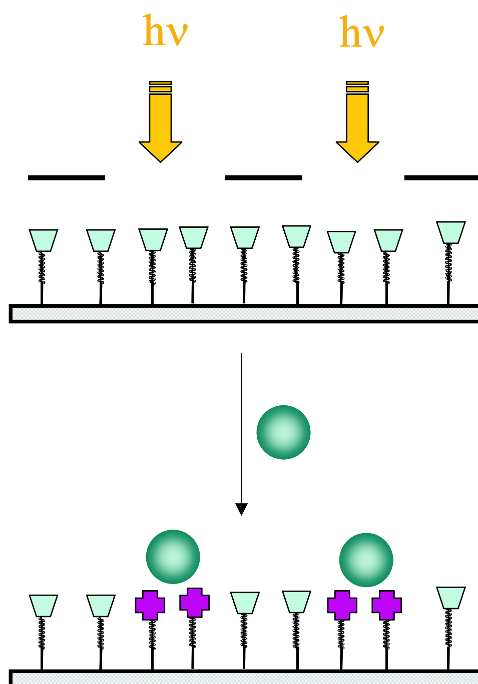

Figure 1.1: *Schematic illustration of a silane layer on a silica surface bearing photoreactive head groups. Upon irradiation through a mask, a photochemical reaction is induced on the surface, which allows for example, particle assembly on the photoactivated regions.*

The characteristic features of silica surfaces, their surface modification and patterning are reviewed in **Chapter 2**. Special emphasis is placed on the alkoxysilane chemistry, considering the process of hydrolysis and condensation in solution and absorption onto the surface. The photolithographic technique is presented, and the synthesis and properties of colloidal particles are described.

After introducing the main characterisation techniques used for this work in **Chapter 3**, site-specific assembly of colloidal particles onto laterally patterned silane layers is described in **Chapter 4**. There, silanisation techniques are presented, concentrating on the formation

of patterned silane layer bearing hydrophilic and hydrophobic regions on the surface. The assembly of hydrophobic silica particles, as well as colloidal polystyrene particles onto these surfaces is investigated. Finally, pH and charge effects on the colloidal assembly are analysed.

A novel photoreactive silane bearing a reactive azide group for chemical patterning is introduced in **Chapter 5**. Synthetic details are given and its hydrolysis and condensation mechanism in solution are investigated by ^{1}H NMR, AFM, and dynamic light scattering. UV measurements are carried out for delineating the optimum irradiation time for silane activation. Charge- and time dependent colloidal assembly is performed onto surfaces modified with this molecule and subsequent irradiation of the substrate is then carried out in order to generate a pattern on the surface.

Finally, **Chapter 6** presents novel alkoxysilanes bearing orthogonal photoprotecting groups. Two different silanes are co-adsorbed simultaneously on the same surface and irradiation with two different wavelengths selectively removes each protecting group individually, thus restoring the initial activity and generating a complex pattern on the silica surface. The synthesis and use of these silanes for surface modification on silica surfaces are illustrated, and optimisation of individual irradiation times for each silane is presented. The existence of reactive head groups is then verified by fluorescent labelling. These patterned surfaces are ultimately used for immobilisation of oligonucleotides and their application as biosensors is proven in hybrid capture experiments of complementary sequences.

Chapter 2

Principles of Patterned Silane Layers

The concept of self-organisation originates from biological processes such as formation of the DNA double helix, folding of polypeptide chains into functional proteins, or formation of cell membranes from phospholipids [Creighton 83, Sanger 86]. The application of self-assembly in modern technology (bottom up approach) is based on the formation of self-assembled monolayers (SAMs) of molecules covalently bound to a substrate surface.

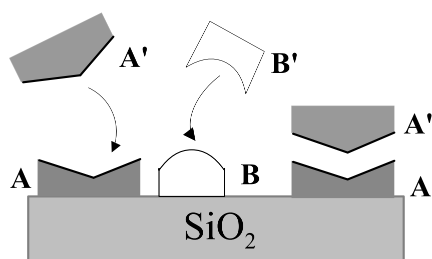

Figure 2.1: *Formation of complex structures* via *self-assembly due to attractive forces.*

When self-assembly is combined with a lithographic top-down technique, lateral patterns onto the planar substrate with nanometer dimensions can be created. This in turn provides a platform for organisation of mesoscale objects on these substrates, based on attractive interactions between the outmost surface molecules on the substrate and the objects. A requirement for the success of this approach is that the objects to be assembled must have a complementary group to the one on the surface, thus allowing attractive interactions to act between them. This approach is represented in Fig. 2.1, where the opposing objects carrying functional groups on their surface (A, A', B, B') form reversible attractive interactions with the complementary layer. These layers can define the spatial location of the objects (A with A' and B with B'). The modified objects are then brought together in an environment that allows reversible assembly and positioning under the control of the surface layers [Jonas 02a, Whitesides 02, Dutta 03]. If appropriate functional groups are included in these layers, they can then be activated by an external stimulus, such as heat or light, for permanent fixation of the structure.

In the 90s Hammond and co-workers managed to self-assemble polyelectrolytes on laterally modified thiol substrates on gold whereas Vossmeyer and co-workers self-assembled gold nano-crystals on photolithographically modified silicon oxide surfaces [Chen 00, Vossmeyer 98]. Even though Hammond was using a metal and Vossmeyer an oxide surface, both groups had modified their patterned surfaces with self-assembled monolayers (SAMs). SAMs are monolayers of either thiols or disulfide groups on gold or silane layers on silicon oxide surfaces that can chemically modify the surface of the substrate.
Other oxide surfaces, such as Al_2O_3, ZrO_2, SnO_2, TiO_2 or NbO_2 are generally modified with carboxylic acids or phosphonic acid, but sometimes also with chloro- or alkoxy silanes. Since metal surfaces, such as gold, are rather of academic interest and somewhat of limited use to a restricted number of technical applications this dissertation will only deal with silanes on silicon oxide surfaces, since it is more relevant for possible applications.

Such silanes that form the monolayers possess either a chloro- or alkoxysilane anchor group that can interact with the silicon surface *via* physisorption or chemisorption. Alkoxy silanes are usually preferred since they are less reactive and therefore much easier to handle under ambient laboratory conditions. Chlorosilanes produce HCl during hydrolysis which auto-catalyses the hydrolysis reaction and silanol condensation. Furthermore, the very high reactivity of the chlorosilanes makes it difficult to handle them under regular laboratory conditions (*e.g.* H_2O in air). Alkoxysilanes on the other hand are easier to handle due to their lower reactivity. In addition, they can be purified by passivating the silica gel column first with an hydrophobic silane such as hexamethlydisilazane (HMDS) or tetramethoxysilane (TMOS). An alkyl spacer separates then the anchor group from the functional head groups (*i.e.* amine, ammonium, ester, epoxy, etc.), which define the surface properties of the substrate and control the interaction with complementary objects.

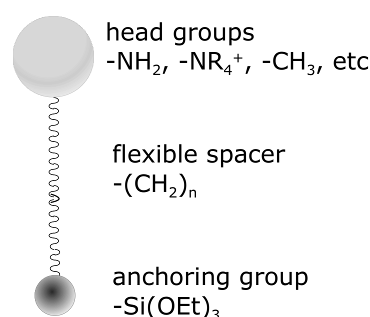

Figure 2.2: *Molecules used for adsorption.*

Monolayers with a thickness of up to 10 nm possess only molecular dimensions and are therefore also referred to as ultra-thin films. Depending on their functionalities, these films can substantially alter the properties of the surface, such as friction, adhesion, chemical resistance, wettability, etc. Colloidal objects are suited perfectly for studying their specific interaction and assembly in these silane layers since they have an isotropic form, can be easily handled in the dispersed state and commercially available or easily synthesised [Xia 00].

2.1 Characteristics of Silica Surfaces

Silicon dioxide (SiO_2) is a hard polymeric solid where the Si atoms in the lattice are sp^3 hybridised and are bound to 4 O-atoms in a 3D tetrahedron. Due to the free p-electron pairs of the oxygen that interact with the empty d-orbitals of silicon the bonding energy of an Si-O bond is very high. Quartz wafers consist of SiO_2 where SiO_4-tetrahedrons are connected at the edges, whereas glass wafers are melts without crystallisation [Riedel 90]. Glass wafers (so called silicates) consist of SiO_2 and alkaline oxides, such as Na_2O, K_2O and CaO, where the oxides have cleaved the 3D network of SiO_4 tetrahedrons thus altering the melting properties of the glass. When silica and silica surfaces are immersed into water they are known to acquire a negative surface charge density, primarily through the dissociation of terminal silanol groups (pK_A of SiOH $\approx$ 7.5). The glass surface carries an effective charge density of -2200$\pm$200 e/μm^2, where e is the elementary charge [Behrens 01].

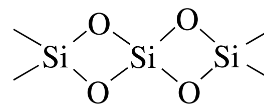

Figure 2.3: *Silicon dioxide lattice.*

Upon reaction with a strong acid such as *Piranha solution* (which is a mixture of conc. H_2SO_4/30% H_2O_2, 7:3 v/v), coordinated Si_2O bonds can be broken, thus generating more "reactive" surfaces. The ions that are dissociated include: the hydronium ions, other counter ions dissociated from the surface and those from the bulk solution due to the auto-dissociation of water. The ions from the bulk solution contribute much more to the overall concentration of mobile ions than the surface-dissociated counter ions if the ratio of surface area to solution volume is exceedingly small. Since in practice even the pure water used in the laboratory also contains some residual electrolyte (*e.g.* CO_2 from air), the surface charge is controlled by these ions and the pH of the bulk solution, just as in the general case of high salt concentrations.

2.2 Silanisation of SiO_2 Surfaces

Surface modification can occur by physisorption, due to attractive forces between the surface and the organosilane, or they can be chemisorbed *via* formation of covalent bonds between the silane and the silanol groups on the surface (Fig.2.4). Chemisorbed layers are more versatile and stable due to the stronger interaction with the surface compared to those with the physisorbed films [Fadeev 99].

The first step in the silanisation process is the hydrolysation of the alkoxysilanes to give hydroxysilanes that can then interact with the silicon dioxide surface and further condensate to form covalent bonds. Another possibility could be that the hydroxysilanes first condensate and then adsorb onto the surface when the anchor groups bear more than one functional group, such as di- or tri-functionalised alkoxysilanes. Condensation of these groups and for-

mation of a pre-polymer leads to aggregates of polymerised silanes which, when adsorbed onto the surface, may form an inhomogeneous layer. Extended silane condensation (forming

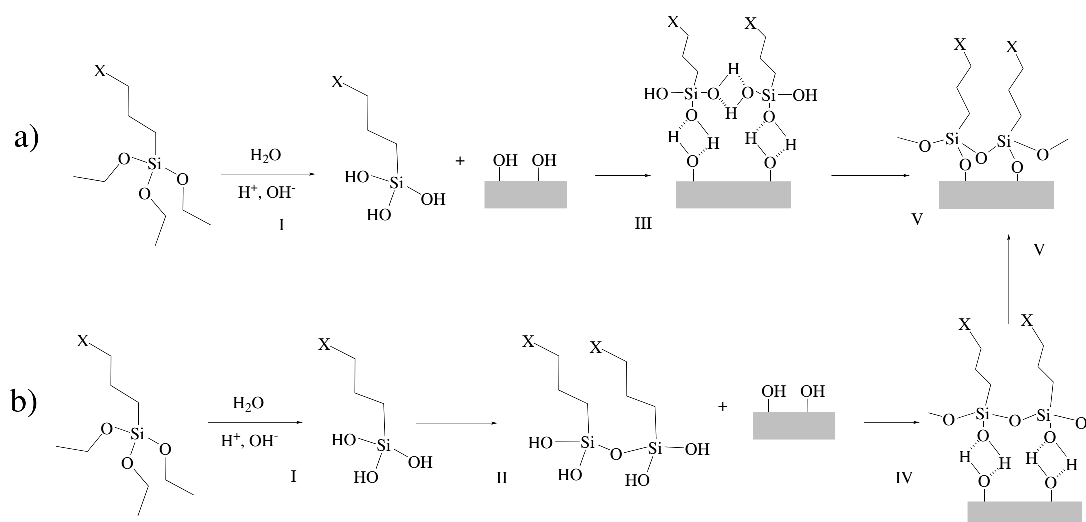

Figure 2.4: *I) Hydrolysis of the alkoxy silane in solution, II) pre-polymer condensation in solution, III) physisorption of hydrolysed alkoxy silane onto silanol surface, IV) physisorption of polymer silane aggregates onto surface, V) condensation of silane with surface and formation of silane layer. Process a) and b) are competing with each other.*

large polymers) prior to adsorption to the surface has to be prevented so that a homogeneous coating can form *via* surface diffusion of physisorbed silanes [Ishida 84].

2.3 Intermolecular and Capillary Forces Acting in Colloidal Assemblies

In colloidal organisation onto patterned surfaces, intermolecular interactions such as Coulomb-, van der Waals-, hydrogen bonds (H-bonds) and capillary forces may have to be considered.
Van der Waals (vdW) forces play a major role when colloids are assembled on the monolayer as model objects with mesoscale dimensions. Whereas interactions between atoms are governed by so-called dispersion forces (London forces) intermolecular interactions are based on the interaction (pair) potentials between two molecules or particles, such as dipole/dipole-, dipole/induced dipole- and induced dipole/induced dipole interactions [Li 00].
An electric dipole consists of two opposite charges separated by a distance R. The arrangement of charges is represented by a vector, the *dipole moment* μ. An applied electric field can distort a polarisable molecule as well as aligning its permanent dipole moment, which results in an *induced dipole* μ^* [Atkins 98]. A non-polar hydrocarbon layer on the wafer surface displays primarily vdW forces based on induced dipole (dispersion) interactions,

while the silica bulk might contribute by long-range vdW attraction. The molecular vdW pair interaction has a general distance r dependence of r^{-6}, while mesoscopic objects like spheres and planar surfaces depend on r^{-2} and r^{-1}, respectively.

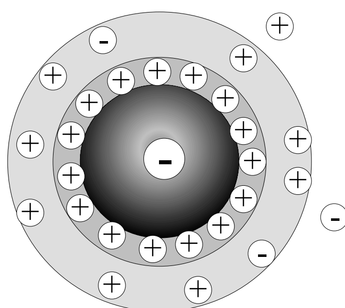

Figure 2.5: *The liquid layer surrounding the negatively charged particle consists of two parts: the inner region, called Stern or Helmholtz layer, where the counter ions are strongly bound and an outer region, the diffuse region, where the ions are bound less firmly. The diffuse layer is called slipping plane, within which the particles act as single entities. The potential around this boundary is called Zeta Potential.*

Non-charged particles agglomerate in solution due to vdW forces and therefore have to be stabilised in order to obtain homogeneous suspensions. Repulsive forces (Coulomb forces) between particles can be provided for balancing this attraction. The most common stabilisation used is electrostatic stabilisation that involves the introduction of surface charges. The Coulomb force F acting between two charges, which are separated by a distance r, depends on the separation by $1/r^2$. Since colloidal assembly usually occurs in an aqueous medium the colloids carry charges that are due to the ionisation of surface groups and specific adsorption of ions. The distribution of the ions close to the surface is then determined by the interaction between surface and thermal motions of the ions. This means that counter-ions are attracted to the surface whereas ions of the same charge repel each other due to Coulombic repulsion. The resulting layer of a charged surface bearing counter ions is called electric double layer and is determined by the electric potential ζ at the inner boundary of the diffusion layer (Fig.2.5).
H-bonds also play an important role when considering molecular interactions. The highly polarised bond of hydrogen with a heteroatom provides a strong protonic character to the hydrogen (proton donor). Therefore the H-atom can interact with an electron donating group / atom / electron lone pair (proton acceptor), which results in an effective H-mediated bond [Israelachvili 85].

Another interaction that should be considered is the hydration force (sometimes also called solvation force) which arises from the specific behaviour of water when it is close to a particle surface [Li 00]. The water molecules are bound more tightly to the surface

via ionic groups or hydrophilic sites on the surface. If two of these hydrated particles are brought together their solvent shells interfere with each other and therefore would have to be dehydrated first for the objects to come into contact, leading to an effective repulsion. However, dehydration is energetically not favourable and therefore hydration forces are always repulsive. On the other hand, when no polar or ionic groups are present on the particle surface, there is no affinity for water and thus no formation of H-bonds, which results in an attraction between hydrophobic surfaces when in close proximity. This is because H-bonds on the surface behave differently than in the bulk: they possess less degrees of freedom and the resulting entropy effects are disfavourable, which in turn leads to an effective attraction. The force acting upon these particles is then called hydrophobic force.

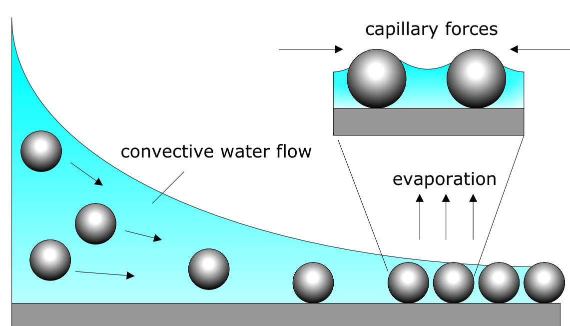

Figure 2.6: *Suspended particles are carried by convective flow of water to the boundary of the particle film where the water evaporates and leaves the dried particles. Enlargement: During evaporation a meniscus remains, which generates lateral capillary forces between the particles and attracts particles to each other.*

When particles adsorb to solid surfaces in suspension they form a submonolayer on the surface of the substrate, which is caused by Coulomb repulsion of the like-charged particles. Particles then aggregate at the rim of the colloidal suspension droplet due to convective water flow, which is stimulated by evaporation at the boundary of the film. As a result the colloids are packed by long-range attractive forces (also called lateral capillary forces) that act between the particles induced by surface tension at the film surface (as visible in Fig. 2.6) [Nagayama 97, Kralchevsky 01]. After complete evaporation an irreversible reorganisation of the particle-substrate interface can occur that prevents resuspension when submerged again into the adsorption liquid.

2.4 Photolithography

Photolithography has been the major tool for micro-fabrication in the semiconductor industry since the 1950s. Its basis is in an optical projection system in which the image of a reticle is

reduced and projected onto a thin film of photoresist that is spin-coated on a wafer, through a high numerical aperture lens system. Contact lithography is the most common technique used

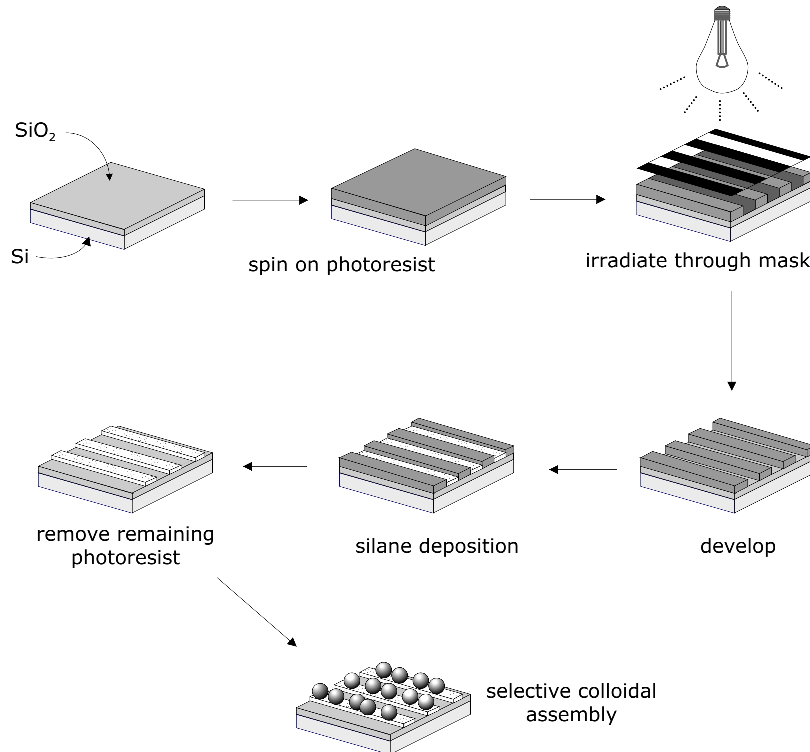

Figure 2.7: *Schematic illustration of photolithography: Spincoating of the photoresist onto a substrate, exposure of the resist layer with UV light through a mask, and developing the exposed parts, which leads to free substrate surface at the irradiated regions. A silane layer is then deposited onto the free silica surfaces and after removal of the remaining resist, a substrate with a laterally structured silane is obtained onto which colloidal particles can be selectively assembled.*

to produce high resolution patterns. It refers to the fact that the irradiation mask is placed right on top of the photo-resist wafer to be patterned. The irradiated parts of the resist undergo a chemical transformation and thus can be removed in an alkaline developer solution. In this case the photoresist is called a positive ”tone” (+)resist whereas a negative ”tone” (-)resist refers to the removal of the non-irradiated parts of the photoresist after irradiation. Negative photoresists form a 3D crosslinked polymer network upon irradiation that is not soluble anymore, hence the non-irradiated parts are removed. The most common (+)photoresist system is the diazonaphthoquinon-Novolak-sytem, which is comprised of 3 major components; namely naphthoquinone as the photoactive component, a Novolak resin and a developer.
The resin is a condensation product of phenol and/or cresol and formaldehyde that does not change upon irradiation. However, the diazonaphthoquinon (DNQ) is transformed into an indene carbonic acid during irradiation *via* a Wolff rearrangement and can be washed off afterwards with a aqueous basic developer.

The resolution is primarily limited by the wavelength λ of the light used, and in practice for light of a Hg lamp with λ = 365 nm the resulting resolution is ca. 350 nm and for deep UV irradiation with a F_2 excimer laser with λ = 157 nm the resolution would be ca. 120 nm [Xia 98, Xia 99].

The first step in the photolithography process (Fig.2.7) is to spin on the photoresist onto the quartz or silicon wafers, which have been cleaned in a Piranha solution before. They are then irradiated through a gold mask with UV light for an appropriate time. The irradiated areas of the resist are then washed off in a developer solution and rinsed gently with Milli-Q water. It is possible to modify these areas with the desired alkoxysilanes and then remove the remaining photoresist afterwards. The remaining free SiOH surface can then subsequently react with another silane, bearing, for example a different charge or polarity. As a final step complementary functionalised objects, such as colloidal particles, can be assembled under conditions that allow specific interaction between the silane surface and the colloid[1].

Photolithographic methods using electromagnetic radiation such as UV can usually create feature sizes of around 90 nm. To go even further down with the resolution is a goal scientist are very eager to achieve. Energetic particles, (*i.e.* electrons and ions) are an attractive means since their de Broglie wavelengths (which depend on the velocity of the electrons) are less than 0.1 nm, which minimises the effects of diffraction that limit many photolithographic processes [Xia 99]. In electron beam lithography an integrated circuit is written by an electron beam into the polymer layer. The extremely high resolution capability comes from the short wavelength that is associated with the high-voltage electron beams (ca. 0,005 nm for 50 keV). The advantage is that the beam cannot be tilted away in atomic dimensions and can be scanned in any desired pattern. It is hence possible to write lines of a few nanometers in width onto a polymer layer. The disadvantage are the high costs of the electron beam lithograph and that the lithography process is slow (ca. 1 h for a 4-in. wafer). Hence, it is not suitable for industrial mass production [Xia 99, Craighead 00].
Chapter 5 and Chapter 6 of this thesis will present an alternative technique to the conventional photolithography that requires less process steps and makes use of a monolayer that carries photoreactive groups *per se*, which when irradiated through a mask forms the lateral pattern on the surface.

A cheaper way of achieving these dimensions is soft-lithography, in particularly microcontact printing (μCP). The stamps for microcontact printing are made using micro-machined silicon wafers. The feature sizes of these master substrates are produced using for example, e-beam or STM lithographies. The wafers form part of a mould in which liquid PDMS (polymethyldisiloxane) is polymerised. On demoulding, a flexible transparent stamp is obtained, with structures that can be smaller than 100 nm. The patterned elastomer is inked with an alkanethiol layer and then brought in contact with a surface (usually gold)

[1]Details on the photolithographic patterning process are given in Chapter 7.2.3

in order to transfer the ink molecules to the regions of the substrate that are in contact with the stamp. Due to the rapid reaction between ink and surface and the fact that highly parallel SAMs can be formed, it has become a successful patterning technique that also minimises waste of starting material. Since an entire area of the substrate is in contact with the stamp at the same time, it is possible to pattern areas of several cm^2 on a single contact. Moreover, this technique can also be used for patterning curved surfaces, which are not suitable for conventional photolithography. Whereas alkane thiols can only form patterns in the scale of roughly 500 nm, μCP patterned SAMs of hexadecanethiolate on gold or silver with successive wet etching can produce structures with lateral dimensions of ca. 50 nm.

2.5 Colloidal Polymer Particles

Polymer colloids are very interesting as model objects for studying mesoscale object self-assembly since they can be synthesised from many different types of monomer with diameters that range from several nanometers to the micrometer regime. By controlling the polymerisation conditions (*i.e.* monomer composition, functional groups and charge) it is possible to determine the final properties of the colloids that make them suitable for self-assembly [Blackley 75].

The main components of an emulsion polymerisation are a water-insoluble monomer, a surfactant, a water-soluble initiator and water as the dispersing medium. Agitating these components results in the formation of colloid particles that are stabilised by the surfactant. Because emulsion polymerisation is based on water its environmental and safety hazards are reduced in an industrial application. Moreover, the fact that the polymer is formed as a colloid particle and not as a solid means that it can be handled more easily. The water can be evaporated in order to obtain the polymer or the polymer can be used as a finely dispersed suspension in water. Another great advantage of emulsion polymerisation is the fact that water absorbs the heat generated in the free radical polymerisation process. This reduces the danger of overheating of the reactors.
Upon heating, a water-soluble initiator decomposes into free radicals in the aqueous phase and a free radical polymerisation begins. Agitation of the mixture results in an emulsion where the monomer is present as large monomer droplets. In the case where surfactant is present in the starting mixture, agitation may also result in micelles [Fitch 71, Winnik 97]. However, it is not essential to have a surfactant present [Egen 04b, Xu 99]. After decomposition of the initiator in the aqueous phase and propagation with rare monomer units the polymerisation reaction of the formed oligomers can be terminated (by disproportionation of a hydrogen atom or by combination of two unpaired free radicals). They can also obtain an even higher degree of polymerisation, become surface-active and hence form micelles. Once the oligomer

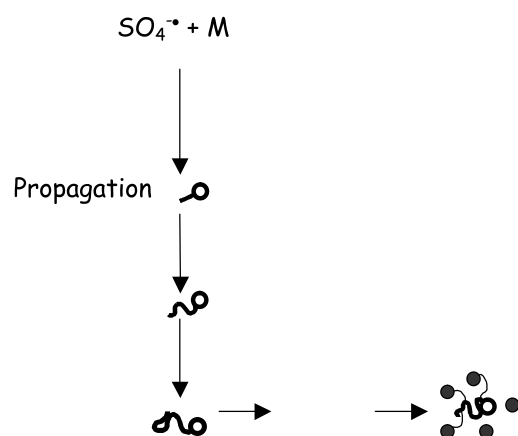
$SO_4^{-\bullet}$ + M
Propagation

allowing the particles to assemble in a thin film of liquid supported on the flat surface into these pre-defined structures [Velev 99, Yin 01, Park 98]. The size of the particles and the size and shape of the templates govern the control of the number of particles in each template. Strong attractive capillary forces that occur upon evaporation at the meniscus between a substrate and the colloid particles, when the substrate is immersed vertically into the colloid suspension, can induce a 3D crystal structure.

This technique has become very useful for growth of photonic band-gap (PBG) crystals where the opal arrays formed can be used as tunable optical notch filters that are capable of selectively rejecting a very narrow wavelength interval of light in the spectral region (ranging from ultraviolet to infrared). PBG-crystals can thus block the propagation of photons irrespective of their polarisation or direction, inhibit the spontaneous emission of excited chromophores and can direct the propagation of photons along a specific direction. This plays an important role for production of light-emitting diodes (LEDs) and for enhancing the performance of many types of optical, electro-optical and quantum electronic devices [Yablonovitch 93, Xia 00, Egen 02, Evers 02]. Crystal flakes, for example, synthesised by Zentel and co-workers were employed as pigments in transparent coatings [Egen 04a].

Chapter 3

Methods of Characterisation

3.1 Optical Microscopy

When light passes from a microscope lamp through a condenser and then either through or around the specimen some of the light passes without disturbance of its path and some of the light is attenuated. The intensity decrease of light passing through a sample can be due to absorption or diffraction and deflection [Davidson 01]. The term *brightfield microscopy* is applied when direct light is projected straight on the retina and the light observed is the brightest where there is no specimen. Thus, the background is brighter than the specimen. Several other contrast enhancing techniques can be applied depending on the specimen that has to be visualised. *Darkfield Microscopy*, for example, only allows diffracted rays to pass to the eye piece so that the specimen appears as a bright object on dark background. Another microscopy technique used is *Differential Interference Contrast* (DIC): light from an incandescent source is passed through a polariser so that all the light getting through must vibrate in a single plane. The light then passes through a prism where it is split in two beams that pass through the condenser lens as parallel beams with perpendicular polarisation. They then pass through the specimen and in any part of the specimen in which adjacent regions differ in refractive index, the two beams are delayed or refracted. When they are combined again by a second prism in the objective lense an interference contrast is created that can be observed as differences in intensity and colour whose shadow effects lead to a kind of 3-dimensional appearance of the specimen.

Whereas in transmission microscopy the observer is on the opposite side of the specimen w.r.t. the light source, in reflected light microscopy both light source and the observer are on the same side of the specimen. Since not all specimen are transparent, reflected light microscopy or epi-illumination is used for opaque specimens, such as silicon wafers, ceramic, metals, plastics, or paper. Light passes from a lamp onto the surfaces with the specimen

pointing upright to the objective where it is reflected and carried back towards the eye piece. Reflected light microscopy can be applied to many modes of light microscopy (brightfield, darkfield, DIC and fluorescence).

Fluorescence microscopy is used when a specimen is either labelled with chemicals that are capable to fluoresce (called secondary fluorescence) or when a material can be made to fluoresce in its natural form (primary fluorescence). The whole spectrum of the lamp hits the excitation filter, which itself only allows a narrow range of wavelengths to pass through (bandpass). Light passing through is then absorbed by the fluorophores in the sample and excited to fluoresce at a higher wavelengths (and hence lower energy). This fluorescent light then passes through an edge filter, which allows only light with wavelengths higher than the emission wavelength to pass through and reach the eye of the observer.

3.2 Dynamic Light Scattering

Dynamic light scattering (also known as Quasi Elastic Light Scattering and Photon Correlation Spectroscopy) is particularly suited for determining small changes in the mean diameter of colloidal particles.
When a beam of light passes through a colloidal dispersion, the particles or droplets scatter some of the light in all directions. When the particles are very small compared with the wavelength of the light, the intensity of the scattered light is uniform in all directions (Rayleigh scattering); for larger particles (above ca. 250 nm diameter), the intensity is angle dependent (Mie scattering). If the light is coherent and monochromatic, as from a laser, it is possible to observe time-dependent fluctuations in the scattered intensity using a suitable detector such as a photomultiplier capable of operating in photon counting mode. These fluctuations arise from the fact that the particles are small enough to undergo random thermal (Brownian) motion and the distance between them is therefore constantly varying. Constructive and destructive interference of light scattered by neighbouring particles within the illuminated zone gives rise to the intensity fluctuation at the detector plane which, as it arises from particle motion, contains information about this motion.

The time dependence of the intensity fluctuation is most commonly analysed using a digital correlator, which determines the intensity autocorrelation function that can be described as the ensemble average of the product of the signal with a delayed version of itself as a function of the delay time. The "signal" in this case is the number of photons counted in one sampling interval. At short delay times, correlation is high and, over time as particles diffuse, correlation diminishes to zero, and the exponential decay of the correlation function is characteristic of the diffusion coefficient of the particles. Analysis of the autocorrelation function in terms of particle size distribution is done by numerically fitting the data with

calculations based on assumed distributions. A truly monodisperse sample would give rise to a single exponential decay to which fitting a calculated particle size distribution is relatively straightforward. In practice, polydisperse samples give rise to a series of exponentials and several quite complex schemes have been devised for the fitting process.
The different directions of the scattered light are measured by the scattering angle θ, between the incident beam defined by the laser ray and the scattered light. Analysis of the time dependence of the intensity fluctuation can therefore yield the diffusion coefficient of the particles from which, when knowing the viscosity of the medium η, the hydrodynamic radius or diameter of the particles, can be calculated *via* the Stokes Einstein equation (Eq.3.1) [Collins 97] .

$$radii = \frac{k_b T}{6\pi\eta D} \tag{3.1}$$

D denotes the diffusion coefficient of the suspended particles in the fluid, and b is a geometric constant determined by the experiment.

3.3 Atomic Force Microscopy

Atomic force microscopy (AFM) probes the surface of a sample with a sharp stylus, called a tip. The tip is a few microns long and located at the end of a cantilever that is 100 to 200 μm long. It is usually made of Si or Si_3N_4 and is capable of measuring forces between 10^{-12} to 10^{-9} N. Forces between the tip and the sample surface cause the cantilever to bend or deflect. A laser beam is reflected from the back side of the cantilever and is focused on a photodiode sensor. When the cantilever is deflected the position of the laser spot on the detector changes. The force acting on the cantilever is proportional to the deflection. Therefore by adjusting a force setpoint, the force between tip and sample is also adjusted. This results in a signal, which is recorded in a computer (Fig. 3.1). The feedback of the computer controls the z translator (called piezoelectric scanner) to adjust the tip or sample up or down in order to restore the tip to its original deflection. The computer stores the vertical position of the z translator at each point and assembles the image [Ulman 91].

Three fundamental operating techniques are usually performed with AFM, namely the contact, the non-contact mode, and the intermittent contact mode (also referred to as tapping mode). In the non-contact regime the cantilever is held on the order of tens to hundreds of angstroms from the sample surface and due to the long-range vdW interactions the force between the cantilever and the sample is attractive. In the contact regime the cantilever is

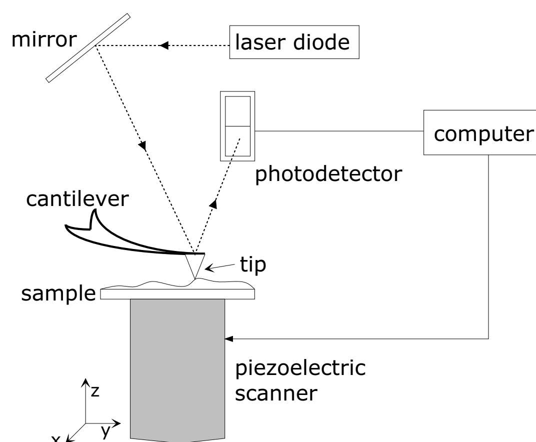

Figure 3.1: *The sample is positioned on the piezoelement that can be moved in xyz. As a raster-scan drags the tip over the sample, the photodetector measures the vertical deflection of the cantilever due to upwards or downwards deflection of the laser beam. The photodiodes can measure displacements of light smaller than 10 Å.*

in contact with the sample surface and the interatomic force between cantilever and sample is repulsive. In the intermittent contact regime the tip is periodically oscillated over the sample and changes in the oscillation frequency or amplitude are detected. Once the AFM has detected the cantilever deflection it can generate the topographic data set by operating in two modes - constant height or constant force mode. In constant height mode the spatial variation of the cantilever deflection can be used directly to generate the topographic data set since the height of the scanner is fixed as it scans. In constant force mode the deflection of the cantilever can be used as an input to a feedback circuit that moves the scanner up and down in z, responding to the topography by keeping the cantilever deflection constant. By doing so the image is generated from the scanner's motion. With the cantilever deflection held constant, the total force applied to the sample is constant.
Contact mode is usually applied to "hard" materials where the rather large force does not damage the surface. For soft materials, such as colloids, non-contact or intermittent contact mode is used.

3.4 Scanning Electron Microscopy

Scanning electron microscopy (SEM) is used to resolve a surface structure down to 5 nm. SEM works analogous to an optical microscope but instead of light and glass lenses an electron beam is focused by lenses consisting of magnetic fields. The electron source is usually a filament of tungsten or lanthanum hexaboride (LaB_6) with a highly negative

potential so that the electrons are accelerated towards an anode that is held at a small positive potential w.r.t. the ground potential. The acceleration voltage used ranges from 0.2 to 30 keV and the high resolution that results from the short wavelength of the electron originates from the de Broglie wavelength. For example, an electron with an acceleration voltage of 25 keV possesses a de Broglie wavelength of 7.76 pm.

As visible in Fig. 3.2 the electron microscope operates under high vacuum and the image is obtained by sweeping the surface in a raster pattern with the focused beam of electrons. Scanning is achieved with the use of electromagnetic coils that deflect the beam in the

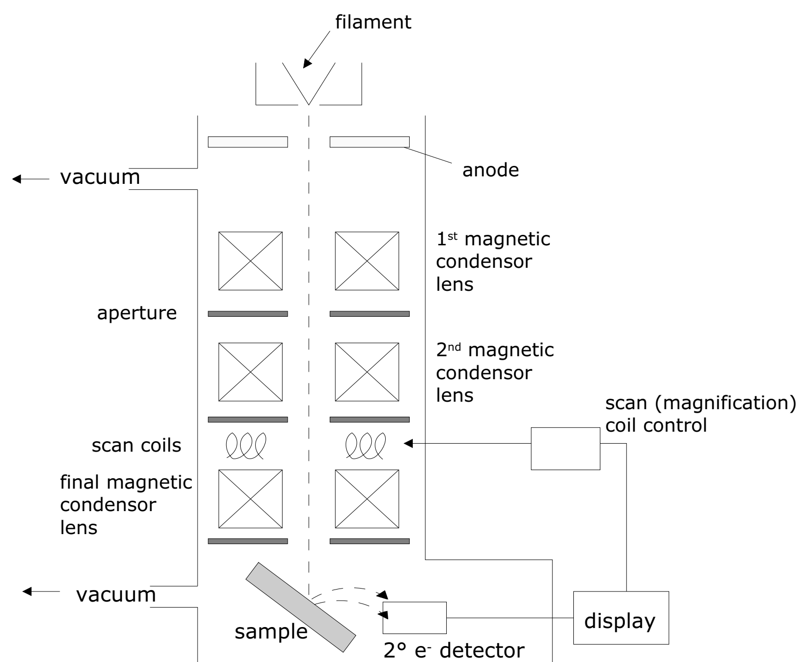

Figure 3.2: *Schematic representation of a Scanning Electron Microscope.*

xy direction. The electrons hit the surface of the sample and yield secondary electrons, backscattered electrons, Auger electrons (0.005-2 keV) and X-ray radiation. The secondary electrons possess a rather low energy of less than 0.005 keV and provide information about the topography and morphology since they are emitted only from the first few nanometers of the specimen. The composition of the specimen can be determined by the intensity of backscattered electrons from deeper regions in the sample since they are correlated to the atomic number of elements within the sampling volume [Skoog 96, Ulman 91].

3.5 UV-Vis Spectroscopy

Ultraviolet/visible spectroscopy involves the absorption of ultraviolet or visible light by a molecule causing the promotion of an electron from a ground electronic state to an excited electronic state. The absorption spectra, which are due to the light absorption, are then measured. The spectra range from 200 to 800nm, where the quantitative absorption is defined by Lambert-Beer's law (3.4), which is based on a beam of light passing through a solution of known thickness *b* and concentration *c* of the adsorbing species depicted by the transmittance *T*

$$T = \frac{P}{P_0}, \tag{3.2}$$

where P_0 is the intensity of the incident beam and *P* the resulting intensity of the beam after absorption by the solution. Upon transmittance the photons interact with the molecules in solution. The absorbance *A* of the solution is then defined as

$$A = -\log_{10} T = \log \frac{P_0}{P}. \tag{3.3}$$

Absorbance is directly proportional to the path length *b* and concentration *c* of the solution, which is described by Lambert-Beer's law:

$$A = \epsilon bc, \tag{3.4}$$

where ϵ is a proportionality constant called "molar absorptivity" with units $\mathrm{Lmol^{-1}cm^{-1}}$. The linear relationship in Beer's law only holds for dilute solutions. With higher concentrated solutions ($>$ 0.01 M) the distance between neighbouring species is reduced leading to interactions that alter the ability to absorb at a given wavelength, which in turn causes deviation from the linear relationship between absorbance and concentration.
Generally it can be said that the spectrum of a given compound exhibits an absorption band of very low intensity ($\epsilon = 10^{-100}$) in the 270-350 nm region, and no other absorptions above 200 nm, if it contains a simple, non-conjugated chromophore. If the spectrum of a given compound exhibits many bands, some of which appear even in the visible region, the compound is likely to contain long-chain conjugated or polycyclic aromatic chromophores. If the compound is coloured, there may be at least 4 to 5 conjugated chromophores and auxochromes. An ϵ value between 10,000 and 20,000 generally represents a simple α,β-unsaturated ketone or diene. Bands with ϵ values between 1,000 and 10,000 normally show the presence of an aromatic system. Substitution on the aromatic nucleus by a functional group which extends the length of the chromophore may give bands with $\epsilon >$ 10,000 along with some which still have $\epsilon >$ 10,000. [Skoog 96]

3.6 Confocal Microscopy

In confocal microscopy (or sometimes called "laser scanning confocal microscopy") a laser beam is used to provide the excitation light. After passing through a dichroic mirror the laser hits two xy galvanometric scanners, which are mounted on motors; these mirrors scan the laser across the sample. Dye in the sample fluoresces and the emitted light gets descanned by the same scanners that are used to scan the excitation light from the laser. The emitted light is reflected by the dichroic mirror and is focused onto the pinhole plane. The light that passes through the pinhole is measured by a detector, *i.e.* a photomultiplier tube.
The confocal aperture (pinhole) is placed in front of the photodetector, such that the fluorescent light from points on the specimen that are not within the focal plane will be largely obstructed by the pinhole. In this way, out-of-focus information (both above and below the focal plane) is greatly reduced (Fig. 3.3). Light excited in the sample in the focal point of

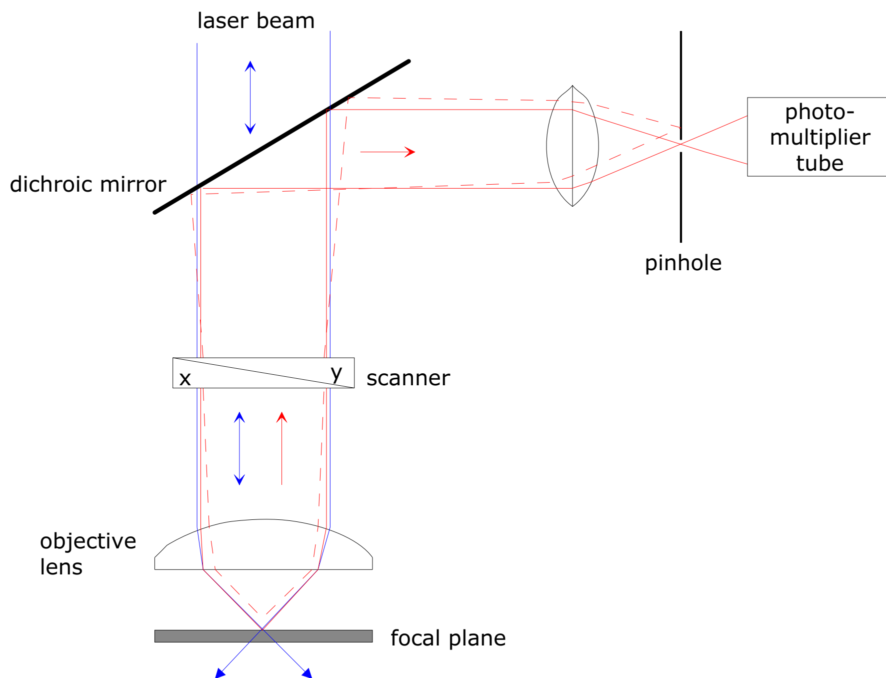

Figure 3.3: *Confocal principle: laser light (blue) passes through dichroic mirror and is emitted at focal point in focal plane (red light). The emitted light is then reflected by dichroic mirror and is focused onto the pinhole by a microscope objective. Light emitted out-of-focus (dashed lines) is not focused on the pinhole.*

the lens is precisely imaged in the opening of the detector pinhole. In this way, a single point anywhere in a 3D sample can be accurately imaged with a resolution of > 1 μm. By scanning this point laterally through the focal plane, a 2D image of a slice through the sample can be made. As the laser scans across the specimen with the help of mirrors, the analog light signal, detected by the photomultiplier, is converted into a digital signal, contributing to

a pixel-based image displayed on a computer monitor attached to the confocal microscope. The relative intensity of the fluorescent light emitted from the laser spot, corresponds to the intensity of the resulting pixel in the image. This becomes especially important when dealing with thick specimens. The spot that is focussed on the center of the pinhole is often referred to as the "confocal spot". A 3D reconstruction of a specimen can be generated by stacking 2D optical sections collected in series.
The advantage of using a confocal microscope is that it is really efficient at rejecting out of focus fluorescent light. The best horizontal resolution of a confocal microscope is about 0.2 microns, and the best vertical resolution is about 0.5 microns [Wilhelm 98].

3.7 Contact Angle Measurement

Contact angle measurement is based on the form that a liquid droplet (usually water) adopts when placed on a solid surface and it is a popular and uncomplicated means to characterise the hydrophobicity or hydrophilicity of a surface [Ulman 91]. According to the interfacial

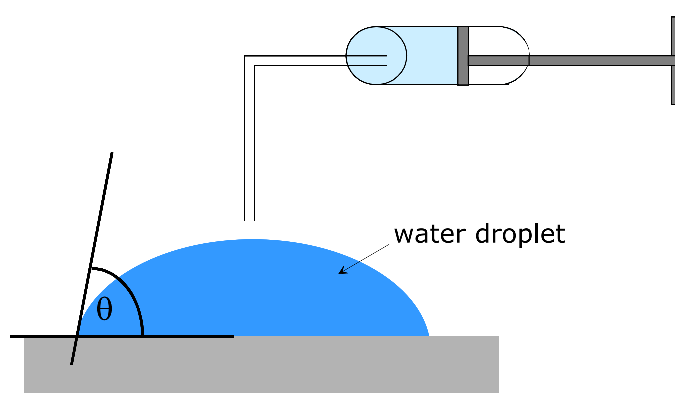

Figure 3.4: *Water from a micro syringe is dropped onto the surface and the angle between liquid-gas boundary and solid-liquid boundary is measured.*

energies given by Young's equation (3.5) the contact angle can be traced to the balance of forces at the liquid / solid boundary which are due to the interfacial and surface energies of the 3-phase system (air-liquid-substrate) [Atkins 98]. If the solid-gas (sg), solid-liquid (sl) and liquid-gas (lg) interfacial energies are denoted γ_{sg}, γ_{sl} and γ_{lg}, respectively, the horizontal forces are in balance if

$$\gamma_{sg} = \gamma_{sl} + \gamma_{lg} \cdot \cos\theta. \tag{3.5}$$

If a small liquid drop is deposited on a surface, it spreads. If additional liquid is added, the contact line advances. Each time motion ceases, the drop exhibits an advancing contact angle (θ_a). Alternatively, if liquid is removed from the drop, the contact angle decreases to a receding value (θ_r) before the contact line retreats. This difference between (θ_a) and (θ_r) is referred to as contact angle hysteresis (from the Greek work *hysterein*, meaning to lag). Surface imperfections, such as contamination, can lead to contact angle hysteresis and removing such anomalies greatly reduced the hysteresis. Consequently, most descriptions assume that contact angle hysteresis is caused by surface flaws. However, even surfaces that are molecularly smooth and homogeneous can show hysteresis. Contact angle hysteresis should be considered a source of information on the behavior of liquid-solid interfaces.
The contact angle is very sensitive towards the chemical composition of the surface and can adopt values from ca. 0° (very hydrophilic, e.g. pure SiO_2) to 120° (very hydrophobic, e.g. methylene head groups on SAM). Thus it is well suited for monitoring the deposition of silanes on the silicon dioxide surface.

Chapter 4

Particle Assembly on Patterned Surfaces

The aim of this chapter is to describe how colloidal particles self-assemble on laterally structured surfaces modified with different ω-functionalised silanes. The lateral structure is obtained by using standard photolithographic and surface modification methods. The assembly of the colloidal particles occurs due to attractive interactions between the particles and the silane surface.

4.1 Formation of Structured Surfaces

For the preparation of the silane monolayers two general techniques are used, namely adsorption from a silane solution and deposition of the silane from the vapour phase (Fig. 4.2).

4.1.1 Solution Phase Deposition

Solution phase silanisation is a common technique where the substrate is immersed into a 0.5-2% solution of the silane in an appropriate solvent. This method also allows controlled hydrolysis of the silane (cf. Chapter 2.2) prior or during substrate immersion [Jonas 02b]. During hydrolysis of the triethoxysilane and adsorption onto the surface different chemical and physical processes occur simultaneously (*e.g.* hydrolytic cleavage of alkoxysilyl bonds, silanol condensation in solution, adsorption of monomeric and oligomeric species to the surface, silanol condensation at the substrate surface, and chemical bonding of the molecule to the SiOH groups on the substrate surface). The reaction conditions thus have to be carefully optimised for each silane derivative in order to prevent undesired three-dimensional aggregation in solution.

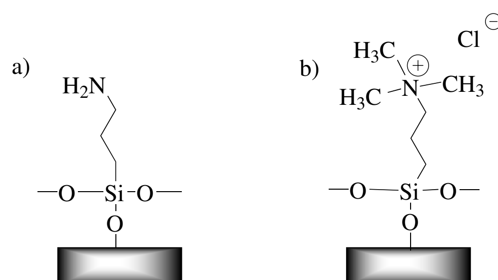

Figure 4.1: *a) APTS and b) NR_4^+ on silica surface.*

Alkoxysilanes, such as aminopropyltriethoxysilane (APTS) and N-trimethoxysilylpropyl-1-N,N,N,-trimethylammoniumchloride (NR_4^+) were deposited on silica surfaces according to Chapter 7.2.1. The static contact angle of ca. 60° for APTS and ca. 70° for NR_4^+ is in good accordance with the results obtained by Krüger *et al.* who also demonstrated that upon storage of APTS-substrate the static contact angle changed to 66° [Krüger 01]. The average thickness of such a layer lies around 0.6 nm [Kallury 94].
While quaternary ammonium groups bear a permanent positive charge at all pHs, amine groups, which have a pK_A of ca. 11, are mostly protonated (positively charged) below pH 11. SiOH groups on the surface possess a pK_A of ca. 7.5 [Behrens 01] and are therefore dissociated at higher pH.

4.1.2 Vapour Phase Deposition

When photoresist structures are used for patterned silane layer preparation, silane deposition is restricted to aqueous solutions since organic solvents (*i.e.* THF) would dissolve the photoresist. This problem can be overcome by using the vapour phase technique, which works well if the boiling point of the silane is low enough at a given pressure. Compared to solution phase deposition, vapour phase deposition should lead to better defined monolayers since hydrolysis, condensation and covalent bonding occur exclusively at the substrate surface.

Two hydrophobic silanes, octadecyltriethoxysilane (OTE) and hexamethyldisilazane (HMDS) were deposited by vapour phase silanisation. OTE has a high boiling point (165°C at 2.7 mbar) and therefore the reaction has to be carried out under vacuum (0.02 mbar) by heating the silane to 95 °C for 2 h in a closed vessel. The triethoxy groups of the OTE then anchor onto the silica surface and due to condensation processes a 3-dimensional network will form.
The contact angles thus obtained (ca. 110 °) were in good accordance with the results obtained by Krüger [Krüger 01] and a thickness of 1.1nm was determined by ellipsometry.
HMDS on the other hand is a monofunctional silane that reacts in a different way with the silanol surface (Fig. 4.3). Upon reaction with the silanol groups on the surface the HMDS

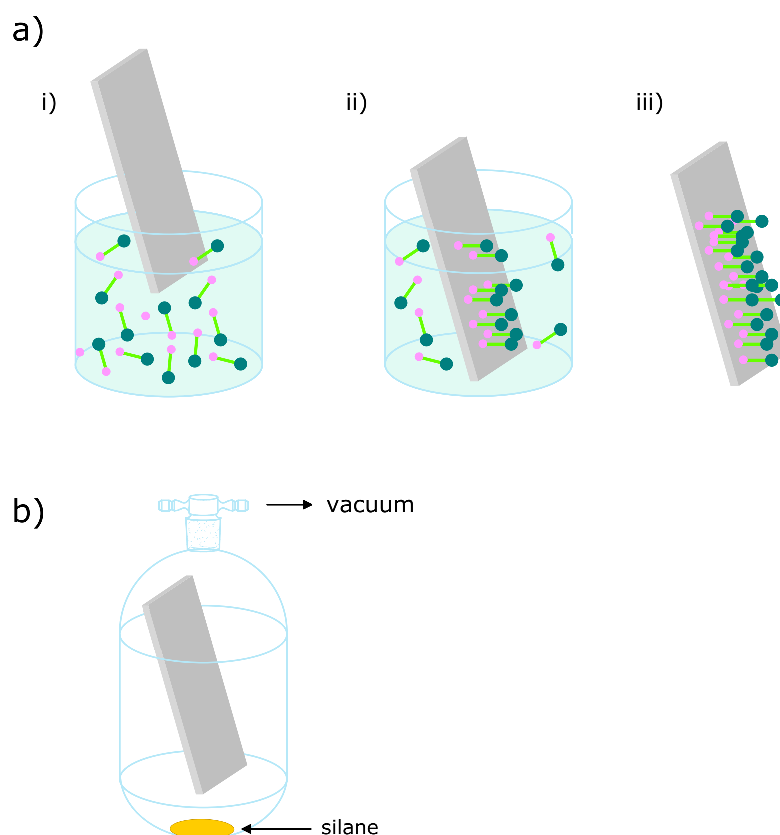

Figure 4.2: *a) Solution phase deposition where substrate is immersed into silane solution (i) so that the silane anchor groups can deposit on the silica surface (ii) to generate SAMs (iii), b) vapour phase deposition in a closed vessel containing only the substrate and the pure silane.*

molecule is cleaved and trimethlylsilyl functions are formed with ammonia as a side product. HMDS possesses a much lower boiling point than OTE (129 °C, 1024 mbar) and a high vapour pressure. It is thus possible to perform the silanisation at room temperature and ambient pressure for 30 min.
The resulting contact angle was 74°, which is characteristic for nonpolar, hydrophobic methyl groups on the surface [Fadeev 99].

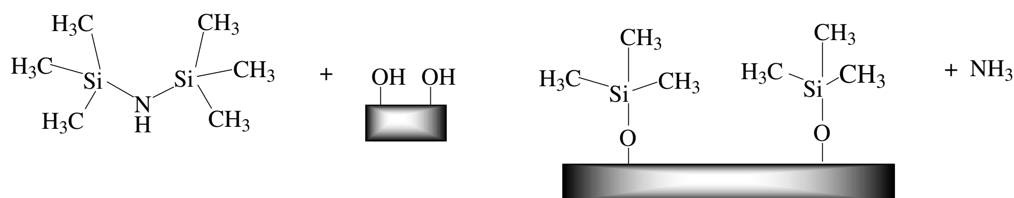

Figure 4.3: *Reaction of HMDS on Si-O surface.*

4.1.3 Combination of Vapour and Solution Phase Deposition

In order to deposit hydrophilic and hydrophobic silanes on the same substrate photolithography combined with the before mentioned silanisation technique was carried out on cleaned silicon dioxide substrates. Once the photoresist pattern is generated, the first silane can be deposited. After removal of the remaining photoresist the second silane can then be deposit on the generated free surface area, thus producing patterned silane layers with a hydrophobic/hydrophilic contrast, (*i.e.* OTE/SiOH or HMDS/SiOH). It is also possible to obtain uncharged/charged patterned surface layers using *e.g.* OTE/NR_4^+, APTS/SiOH or NR_4^+/SiOH.

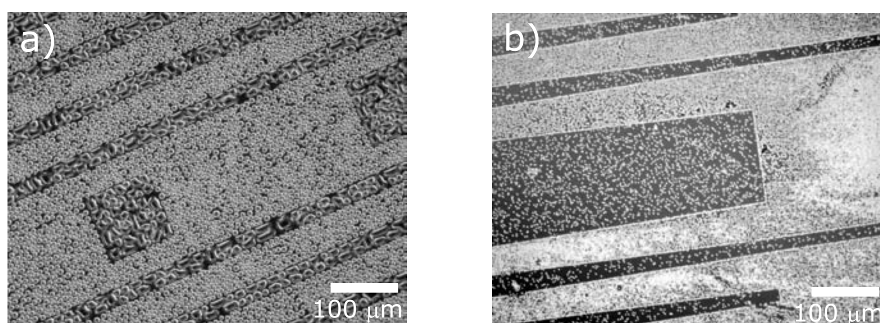

Figure 4.4: *Optical microscopy image (DIC) of H_2O condensation on an OTE/SiOH monolayer pattern: a) water condensation pattern after substrate cooling with hydrophilic SiOH squares and stripes, surrounded by hydrophobic OTE, almost completely wetted on hydrophilic regions, b) breath pattern at room temperature with the bright SiOH regions and darker OTE regions.*

For the OTE/SiOH pattern shown in Fig. 4.4 octadecyltriethoxysilane was deposited *via* vapour phase silanisation after the photoresist had been developed. The remaining photoresist was then removed in an ultrasound bath and a picture of the condensation pattern was recorded.
It is visible from the condensation pattern on a cooled substrate (Fig. 4.4a) that the hydrophilic SiOH squares are almost completely wetted (water contact angle ca. 12°) whereas the water is mostly repelled from the hydrophobic OTE surface (water contact angle ca. 108°). A bright contrast is also observed when a breath pattern was recorded at room temperature.
Fig. 4.4 shows that it is possible to influence the polarity and wetting behaviour of the surface by choosing appropriate functionalised head groups on the silane layers.

The remaining free SiOH groups on the surface can be further modified with a second silane in order to form a more complex functionalised surface layer. NR_4^+ functionalised silane was deposited on the OTE/SiOH patterned substrate *via* solution phase deposition, and

after tempering and washing a breath pattern was recorded with the optical microscope.
The condensation pattern on OTE/NR_4^+ substrate is visible in Fig. 4.5, where the brighter regions correspond to the ammonium covered areas on the surface. Compared to OTE/SiOH

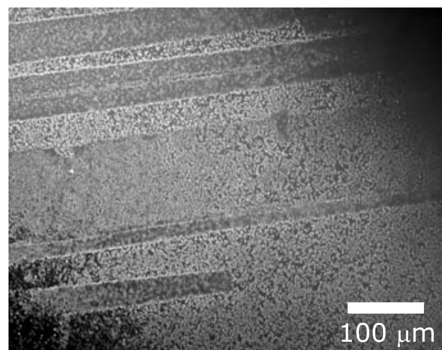

Figure 4.5: *Optical microscopy image (DIC) of OTE/NR_4^+ monolayer condensation pattern at room temperature with the bright regions being NR_4^+ and the darker regions OTE.*

the wetting contrast is reduced, which is due to the larger contact angle of the NR_4^+ layers resulting in a smaller difference in the water contact angle between the uncharged OTE and the charged ammonium groups. Measurements show that NR_4^+ covered surfaces possess a water contact angle ca. 70° as compared to ca. 12° for SiOH. Therefore the selectivity of the water droplets on the surface is less specific than with OTE and SiOH. However, the wetting contrast is still high enough to be visualised in the condensation pattern.

4.2 Colloidal Assembly on Patterned Surfaces

Tailoring the surface functionalities allows colloidal particles to selectively self-assemble on silane layer patterns and thus study mesoscale assembly in a model system [Lee 02, Tieke 01]. Selective self-assembly of colloidal particles at surfaces due to attractive electrostatic interactions has become very popular in recent years. The ability to harness intrinsic interactions between surfaces leads to novel and elegant methods for self-organised deposition of colloidal particles, where the driving forces are electrostatic interactions, surface tension, vdW forces and capillary forces. 2D or even 3D structures can be created by controlling these forces [Im 02, Burmeister 99].
To immobilise colloids (primarily polymer and silica particles with diameters $>$100 nm) at planar substrates various methods utilising charge and polar interactions are available [Wit 98, Kampes 99, Tieke 01] with the more sophisticated techniques leading to laterally structured colloid assemblies [Nakagawa 00, Hattori 01, Aizenberg 00, Zheng 02a, Zheng 02b]. However, whereas in former years scientific groups were interested in the formation of 2-D crys-

tals from latex particles on unpatterned substrates, this chapter will deal with colloidal self-assembly on patterned surfaces [Denkov 92, Iler 66, Johnson 96, Serizawa 98].

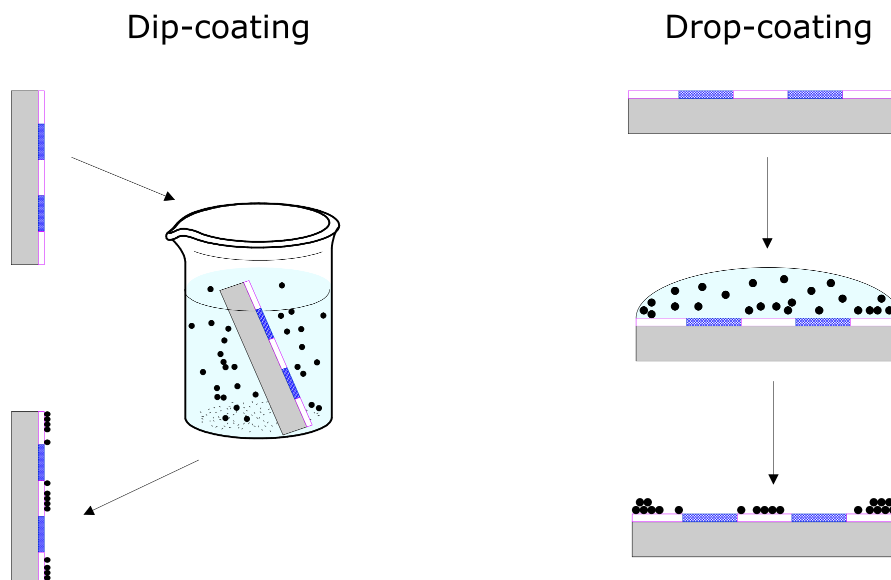

Figure 4.6: *Organisation of colloidal particles with drop-coating and dip-coating methods.*

Colloidal adsorption (usually from aqueous suspensions) can be carried out using either the drop-coating method, where a droplet of the dispersion is applied to the surface or the dip-coating method, where the substrates are immersed into the colloidal solution (Fig. 4.6). After removal of the droplet or the substrate out of the suspension, the wafers are rinsed gently with the suspending liquid to wash off any unspecifically bound particles.

Since weakly adsorbed particles might also be removed in the washing process no rinsing step was applied in such cases. During removal of the substrate the contact line runs over the substrate and interferes with particle selectivity by particle rearrangement mediated by capillary forces.
Drop-coating is usually preferred since the volume of the removing liquid can be controlled so that the substrate surface does not run dry.

4.2.1 Assembly of Hydrophobic Aerosil Particles

In order to study in more detail the interaction between hydrophobic/hydrophilic surfaces with hydrophobic particles, octyl-modified colloidal silica particles[1] were assembled on silica surfaces from suspensions in toluene, THF and EtOH. The assembly was carried out on

[1] Aerosil R805, Degussa, 100-200 nm in diameter

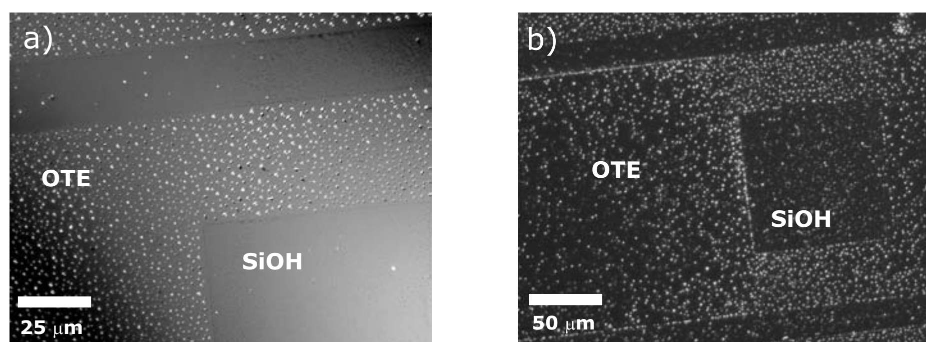

Figure 4.7: *Optical microscope image (DF) of Aerosil particles deposited from toluene suspension on SiOH/OTE patterned surface: a) substrate with wet suspension with almost complete coverage of the particles outside the square on the OTE regions, b) substrate after drying of suspension for 24 h.*

photolithographically patterned OTE/SiOH silica surfaces. The selectivity of the particle adsorption was then studied w.r.t. the solvent polarity.
For all assembly processes the Aerosil particles were redispersed in their respective solvent as a 0.3 wt% solution and the substrates were then immersed into the suspension overnight. Optical microscopy images were recorded on the particle layers before and after drying for 24 h.

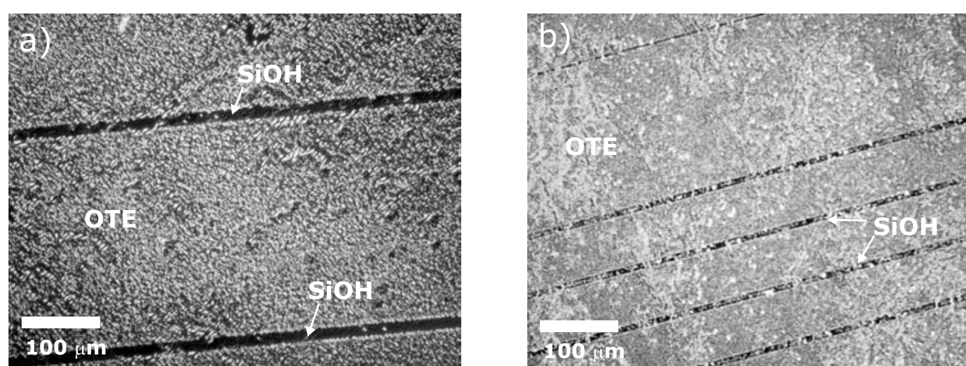

Figure 4.8: *Optical microscope image (DIC) of Aerosil particles from THF suspension on SiOH/OTE patterned surface: a) substrate with wet suspension with almost complete coverage of the particles outside the SiOH stripes on the OTE regions, b) substrate after drying of suspension for 24 h with most particles on the OTE region outside the stripes.*

When adsorbing hydrophobic Aerosil particles from a toluene suspension (Fig. 4.7a), it becomes apparent that the particles primarily adsorb onto the OTE regions when being in the wet state. After 24 h drying (Fig. 4.7b) most of the particles are still present in the OTE

regions, but due to the wet/dry contrast some particles are visible in the hydrophilic SiOH region.

When adsorbing the particles from a suspension in THF (Fig. 4.8a) most Aerosil particles have adsorbed in the wet state onto the hydrophobic OTE regions outside the stripes. After 24 h drying particle contrast is reduced with more particles being visible also on the hydrophilic regions inside the stripes (Fig. 4.8b). Again this might be due to optical effects that occur upon drying.

A change in selectivity is observed when adsorbing the hydrophobic particles in hydrophilic and protic ethanol. Fig. 4.9a shows the fresh particle deposition in the wet state and Fig. 4.9b shows the particles after 24 h of drying. Even though a pattern can hardly be detected, it is visible that the particles are adsorbed mostly on the hydrophilic SiOH regions of the surface (inside the stripes).

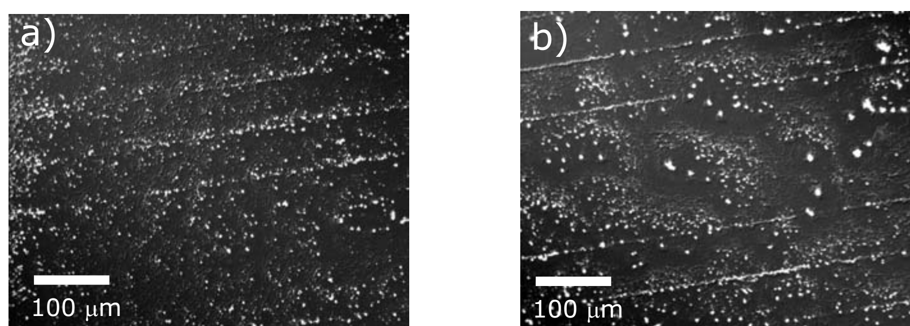

Figure 4.9: *Optical microscope image (DIC) of Aerosil particles from EtOH suspension on SiOH/OTE patterned surface: a) wet substrate showing lower selectivity and particle adsorption coverage of the particles, b) substrate after drying of suspension for 24 h, showing no substantial change.*

Since both the OTE surface and the Aerosil particles possess a hydrocarbon layer and are uncharged the interactions between them are primarily due to vdW forces based on induced dipoles. The polar solvent on the other hand has a preference for itself or for the polar SiOH groups on the surface. This leads to an effective reduction of the preference of the Aerosil particles for the polar surface. The attractions between the surface and adsorbed particles under those conditions are therefore of a strong Coulombic nature.

When colloidal particles self-assemble on a surface many parameters have to be considered: the interactions between the solvent and substrate, particles and substrate, particles and solvent, and between the solvent molecules themselves.
Toluene for example is a hydrophobic solvent with a weak dipole moment (0.36 D) and

can undergo vdW interactions with the OTE layer and the Aerosil particles. THF is also a molecule with a higher dipole moment of 1.6 D. Being an ether it can form stronger dipole interactions than toluene. In addition, it can accept H-bonds and thus act as a Lewis base. Due to the complexity of the system one can only speculate that solvents with lower polarity (*i.e.* toluene) will form stronger interactions with the OTE layer than with the SiOH regions. As a result, particle adsorption onto the hydrophilic SiOH surface is aggravated, whereas vdW interactions between hydrophobic particles and the OTE layer remains unaffected.
When the Aerosil particles are adsorbed from a THF suspension they primarily adsorb onto the OTE regions. This is again due to the rather strong attraction between THF solvent molecules and SiOH groups on the surface. Therefore the solvent particles cannot be displaced from the SiOH regions by the Aerosil particles, thus preventing particle adsorption on the SiOH layer.
Ethanol on the other hand is a more polar molecule with a dipole moment of 1.7 D. It can both accept and donate H-bonds and can undergo strong dipole interactions. The surface tension of ethanol (22 mJm^{-2}) exerts a strong drying effect on the substrate surface emphasised by lateral capillary forces that act between the particles. This also results in dewetting of the OTE regions and pinning of the solvent at the hydrophilic SiOH regions. By this mechanism particles can be substantially rearranged during the drying process, which explains the low selectivity contrast and the higher particle density on the SiOH regions.

From these experiments it can be deduced that hydrophobic particles assembly in organic solvents with low polarity are most suited to achieve an appropriate selectivity.

4.2.2 Self-Organisation of Charged Colloidal Particles on Patterned Substrates

4.2.2.1 Carboxylated PBA Particles on $NR_4{}^+$/SiOH Surfaces

In order to investigate further the assembly of charged colloidal particles onto surfaces, carboxylated latex particles were assembled on patterned $NR_4{}^+$/SiOH surfaces.

Assembly experiments were first carried out using trimethylammonium modified silanes, whose head groups are not affected by the pH. In order to confirm this, colloidal assembly of carboxylated PBA particles (44 $Å^2$ per charge) was carried out at pH 4 and 9.
The colloidal suspension was diluted to 0.04 wt% using pH adjusted Milli-Q water for dilution.[2] The colloidal deposition was carried out *via* the drop-coating method, and the substrates rinsed in Milli-Q water afterwards. They were then examined with optical microscopy.

[2]Water for dilution was first adjusted to the desired pH using HCl and NaOH

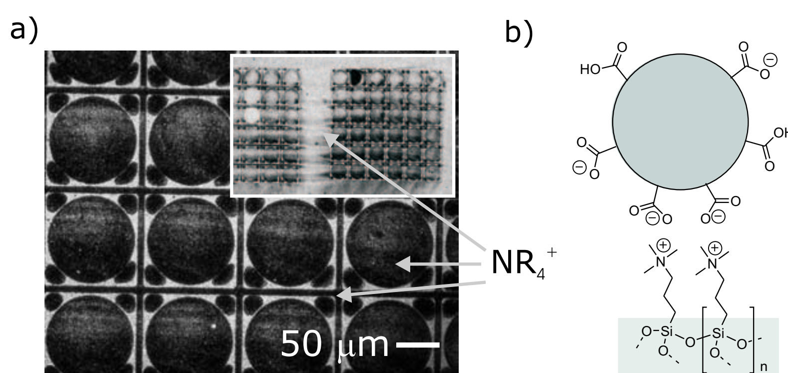

Figure 4.10: *a) optical microscope image (DF) of carboxylated PBA particles adsorbed at pH 4 on NR_4^+/SiOH patterned surface, b) schematic representation of colloid on surface.*

Colloidal particles adsorb to the SiOH regions, as well as the NR_4^+ regions (Fig. 4.10). The results are in accordance with experiments carried out by Jonas and co-workers [Jonas 02a]. At pH 4 the COOH groups of the colloidal particles are protonated and thus can form strong hydrogen bonds with the silanol groups on the surface that are only weakly dissociated [Behrens 01]. The ammonium groups on the other hand primarily interact *via* electrostatic interactions with the colloids at this pH. Since the COOH groups are sufficiently negatively charged at this pH, the particles adhere to the surface predominantly by electrostatic interactions with the cationic surface.

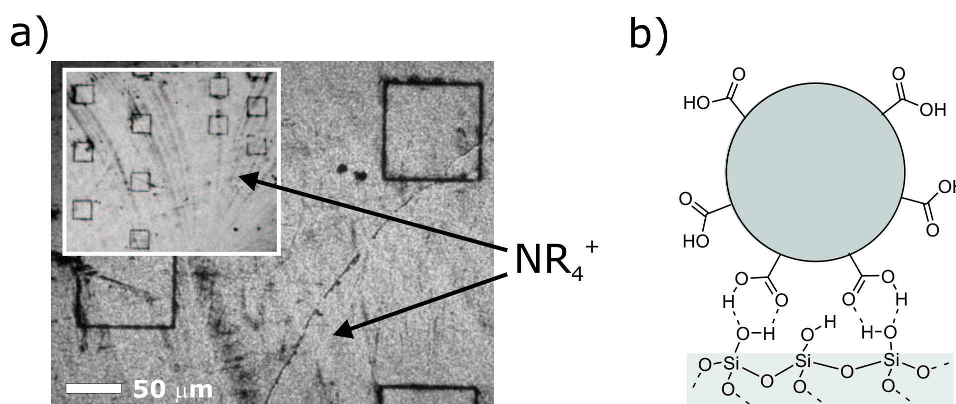

Figure 4.11: *a) optical microscope image (DF) of carboxylated PBA particles adsorbed at pH 9 on NR_4^+/SiOH patterned surface, b) schematic representation of colloid on surface.*

When the same experiment was carried out at pH 9, all the particles were selectively adsorbed on the ammonium layer, as visible in Fig. 4.11. The COOH groups are dissociated at pH 9

and can therefore form attractive interactions with the positively charged ammonium surface. SiOH groups (pK_A ca. 7.5) are dissociated at pH 9. As a result, Coulomb repulsions between surface and particles prevent a colloidal adsorption on the silica layer. The resulting selectivity contrast is observed around the squares in Fig. 4.11a.

4.2.2.2 Carboxylated and Non-Carboxylated Polystyrene Particles on NH_2/SiOH and NH_2/HMDS Patterned Surfaces

The influence of pH and particle charge during colloidal adsorption were investigated in more detail by conducting experiments with three types of latex particles with different charges ((PS-7) with a parking area[3] of 98 Å^2/COOH, polystyrene particles (PS-10) with a parking area of 527 Å^2/COOH, rendering the surface rather nonpolar with little charge, and uncharged particles (PS-cell) at pH 4, 7, and 9. The latter gratefully provided by Marc Egen in the group of Prof. Zentel of the University of Mainz and consisted of a polystyrene core with hydroxypropylcellulose arms outside the shell. All particles were assembled using the drop-coating method and rinsed with Milli-Q water afterwards.

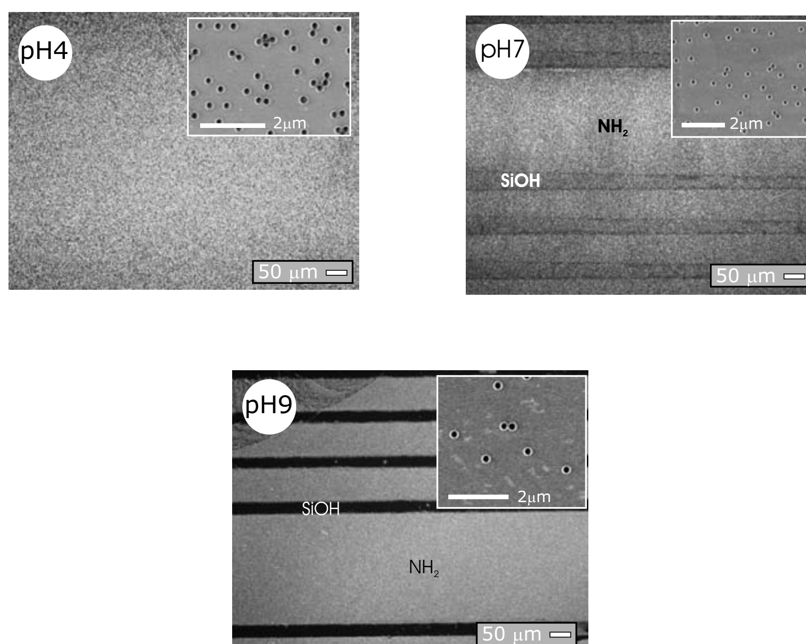

Figure 4.12: *Optical microscope image (DIC) of NH_2/SiOH modified surface with PS-7 particles; smaller picture: SEM image of the particles on the amine layer.*

[3] parking area = average surface area of a colloidal particle containing an acid group

Colloidal deposition was first carried out on charged/uncharged surfaces and then on polar/nonpolar surfaces. NH_2/SiOH patterned substrates were first coated with a colloidal suspension of higher charged particles (PS-7) at pH 4, 7 and 9, respectively.

As visible from Fig. 4.12, at pH 4 the particles have adsorbed onto all regions of the substrate. At pH 7 a weak pattern can be recorded and at pH 9 the pattern is clearly visible. Since at pH 4 nearly all amine groups are protonated and the carboxylic acid function is also protonated, the attraction between surface and particle are mediated by polar and hydrogen bonding interactions. The free SiOH surface exposes polar OH groups to the solution that can participate in dipoledipole interactions and hydrogen bonding. The OH-bond is amphoteric and can dissociate under basic conditions to form a negatively charged surface or it can be protonated at very low pH < 1, yielding a cationic surface.

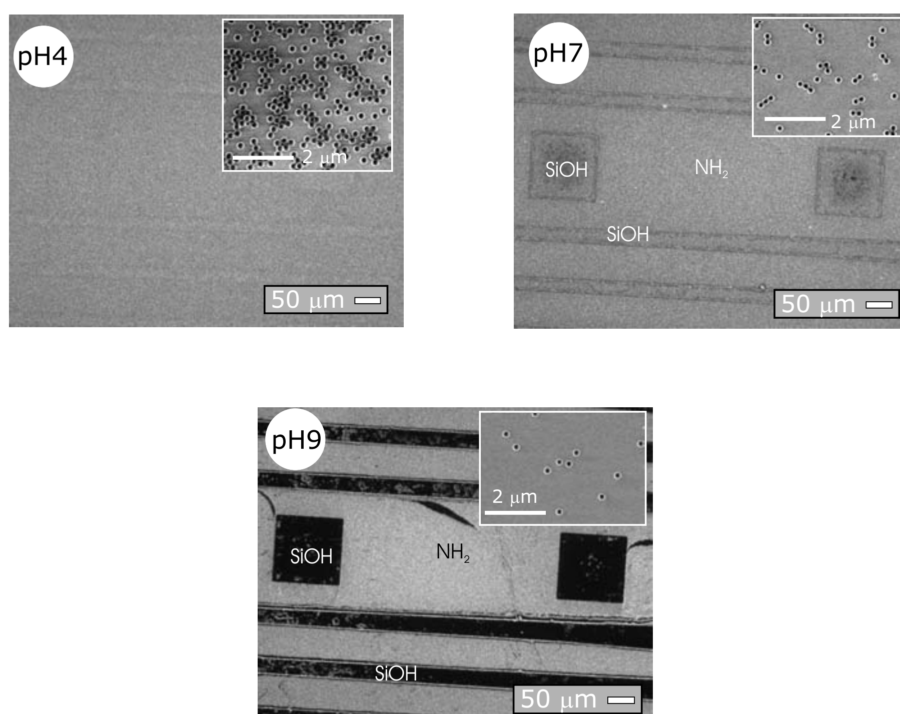

Figure 4.13: *Optical microscope image (DIC) of NH_2/SiOH modified surface with PS-10 particles; smaller picture: SEM image of the particles on the amine layer.*

As a result, the silanol will form strong H-bonds with the COOH functionality at pH 4, leading to a complete coverage of the surface. At pH 7 the silanol groups are partly dissociated leading to Coulomb repulsions between the silanol and the colloid and therefore to a smaller surface coverage of the particles on those areas, as visible in Fig. 4.12. However, since the attraction between the protonated amine groups and the dissociated COO^- groups of the PS-7 particles

are still strong, a weak pattern is visible. Changing the pH to 9 increases the selectivity tremendously since the repulsion between the particles and the SiO^- is now strong enough to effectively prevent colloid adsorption, whereas the electrostatic interaction between the positively charged amine groups on the surface and the dissociated COO^- groups lead to a colloidal assembly on those regions.
From the SEM pictures it can be seen that the particle density also decreases on both regions. At pH 4 the particle density is ca. 7 particles μm^{-2}, for both NH_2 and SiOH. At pH 7 the number decreases to ca. 5 on the NH_2 and ca. 2 particles μm^{-2} on the SiOH regions, whereas at pH 9 the numbers are 1.4 and 0.3 particles μm^{-2} on the NH_2 and SiOH, respectively. Since at higher pH the dissociation of the functional groups increases for both colloids and surface groups, the inter-particle repulsion increases, which consequently leads to a smaller particle density at high pH.
In contrast, at pH 4 all groups involved are protonated and therefore the particles can aggregate by strong hydrogen bonding, which also leads to the complete coverage of the surface.

Assembly with less charged polystyrene particles (PS-10) follows the same trend as observed with more charged colloids above (Fig. 4.13). The selectivity of particle assembly on the amine layer increases from pH 4 to pH 9. Whereas no pattern is visible at pH 4 using the PS-7 particles, a faint selectivity is observed using the PS-10 particles.
It is also clearly visible from the SEM pictures that the particle density decreases from pH 4 to pH 9 due to dissociation of the functional groups and therefore increasing inter-particle repulsion. The particle density on the amine layer is ca. 12 particles μm^{-2} at pH 4, ca. 9 particles μm^{-2} at pH 7 and ca. 4 particles μm^{-2} at pH 9. At pH 9 the particle density on the SiOH layer is also slightly higher with the less charged PS-10 particles, namely 0.3 particles μm^{-2}. The higher particle density arises from the fact that the less charged particles do not repel each other to such an extend as the more charged PS-7 particles. Due to a parking area of 527 $Å^2$ charge^{-1} intermolecular repulsion is reduced, resulting in a higher surface coverage with the colloidal particles at all pHs.

When using the completely uncharged PS-cellulose particles (sterically stabilised) at the different pHs (Fig. 4.14) no selectivity is visible at pH 4, 7 and 9. Since the particles are not affected by the pH they are not amenable to electrostatic interactions with the surface groups and hence form polar and vdW interactions with all surface groups, which leads to a non-selective coverage of the whole substrate. The OH groups in the cellulose chain might also form H-bonds with both the silanol and amine groups on the substrate surface, which can result in a complete coverage of the surface layer with particles. The average particle density at all pH values is roughly 0.1 particles μm^{-2}.

The same assembly experiments were then carried out using a NH_2/HMDS modified surface. By using a hydrophobic counter layer to the amine groups on the surface, it was expected that particle adsorption on the HMDS region should be blocked at all pHs. However, when carrying out the assembly experiments with the higher charged PS-7 particles the selectivity

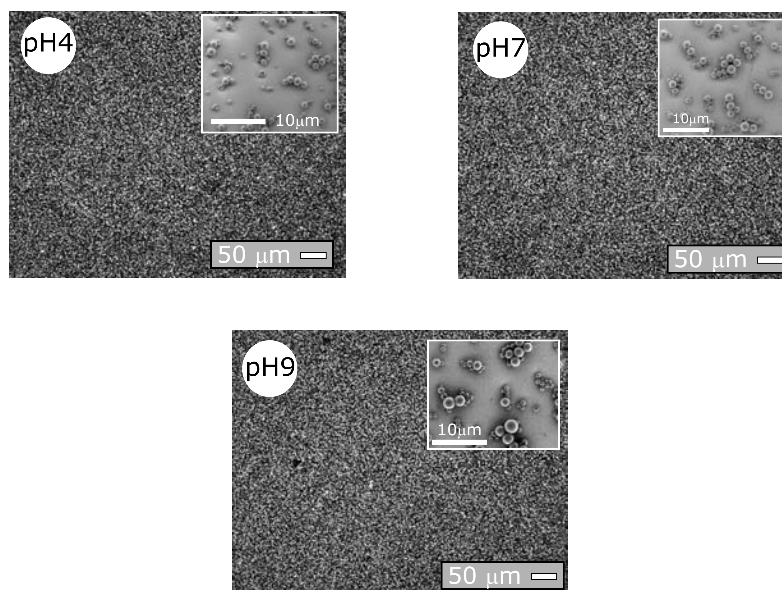

Figure 4.14: *Optical microscope image (DIC) of NH_2/SiOH modified surface with PS-cellulose particles; smaller picture: SEM image of the particles on the amine layer.*

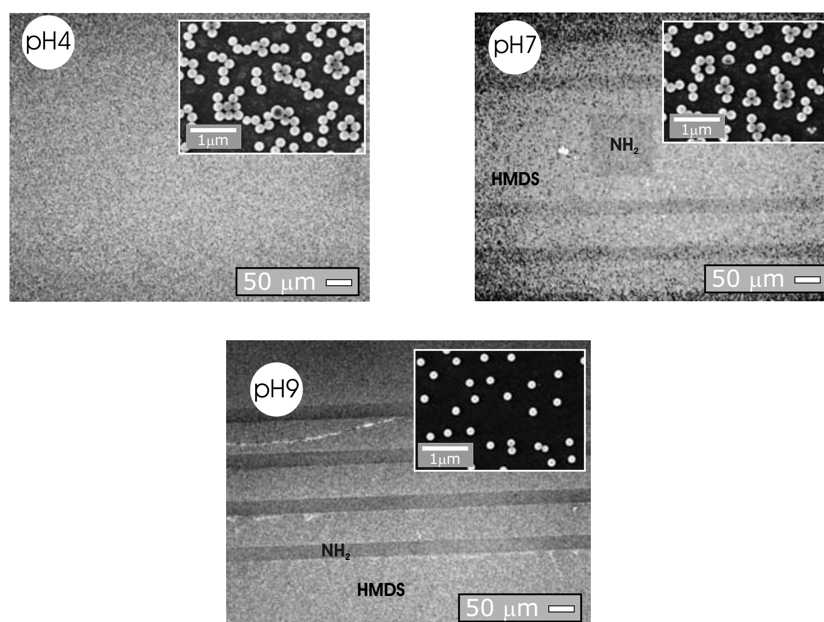

Figure 4.15: *Optical microscope image (DIC) of NH_2/HMDS modified surface with PS-7 particles; smaller picture:SEM image of the particles on the amine layer.*

was lower at pH 7 and 9 than before (Fig. 4.15). This is due to the fact that all SiOH functions are converted into $SiOSi(Me)_3$ group, which do not dissociate at higher pH and therefore do not exert any Coulomb repulsions. The attraction between negatively charged particles and the hydrophobic surface is mainly due to vdW interactions. The particle density on both amine and HMDS layer is rather high, with the number of particles being the same in both regions. Again particle density decreases from pH 4 (ca. 7 particles μm^{-2}) to pH 9 (ca. 1 particle μm^{-2}).

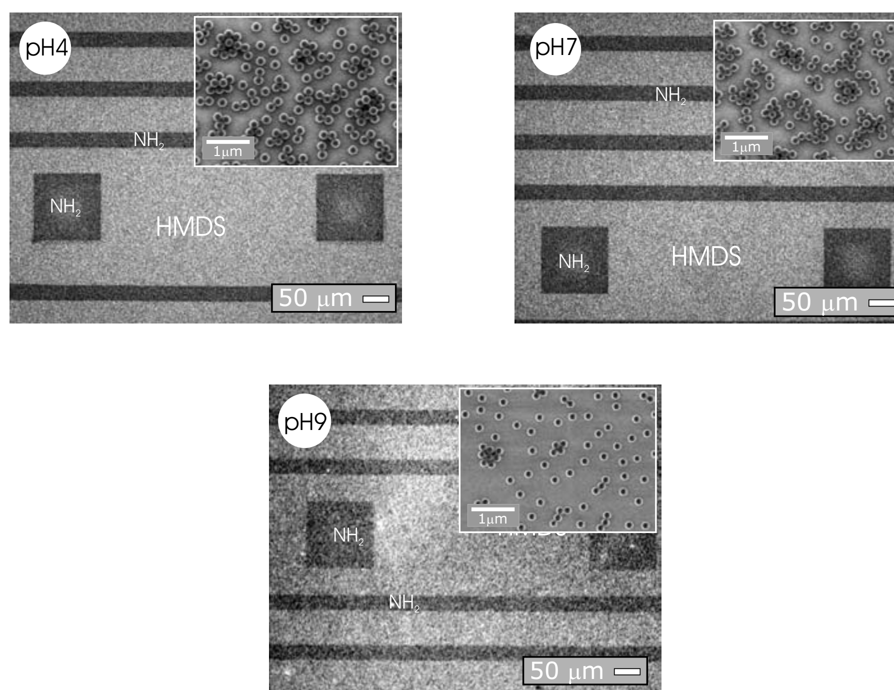

Figure 4.16: *Optical microscope image (DIC) of HMDS/NH_2 modified surface with PS-10 particles; smaller picture: SEM image of the particles on the amine layer.*

When assembling the less charged PS-10 particles on the HMDS/NH_2 modified surface (Fig. 4.16) the adsorption selectivity appears increased compared to PS-7 and is the same at all pHs. The PS-10 particles have mostly adsorbed onto the hydrophobic HMDS region. Due to inter-particle repulsion, particle density decreases on both layers when going from pH 4 (ca. 9 particles μm^{-2} on NH_2 layer) to pH 9 (ca. 4 particles μm^{-2} on NH_2 layer), as can be seen from the SEM pictures. Furthermore, at pH 4 there are more particles on the HMDS region than on the amine layer, whereas at pH 9 the particle number on both regions are roughly the same, as determined by scanning electron microscopy.

The increased selectivity of the less charged PS-10 particles (compared to PS-7) might be due to a stronger dependence of the inter-particle repulsion influenced by the substrate. Thus the

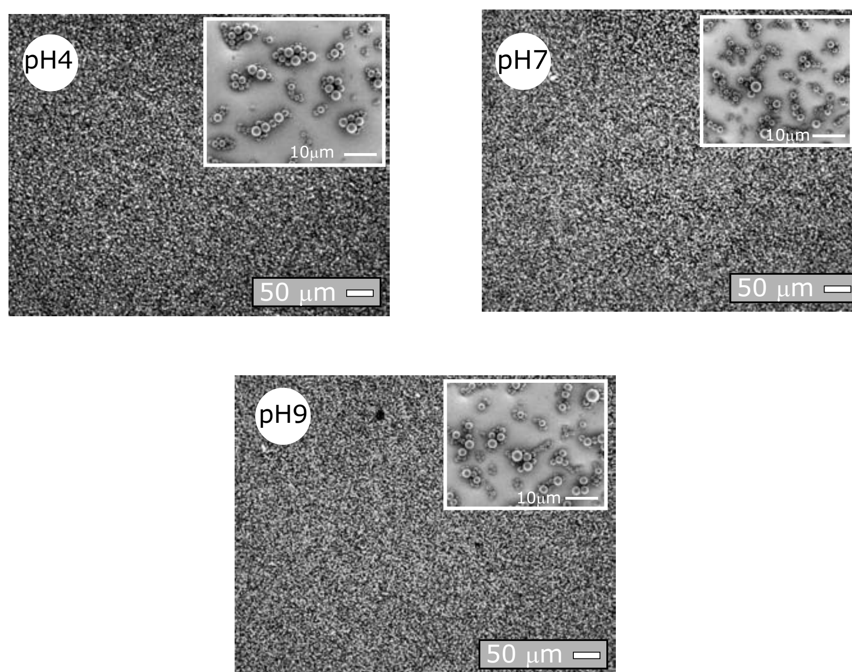

Figure 4.17: *Optical microscope image (DIC) of HMDS/NH_2 modified surface with PS-cellulose particles; smaller picture: SEM image of the particles on the amine layer.*

basic NH_2 surface might lead to a stronger particle charge and a corresponding lower surface density than on HMDS regions. At pH 9 particle selectivity is further reduced because the charge of the particles is fully controlled by the suspending medium and not by the substrate surface.

When uncharged polystyrene-cellulose particles were used for self-assembly on a HMDS/NH_2 modified surface (Fig. 4.17) again no selectivity was visible at any of the pHs. These results are in full accordance with experiments carried of the PS-cellulose particles on NH_2/SiOH surfaces (cf. Fig. 4.14). The SEM pictures show clearly that the nonpolar PS-cell particles have formed aggregates at all pHs, which again leads to a complete coverage of the surface. As with before with NH_2/SiOH patterned surfaces, particle density remains the same at all pHs with 0.1 particles μm^{-2}.

The number of particles on each patterned substrate are summarised in Table 4.1. The particle number densities on the NR_4^+/SiOH and NR_4^+/HMDS patterned surfaces were gratefully provided by Ch.-A. F. (Max Planck Institute for Polymer Research, Mainz).

		PS-7 [98 Å^2 charge^{-1}]	PS-10 [527 Å^2 charge^{-1}]	PS-cell [no charge]
NH_2/SiOH				
	pH 4	7.0	12.3	0.1
	pH 7	5.3 (1.9 on SiOH)	8.9	0.1
	pH 9	1.4 (0.3 on SiOH)	4.2 (0.3 on SiOH)	0.1
NH_2/HMDS				
	pH 4	7.0 (7.1 on HMDS)	9.7 (12 on HMDS)	0.1
	pH 7	5.5 (5.4 on HMDS)	8.1 (8.9 on HMDS)	0.1
	pH 9	1.4 (1.6 on HMDS)	3.6 (3.4 on HMDS)	0.1
NR_4^+/SiOH				
	pH 4	5.4	8.7	/
	pH 7	0.9	1.3	/
	pH 9	0.4	1.5	/
NR_4^+/HMDS				
	pH 4	4.4	8	/
	pH 7	0.7	1.0	/
	pH 9	1.0	1.4	/

Table 4.1: *Number of particles μm^{-2}, calculated from the amino or ammonium layer on the substrate surface.*

4.3 Summary

Colloidal deposition of hydrophobic Aerosil particles in different suspensions showed the best selectivity pattern when adsorbed from an hydrophobic solvent (toluene), as it had been expected. The adsorption experiments with differently charged polystyrene particles have shown that with both higher (PS-7) and lower charged colloidal particles (PS-10) a total coverage of the substrate is obtained at pH 4 on the NH_2/SiOH and NH_2/HMDS surfaces; whereas, a selective contrast is obtained throughout at pH 9. Both particles types show a similar behaviour w.r.t. the particle density on the surface. That is, due to inter-particle repulsion the particle density decreases on all surfaces when going from pH 4 to pH 9, as can be seen from Table 4.1.
The lower charged particles (PS-10) result in higher particle densities compared to PS-7 since less inter-particle repulsions are present. The more the particles are charged on their surfaces (hence the smaller the parking area), the lower is the resulting particle density on the substrate. Table 4.1 also shows that the same trend holds for pH dependant particle assembly on NR_4^+/SiOH and NR_4^+/HMDS surfaces.

When sterically stabilised, uncharged particles (PS-cellulose) were assembled on both

NH_2/SiOH and NH_2/HMDS surfaces, no pH dependence was observed. As a result, particle density was not affected by the pH dependent assembly of the colloidal particles.

Chapter 5

Photo-Reactive Silane for Chemical Patterning

5.1 Introduction

Photochemical transformation of polymers induced by the irradiation of light is of paramount interest from an academic point of view as well as for industrial applications. For example, photoactivated cross-linking experiments of polymers have a major application in photo-resist technology or for curing of surface coatings to protect a metal against corrosion [Suppan 94]. Photoresist technology is a key technology in the structuring and functionalisation of silicon oxide surfaces, as used in the modern microelectronic industry.
Using light as the major tool for chemical transformations on the surface is appealing from a technical point of view since a complex pattern can easily be generated in a parallel fashion.

Light can be used to either degrade a compound on the surface or to activate certain groups by UV irradiation [DePuy 77]. For instance, amphiphilic titanium dioxide surfaces are photogenerated by ultraviolet irradiation to produces TiO_2 surfaces that are antifogging [Wang 97, Machida 99]. Activation of chemical compounds by light was also used by Fodor and co-workers to spatially direct the simultaneous synthesis of peptides on a surface. They demonstrated in 1991 that photo-protected amine groups (*e.g.* amino acids) could be activated by irradiating the layer through a mask, thereby removing the photolabile protecting group on the regions that had been addressed by the light [Fodor 91]. The free amine groups can then couple with another photo-protected amino acid and irradiation through a second mask will activate other regions on the substrate bearing a different chemistry, thus generating different building blocks on the surface. In the same year Calvert and co-workers showed that organosilane layers on silicon surfaces bearing a native oxide layer could be cleaved with high energy deep UV light, rendering the surface amenable to further SAM

modification or even mammalian cell adhesion and growth [Dulcey 91, Brandow 99]. Tarlov *et.al.* demonstrated that it was possible to degrade only specific anchor groups on the surface by photo-conversion, such as alkyl thiol layers, where the thiol anchor is converted into the corresponding sulphonate that binds much weaker to the gold substrate and can therefore be displaced by a second thiol [Tarlov 93].
The advantage of using only light for creation of a chemical pattern is not only the cheap nature of this reagent but also no additional reagents (*i.e.* solvents) are required thus generating less chemical waste. Furthermore, the absence of solvents makes this technique suitable for very sensitive functionalities.
Light directed chemical patterning has so far found many applications in medicinal-biological areas, such as addressable use of photo-chelators that release Ca^{2+} upon illumination. It is thus possible to study the kinetics of Ca^{2+} regulation of troponin hormone in skeletal muscle [Adams 89]. Especially in the modern microelectronic industries the use of semiconducting and metallic nano-particles is advancing rapidly. Vossmeyer *et. al.* have developed a process for generating complex, spatially separated patterns of multiple types of these nano-particles by using lithographic patterning of organic monolayers that contain a photolabile groups and are covalently bound to the SiO_2 surface [Vossmeyer 98]. Jonas and co-workers demonstrated a further expansion of this concept towards the control of mesoscale assembly by showing regioselective colloid assembly after direct monopatterning with light [Jonas 02a]. Moreover, light directed synthesis of DNA arrays has emerged as a powerful tool for parallel hybridisation-based analysis of DNA and RNA sequences and provides a versatile probe method for microfabricating probe arrays with densities of 1,000,000 unique sequences per cm^2 [McGall 96]. Patterning proteins, cells and oligonucleotides on a surface has become a versatile tool for high throughput screening (HTPS) of microarrays in the field of medicinal or molecular biology, which allows investigation of for example, associate cellular dysfunctions, diseases or even the human genome.

The general procedure to introduce photosensitive moieties onto a substrate involves first the modification of a surface with organic groups, which then react in a second step with the photosensitive units. Since all of the chemistry occurs at the surface the disadvantage of this approach lies in the limited control over the reaction yield, layer composition and analysis of the product. Nevertheless, many scientist have used this technique in the past for postmodification of functionalised gold or silica surfaces [Vossmeyer 97, Stenger 92, Elender 96].
The approach taken in this thesis is based on a surface modification process that uses functionalised alkoxysilanes, carrying photolabile protecting groups. These silanes are synthesised prior to deposition onto the surface. The advantage of synthesising a silane that directly incorporates a photoprotecting group versus postmodification of a surface lies in the simple preparation of a well defined structure and the possibility to prepare mixed monolayers depending on the photoreactive groups present. Furthermore, the photoreactive silane can be fully characterised by NMR, mass spectrometry, etc. prior to deposition, a

feature which is not possible after postmodification of a surface. After silane deposition on the surface, the pattern can be achieved in the same way as in conventional photolithography, namely by irradiation through a mask. Together with the sequence of reactants they define the final products and their location. Surface modification is not limited to silica surfaces but can be applied to other oxide surfaces, such as TiO_2, Fe_3O_4 or ZrO_2.

The above mentioned strategies are all based on the introduction of functional groups after selective removal of surface-bound photoprotecting groups by light. An alternative strategy for the generation of chemical lateral patterns on a surface involves the direct activation of the photoreactive surface layer. Thereby a pattern is generated of reactive and non-reactive regions. This pattern can subsequently be used to covalently attach other molecules or objects to selected positions (the irradiated ones) on the surface.
Aryl azides are a particular example of photoreactive groups, which have been extensively used due to their acceptable chemical stability in the dark and their photochemical fragmentation into reactive nitrene and the inert N_2 gas. This group has already been used in the literature for "photoaffinity labelling", where antibodies are chemically immobilised to the antigen binding site by irradiation of bound azide groups [Kotzyba-Hilbe 95].

The aim of this chapter is to combine the photochemical reactivity of an aryl azide with the site-selective assembly of colloidal polymer particles on laterally patterned silane layers. Therefore an alkoxysilane was synthesised bearing an aryl azide head group that could be transformed into the highly reactive nitrene upon irradiation. This activated group could then insert into any C-H or heteroatom-H bond, thus creating a covalent bond between the silane and the species of insertion, *i.e.* polymer particles.
This chapter will cover the synthetic details, as well as the characterisation methods used in order to optimise the surface modification of silicon or quartz wafers: kinetic experiments for tailoring the hydrolysis conditions, dynamic light scattering for investigating the silane behaviour in solution, and kinetic UV measurements for optimising the irradiation time. The experimental details are then described and finally summarised.

5.2 Azides and Nitrenes

The requirements for a photochemical patterning reagent are first, chemical stability in the dark and in the presence of water (since the polymer colloids to be assembled are present in an aqueous solution) and second, the absorbance of light at a suitable wavelength. If proteins or nucleic acids, which absorb below 300 nm, were to be attached, the ideal λ_{max} of the reagent should be above 300 nm. The reagent should have a high extinction coefficient and a high quantum yield, ϕ, so that the photolysis would occur much faster than the rate at which the sample is damaged. Ideally, the intermediates formed upon photolysis should be highly

reactive and therefore short-lived.

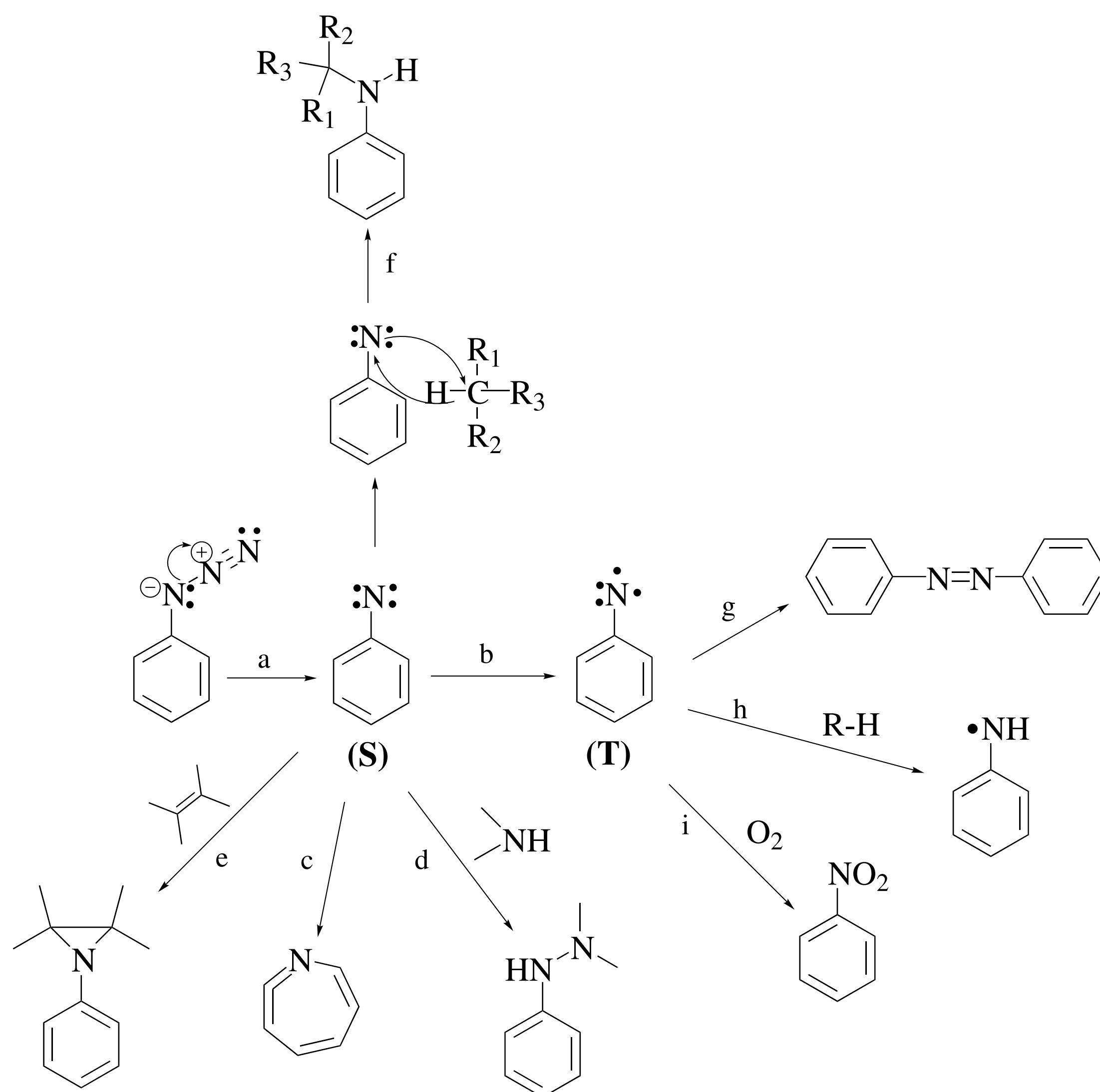

Figure 5.1: *Photochemistry of aryl azides; a) conversion of aryl azide to singlet nitrene, which can then add directly to a double bond (e), or form cycloheptatetraene by incorporation of the nitrogen into the ring (c); they can be attacked by amines, especially when generated using long wavelength light (d), or they can insert into C-H bonds* via *an intermolecular reaction (f); singlet nitrenes can also undergo irreversible intersystem crossing to a triplet (b), which then dimerises to give an azo compound (g), it can abstract another hydrogen to form an amine radical (h) or it can be oxidised to a nitro compound (i) [Bayley 84].*

Upon photolysis (Fig. 5.1), the aryl azide is converted into a highly reactive nitrene, which only possesses 6 electrons in its outer shell and therefore undergoes rapid transformation

in order to complete its valence shell. Nitrenes are the nitrogen analogues of carbenes and undergo similar reactions: upon irradiation, the azide is converted into a singlet nitrene. The nitrene will either form electrophiles by rearrangement (*e.g.* cycloheptatetraene analogues), which can then be attacked by a nucleophile (*e.g.* R_2NH or RSH) or it will undergo an indirect insertion reaction with a carbon-hydrogen bond by addition and rearrangement. Reactions with nucleophiles are very common and largely occur *via* the electrophilic species that are generated by rearrangement of the singlet nitrene. The singlet nitrene can also undergo an intersystem crossing (ISC) from its excited state to its ground state to form a triplet nitrene, which is generally less reactive. Triplet nitrenes can form dimers (azo compounds), react with oxygen to form nitro compounds or can also undergo insertion reactions with a C-H bond by hydrogen abstraction and radical recombination [Smith 84].

The irradiation of the azides can be monitored by the change or disappearance of the chromophores present. Phenyl azide, for example, shows an intense absorption band in the UV/Vis spectrum near 250 nm and a weaker band at 280-290 nm, which is assigned to the π-π^* transition [Reiser 71]. Another absorption band is visible at 330 nm and assigned to the n-π^* transition. Since nitrenes themselves are very reactive at room temperature (lifetime $\sim 10^{-4}$ s) they can only be kept and studied at liquid-nitrogen temperatures (77 K) [Smirnov 82].

5.3 Synthetic Approach

The synthesis of an aromatic azide silane, having the azide group as the head group and a silane group for anchoring onto the silicon surface, was proposed. Therefore, a precursor bearing two functional groups was required, that could be converted into an azide and a carboxyl group, which was needed for further coupling to the silica surface. The introduction of an additional nitro group on the aromatic ring allows photoactivation at 320-360 nm and increases the reactivity of the photogenerated aryl nitrene [Lewis 77].

The starting material was chosen to be 2-cyano-4-nitroaniline, where the nitrile group was to be converted into the carboxylate by refluxing in strong basic medium (Fig. 5.2). Upon acidification with sulfuric acid, the desired product **2** was obtained in a 60% yield. Thin layer chromatography gave the characteristic streak and ^{1}H and ^{13}C NMR confirmed the existence and purity of **2**.
The next step was to convert the amine group into an azide group using HCl and sodium nitrite to generate the nitrosyl cation NO^+, which reacts with the amine group to give a diazonium salt. Addition of sodium azide to the solution affords the aromatic azide **3**. Even though the reaction procedure was straightforward, the desired product was not obtained. The

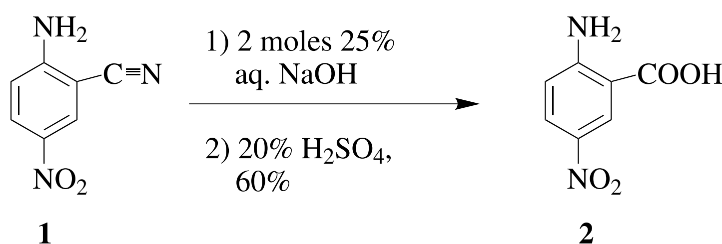

Figure 5.2: *Conversion of 2-cyano-4-nitroaniline **1** to 2-amino-5-nitrobenzoic acid **2**.*

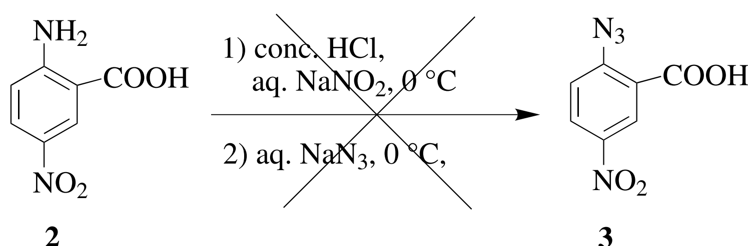

Figure 5.3: *Attempted conversion of 2-amino-5-nitrobenzoic-acid (2) to 2-azido-5-nitrobenzoic acid (3).*

molar percentage of $NaNO_2$ was therefore increased and the reaction mixture was allowed to stir for 3 h instead of 1 h before the cold NaN_3 was added. After 6 additional hours of reaction the product was not obtained.
Besides steric reasons, hydrogen bonding between the amino group and the carboxylic acid in the *ortho* position may be responsible for the lack of reactivity. Hence, the amine could not attack the nitrosyl group in order to generate the intermediate diazonium salt. Maybe this problem could be overcome by converting the amine first into the azide and then subsequently hydrolyse the nitrile group.

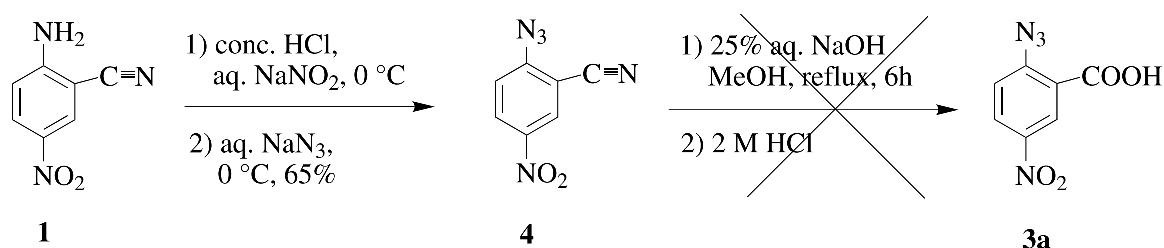

Figure 5.4: *Conversion of 2-cyano-4-nitroaniline **1** to 2-azido-5-nitrobenzonitrile **4**, and further attempted conversion to 2-azido-5-nitrobenzoic acid **3a**.*

By doing so, the crude 2-azido-5-nitrobenzonitrile **4** was obtained and reactants and products were separated by passing through a plug of silica using dichloromethane/acetone (1:1) as eluent. Thus, the reactants were adsorbed onto the silica gel and the product was present in the filtrate. ^{1}H and ^{13}C NMR and IR spectroscopy showed the characteristic peaks and absorption bands of the product, which was obtained in a 65% yield.

The next step was the hydrolysis of the nitrile group (Fig.5.4) to give **3a**. However, the reaction yielded too many side products (as visible on the TLC plate) and the pure product could not be isolated. The influence of heat might have been a possible reason but also the *ortho* position of the nitrile group to the azide. Thus, the nitrile and the azide groups might have undergone [3+2] cycloaddition to form a tetrazole.

An alternative isomer strategy was devised by changing the location of the carboxy groups using 5-amino-2-nitrobenzoic acid, **5**. The conversion to the azide with HCl, $NaNO_2$, and NaN_3 afforded product **6** in 82% yield and IR spectroscopy showed the characteristic azide absorption at 2100 cm^{-1}. No further purification was necessary and the next step was

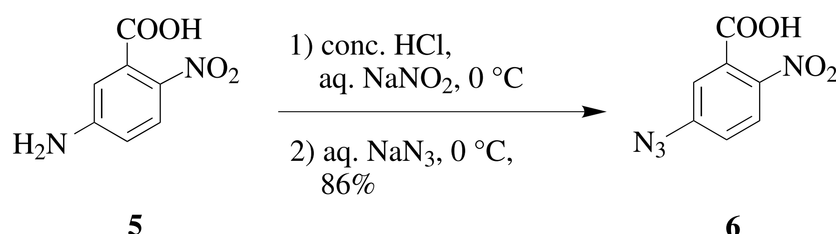

Figure 5.5: *Conversion of 5-amino-2-nitrobenzoic acid* ***5*** *to 5-azido-2-nitrobenzoic acid* ***6.***

to convert **6** into an allyl-benzamide **10** using allylamine in the presence of DCC and DMAP (Fig. 5.6). The allyl group would then be hydrosilylated with triethoxy silane. However, when carrying out the reaction with allylamine, DCC, and DMAP at 0 °C, too many side products formed and after column chromatography the yield was very low. The reaction was therefore repeated using N-hydroxysuccinimide first to activate the carboxylic acid **9** and then add allylamine in order to form the amide bond. Flash column chromatography afforded the product **9** in a 88% yield. Conversion to the benzamide with allyl amine in acetonitrile and THF gave the desired product **10** in 96% yield.

Hydrosilylation was then carried out using $HSi(OEt)_3$ and hexachloroplatinic acid as the catalyst. Hydrosilylation itself occurs *via* a heterolytic mechanism where the unsaturated olefin is coordinated to the Pt-metal center. Oxidative addition of the olefin to the metal center and insertion of the ligand into M-H bond is followed by reductive elimination of the product and the regeneration of the catalyst. H_2PtCl_6 in *i*-PrOH is a homogeneous catalyst, called Speier's catalyst that is reactive enough to forgo the need for any co-catalyst to enhance

its activity. The hydrosilylation reaction did not take place after 8 h reaction time, as visible from the reactant's double bond in the ^{1}H NMR. Further additional catalyst or longer reaction times did not lead to the product, but resulted in the polymerisation of **10** and in the complete saturation of the double bond. Even after column chromatography of the crude, compound **9** still showed some impurities in the ^{1}H NMR spectrum that could not be removed completely. Catalyst contamination with these impurities might be the reason why hydrosilylation did not work. However, the azide might not be compatible with the harsh reaction conditions, either.

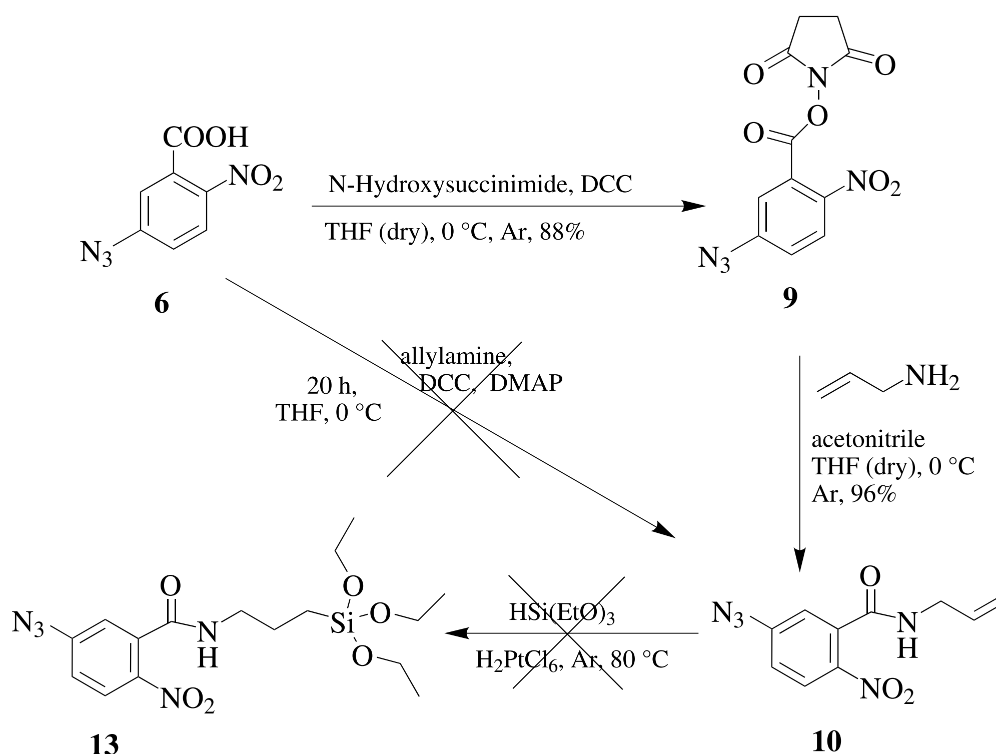

Figure 5.6: *Activation of the carboxy group of 5-azido-2-nitrobenzoic acid **6** to N-Hydroxylsuccinimidyl-5-azido-2-nitrobenzoate **9**. This is further reacted with allylamine to form the amide **10**, which can be hydrosilylated using triethoxysilane in the presence of Speier's catalyst to give (5-azido-2-nitrobenzyl)-triethoxysilylpropylbenzamide **ANTSP**.*

A new synthetic strategy was found, starting from aminopropyltriethoxysilane (APTS). NHS-activated benzoic acid **6** was reacted with APTS at room temperature for 24 h and after filtration of the precipitated N-hydroxysuccinimide and removal of excess APTS under vacuum, the crude product was purified on a passivated silica gel column to afford **13** in a 46 % yield Fig. 5.7.

Purification of alkoxysilanes using passivated silica gel is a strategy which was elabo-

rated by del Campo and co-workers. It allows the chromatography of alkoxysilanes on conventional silica gel supports without loosing a significant amount of the product due to its reaction with the Si-OH groups of the silica gel [del Campo c]. For this purpose, the silica gel was first reacted with hexamethyldisilazane (HMDS) to partly convert the most reactive hydroxyl groups of the silica gel into hydrophobic methyl groups. After packing, the column was completely washed with the pure eluent in order to remove any excess HMDS before adding the crude compound for separation. It was possible to obtain 46% of the product **13**, namely (5-azido-2-nitrobenzyl)-triethoxysilylpropylbenzamide (**ANTSP**). ^{1}H NMR showed the characteristic methylene peaks of the propyl chain in α, β, and γ positions w.r.t. the silicon. IR measurements confirmed the success of the reaction and showed the azide peak absorption at around 2100 cm^{-1}.

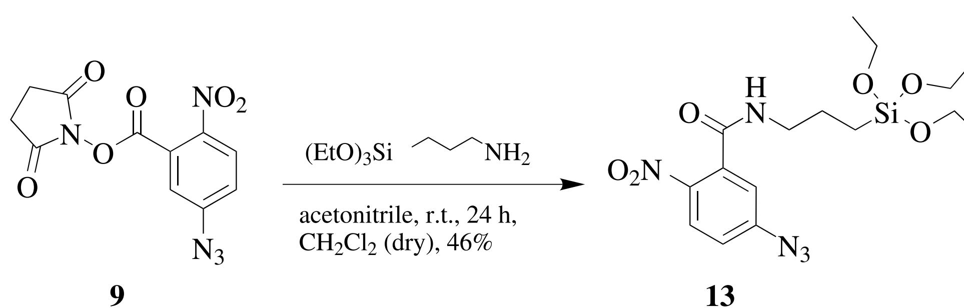

Figure 5.7: *Conversion of 5-azido-2-nitrobenzoic acid **6** to ANTSP **13** using aminopropyltriethoxysilane (APTS).*

5.4 Surface Modification and Characterisation

In order to anchor ANTSP to the silanol groups on the silica surface, its alkoxy groups had to be hydrolysed in solution to the more reactive silanol species that can bind covalently to the silica surface. In order to investigate the kinetics of hydrolysis, ^{1}H NMR spectra of the solution were recorded at different reaction times. Since hydrolysis results in the formation of three hydroxyl groups attached to the silicon atom and 3 molar equivalents of ethanol, the decrease of the ethoxy methyl and methylene groups and the increase of the ethanol methyl and methylene groups in the ^{1}H NMR can be used to quantitatively follow the process (Fig. 5.8b). The reactions of alkoxy silanes with the surface and the condensation of the silanols in solution are competing processes when triethoxysilanes are used [Ishida 84]. To find the optimum reaction conditions for obtaining a smooth surface layer, contact angle measurements were used to monitor the quality of the final surface after surface modification in different conditions.

5.4.1 Kinetic Experiments

The ^{1}H NMR kinetic experiments for the hydrolysis in solution were carried out using a 1 % solution of ANTSP in THF with water or aq. NaOH solution as the catalyst. When only water was used, no hydrolysis was visible in the ^{1}H NMR over a period of 2 days. When a catalytic amount of 0.1 M NaOH was added, after 100 min more ethanol was present in the mixture than ethoxy groups and after around 450 min nearly all ethoxy groups had been hydrolysed (Fig. 5.8c). Condensation of the silanols in solution is present, as visible from the formation of a broad peak (δ ca. 0.7 ppm) in the spectrum. This corresponds to the Si-CH_2 groups of the condensate at long hydrolysis times.

5.4.2 Silane Deposition on Silica Surfaces

Chemisorption on silica surfaces occurs when the silicon or quartz wafers are immersed into the hydrolysed silane solution. The optimum time for the surface reaction can be monitored by placing the silicon-wafers into the hydrolysing solution at different hydrolysis times and measuring the contact angle of the resulting layers. The contact angle increases with time from ca. 10° (which is the contact angle of the pure silica surface) to a steady value of ca. 70° after 30 min of hydrolysis (Fig. 5.9). An increase in the contact angle indicates increasing hydrophobicity of the surface as a consequence of the surface modification with the silane. When the contact angle remains constant, monolayer formation is completed, possibly followed by multilayer formation after longer adsorption times. A contact angle value of ca. 70° is in accordance with measurements carried out in the group of J. M. Calvert [Dulcey 91], where benzyltrichlorosilane layers on silicon surfaces showed a static contact angle between 65° and 74°.

The surface roughness of deposited ANTSP on the silica surface was further investigated with atomic force microscopy. To carry out the measurements, two silane solutions in THF were hydrolysed for 30 minutes using water and base as catalysts. AFM[1] measurements revealed rather than a smooth surface, a bulky surface with deformed spherical objects with an average size of 230 nm in diameter and 18 nm in height. (Fig.5.10).
Since no hydrolysis was visible in the solution ^{1}H NMR spectrum with d-$_{8}$THF, the spheres cannot be due to pre-polymer formation. They can be due to micelle formation of the trialkoxysilanes on the silicon-wafers. In addition, the added water can act as a nucleation center for clustering of micelles, which results in the formation of larger spheres.

When the silane deposition was carried out in the presence of a catalytic amount of

[1]AFM measurements were generously provided by A.-S. D. and R. B., Max Planck Institute for Polymer Research, Mainz, Germany

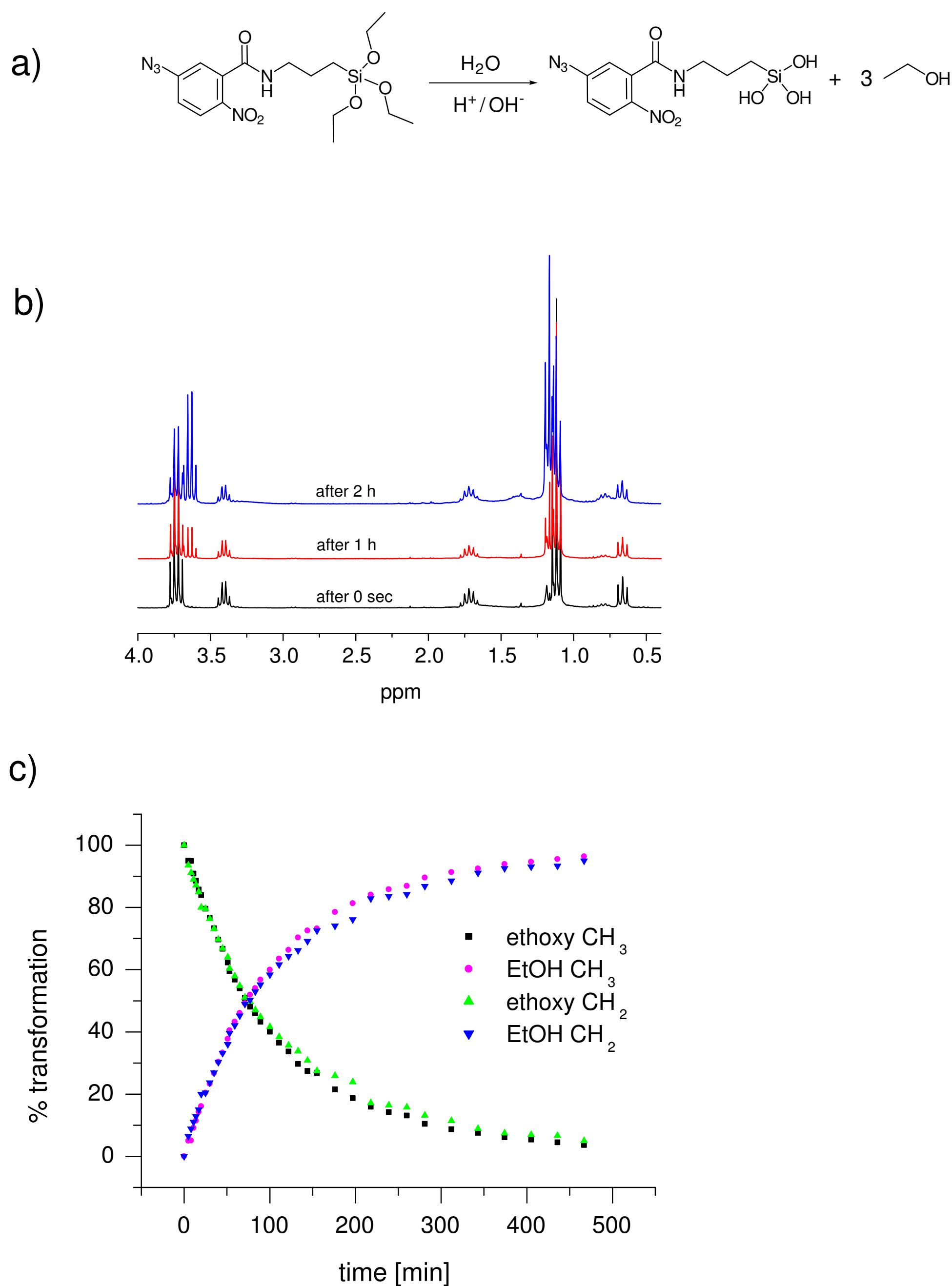

Figure 5.8: *a) Reaction scheme of the hydrolysis of **13** in presence of catalytic amount of acid or base b) ^{1}H NMR of **13** showing the decrease of ethoxy CH_2/CH_3 and increase of ethanol CH_2/CH_3 c) kinetic curve showing the % transformation of hydrolysed ethoxy groups and resulting ethanol molecules.*

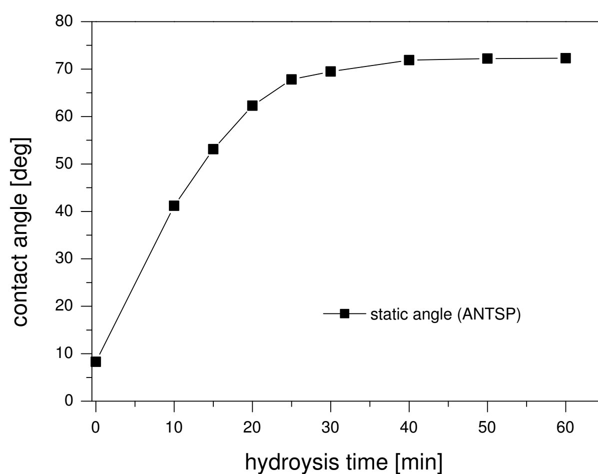

Figure 5.9: *Increase of hydrophobicity as a function of time and visible as increase of contact angle.*

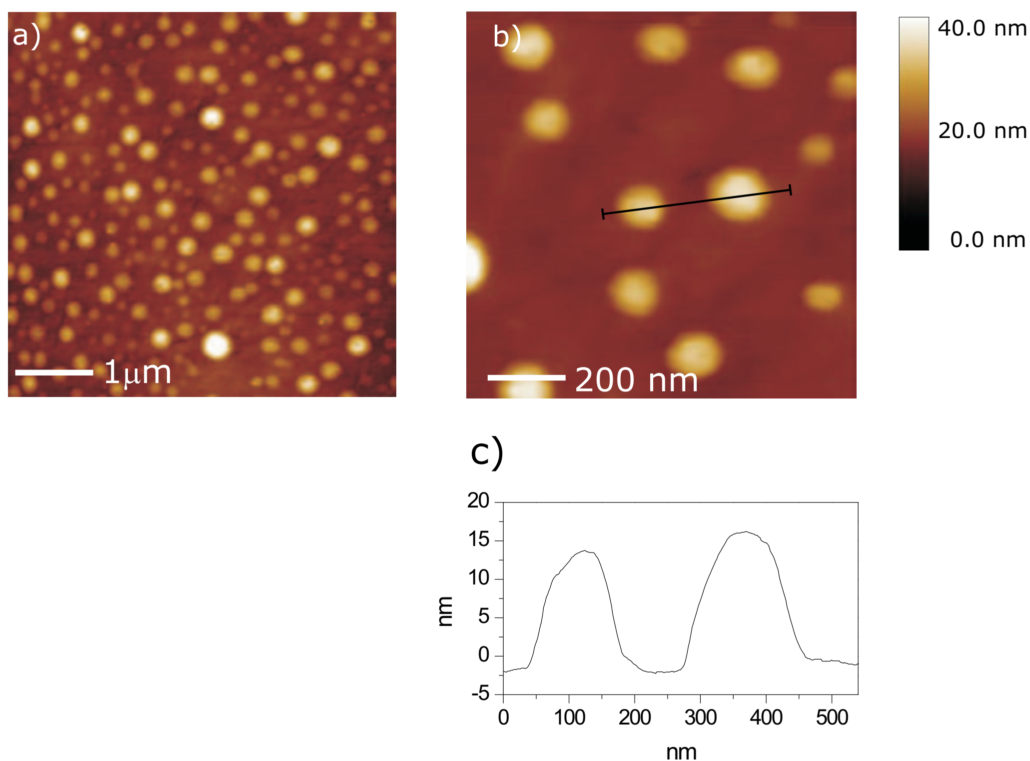

Figure 5.10: *AFM images (contact mode): silica surface with ANTSP after hydrolysis with water and silane deposition for 1 h; a) large scan, b) enlargement, c) cross-section analysis.*

NaOH, the same bulky spheres were visible, but this time even larger and with a more evolved internal structure (Fig.5.11). The average diameter was ca. 400 nm (compared to 40 nm

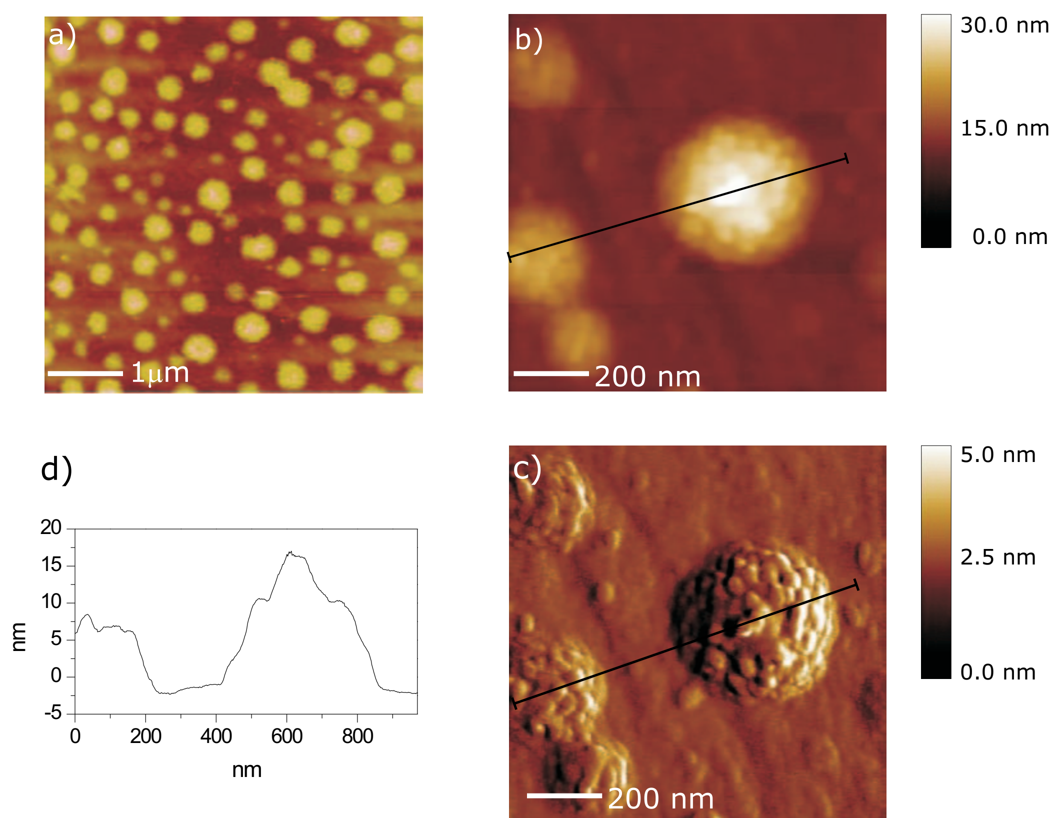

Figure 5.11: *AFM images (contact mode): silica surface with ANTSP after hydrolysation with water and NaOH after silane deposition for 1 h; a) large scan, b) enlargement, c) deflection image of enlargement, d) cross-section analysis.*

diameter without water) and the height was ca. 17 nm.

It is assumed that the smaller spheres are micelles of ANTSP molecules, which can then in turn form micellar clusters by further aggregation. When NaOH is present in the solution mixture, ANTSP is hydrolysed (Fig. 5.8) and can form condensates. This can result in pre-polymer and/or in micelle formation, depending on the amount of hydroxyl groups present. A schematic representation of the micelle and cluster formation in solution is shown in Fig. 5.12.

The deposition experiment was therefore repeated without the addition of water to the silane solution in dry THF and analysed by AFM. Without the presence of water in the hydrolysate, the size of the clusters is reduced by a factor of ca. 6 and only small aggregates are present with an average diameter of 30 nm (Fig. 5.13). It can further be concluded that water mediates the micelle clustering. When no water is present in the solution, only micelles are formed but no clusters.

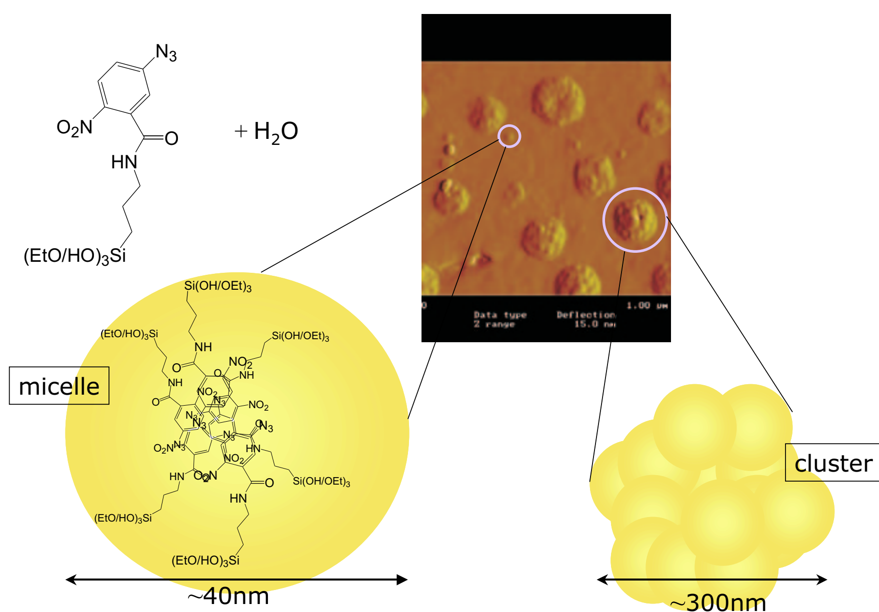

Figure 5.12: *Schematic representation of micelle formation and micelle clustering occurring in a THF solution mixture in presence of water.*

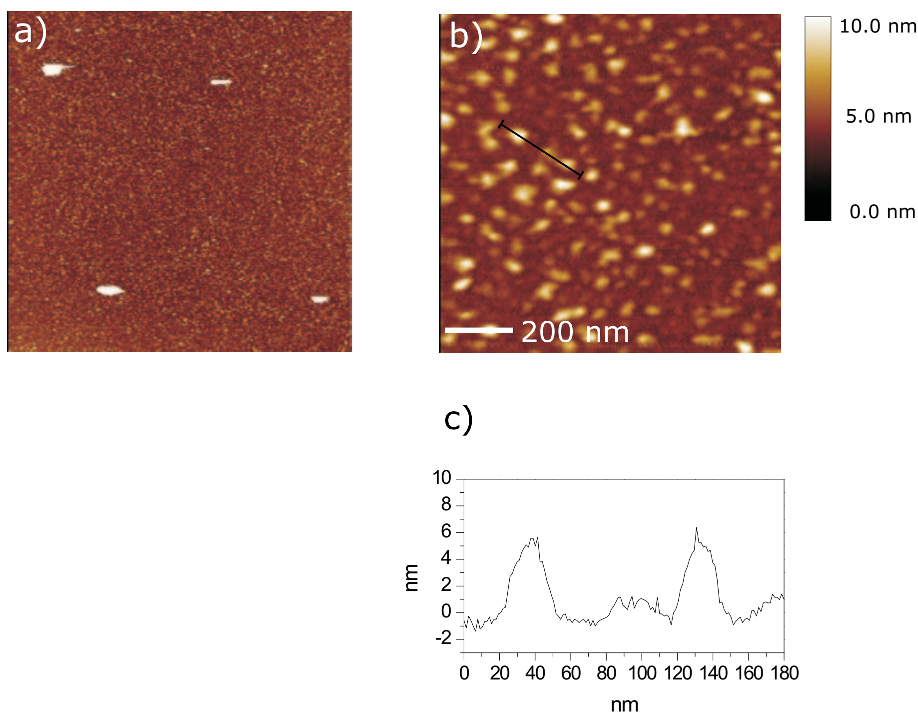

Figure 5.13: *AFM images (tapping mode): silica surface with ANTSP after hydrolysis without water and silane deposition for 1 h; a) large scan, b) enlargement, c) cross-section analysis.*

5.4.3 Dynamic Light Scattering

5.4.3.1 Sample Preparation and Experiments

In order to investigate further the influence of water present in the silane/THF solution, dynamic light scattering[2] experiments were carried out in the following solutions:

a) 5 ml 0.02 M ANTSP in stabilised[3] THF
b) 5 ml 0.02 M ANTSP in dry THF (HPLC grade)
c) 5 ml 0.02 M ANTSP in stabilised THF with 20 μl H_2O
d) 5 ml 0.02 M ANTSP in stabilised THF, where more water was added gradually over time
e) 5 ml 0.02 M ANTSP in stabilised THF with 20 μl H_2O and 10 μl 1N NaOH

In order to minimise the presence of dust particles, the solutions were filtered through a 0.2 μm PTFE filter into an acetone washed cuvette prior to the measurement. The hydrodynamic radii were then recorded from the autocorrelation function of the light scattering experiments.

Solution a) was examined with dynamic light scattering at different angles (Fig. 5.14). Two types of aggregations are present in the solution, with an average radius of 70 nm and 2.5 nm. These values are in correlation with the AFM measurements carried out in Fig.5.13, where 0.02 M ANTSP in THF (without water) was deposited on a silica surface. Time dependant DLS was then carried out with an ANTSP solution in dry THF (solution b), where the hydrodynamic radii were recorded over a time span of 8 h. 15 minutes after preparing the solution the particles present possess an average radius of 70 nm, which then decreases over time so that after 6 h, the particles show an average radius of 60 nm (Fig. 5.15). Again, these fluctuations lie in the same range of hydrodynamic radii as obtained from AFM measurements with stabilised THF (Fig. 5.13). The radii correspond to small micelle aggregates of hydrolysed ANTSP. It is also visible that no hydrodynamic radii were present corresponding to clusters with a size of 100-200 nm radius, as were detected by AFM in a THF-water solution.

When the same experiment was carried out with 20 μl of water present in the 5 ml ANTSP-THF solution (solution c) larger particle sizes were detected than without water (Fig.5.16). It is noticeable that two sizes of particles are present, just as with the stabilised ANTSP-THF solution. The hydrodynamic radii obtained correspond roughly to the average diameters of the bulky spheres detected by AFM (cf. Fig. 5.10), thus verifying the initial concept that upon

[2]All DLS measurements were generously carried out by B. M., Max Planck Institute for Polymer Research, Mainz, Germany

[3]THF was stabilised using di(tert)-butylmethylphenol

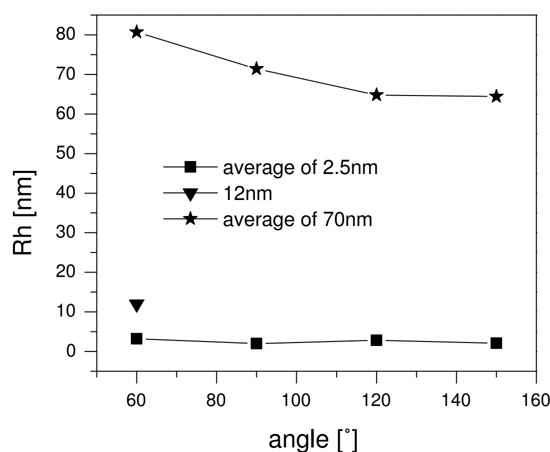

Figure 5.14: *Angle dependant hydrodynamic radii calculated from dynamic light scattering of ANTSP solution in THF.*

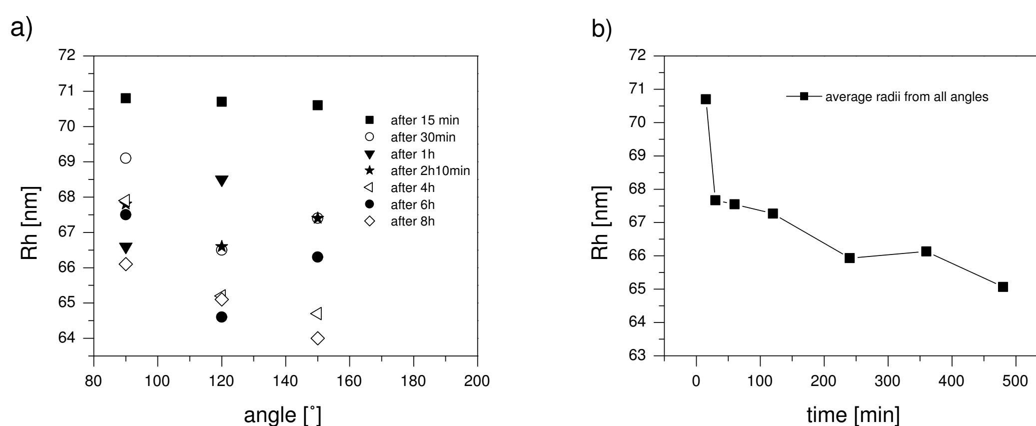

Figure 5.15: *Dynamic light scattering of ANTSP solution in HPLC grade THF a) angle dependant hydrodynamic radii (Rh) measured over time and b) time dependant average Rh of all angles.*

addition of water to the silane-THF solution, the ethoxysilane forms bigger aggregates than without water. The hydrodynamic radii for the larger particles ca. 85 nm and the smaller particles ca. 7 nm also seemed to increase slightly with time due to micelle growth. Since the ANTSP deposition onto the SiO_2 surface in presence of water did not take longer than 2 h, no further light scattering experiment were carried out after 4 h.

Dynamic light scattering experiments were carried out with solution d), where water was added gradually to the 5 ml ANTSP-THF solution (Fig. 5.17). The solution was first analysed without the presence of water, then 10 μl of Milli-Q water were added and then another 50 μl of Milli-Q water (Fig.5.17a). This final solution was then left to stand for 6 d and

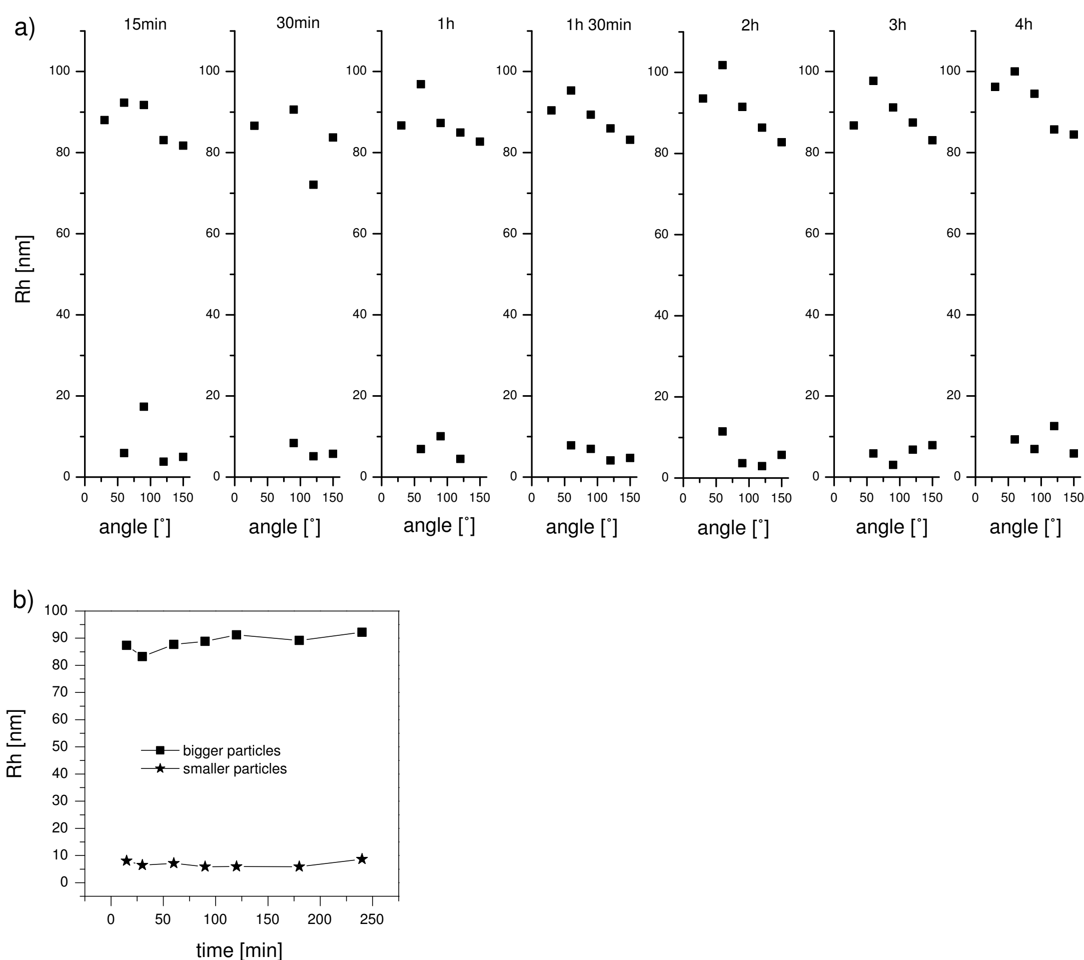

Figure 5.16: *Dynamic light scattering of ANTSP solution in THF plus 0.4% water a) angle dependant hydrodynamic radii (Rh) measured over time, b) time dependent average Rh of all angles.*

was then measured again with DLS (Fig.5.17b). Upon addition of water, the hydrodynamic radii of the particles increased slightly after decreasing first when 10 μl of water were added to the 0.02 M solution. The average radii stayed the same when the sample was analysed again after 6 d. It can therefore be concluded that the addition of water to the silane-THF solution does not lead to the formation of large micelle clusters with radii of around 150 nm. Instead smaller micelle aggregates are formed that are in good accordance with the AFM images (Fig.5.10). In a first approximation, the clusters visible by AFM are aggregated micelles. They appear globular in solution; whereas, they are more flattened out on the silica surface. Therefore particle sizes obtained from AFM and DLS cannot be directly correlated. This is due to the fact that AFM measurements are merely topographic whereas more parameters have to be considered in dynamic light scattering (*i.e.* local refractive index changes).

To confirm the formation of large micelle clusters as visible with AFM (Fig.5.11),

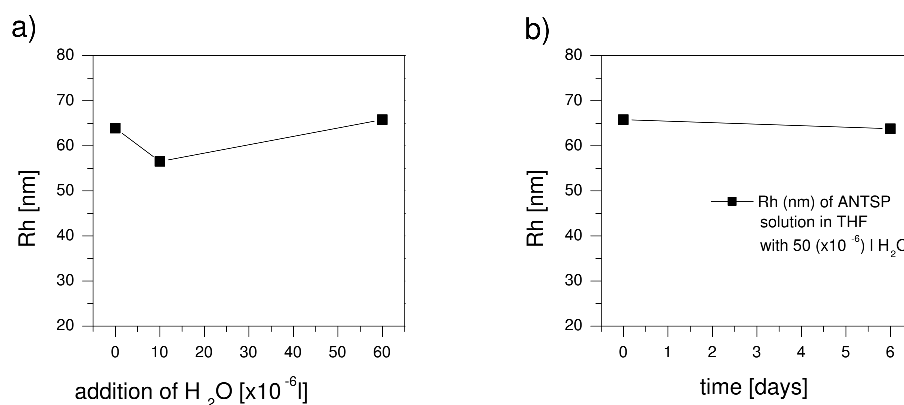

Figure 5.17: *Dynamic light scattering of 0.02 M ANTSP solution in stabilised THF (plus 20 μl H_2O) a) hydrodynamic radii (Rh) measured when water was added gradually, b) Rh of ANTSP solution with 50 μl H_2O, measured over time*

DLS experiments were carried out with a 5 ml ANTSP solution to which water (20 μl) and 1 N NaOH (10 μl) were added (solution e). The hydrodynamic radii of the particles in the

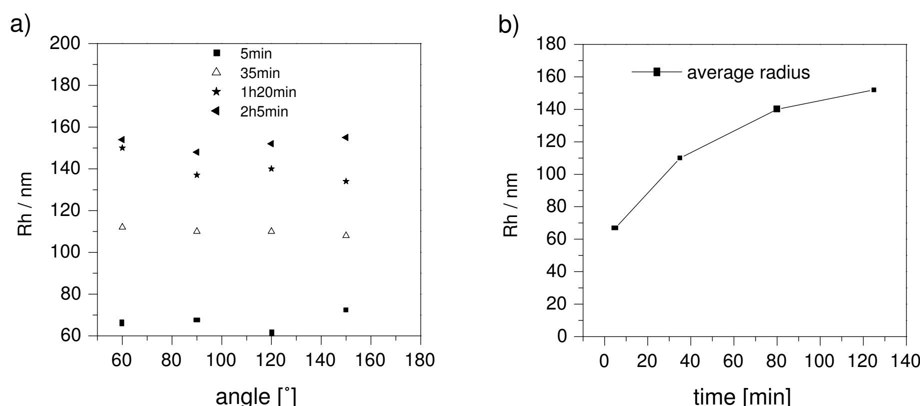

Figure 5.18: *Dynamic light scattering of 0.02 M ANTSP solution in THF (plus 20 μl H_2O and 10 μl 1 N NaOH) a) angle dependent hydrodynamic radii (Rh) measured over time, b) time dependant average Rh of all angles.*

solution increase rapidly upon addition of 1N NaOH, so that after 2 hours the average radii are around 160 nm (Fig. 5.18). This result is also in accordance with the AFM measurements (Fig. 5.11) and with the kinetic experiment (Fig. 5.8), which confirm fast hydrolysis due to NaOH, and thus the formation of micellar clusters with radii of ca. 160 nm and more. In addition, NaOH has a miscibility problem with THF, particularly in the presence of alkoxysilanes. The effect this might have on the deposition process has not been fully understood, but has also been observed by others [del Campo b].

5.4.4 UV Irradiation

Since the ANTSP molecule bears chromophores, its deposition to the surface can be monitored by UV spectroscopy of the substrates. Irradiation removes the chromophore from the surface, and the extent of the cleavage can be analysed by comparing the intensity of the UV spectra recorded before and after irradiation and washing. Pure phenyl azide absorbs in the near ultraviolet region with a λ_{max} around 280 nm. ANTSP exhibits a strong absorption band with λ_{max} around 320 nm that arises from the nitro group in the *para* position and from the amide present in the molecule (Fig. 5.19). The quartz UV spectra show that the local maxi-

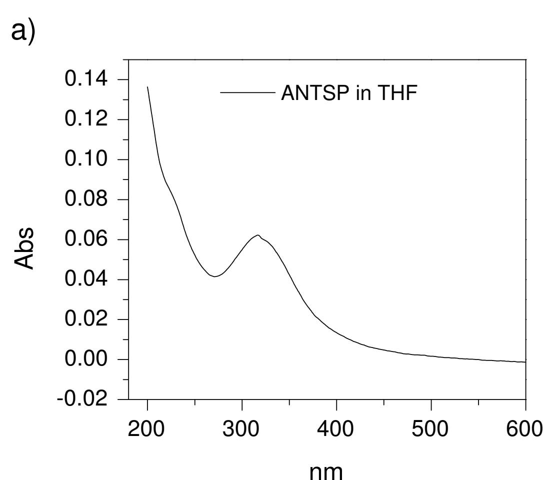

Figure 5.19: *UV spectra of ANTSP on quartz with hydrolysis carried out as 1% ANTSP solution in THF, using NaOH as catalyst.*

mum occurs at ca. 320nm, which is in good accordance with the solution spectrum of ANTSP. An absorbance of ca. 0.06 is a rather high value for a single self-assembled monolayer. In fact, it is common to obtain smaller absorbance values for SAMs (0.001-0.002) so that the absorbance measured in Fig.5.19 hints to a dense surface layer with 3-D aggregates or multilayers. In addition, an average layer thickness of 1.6 nm was measured by ellipsometry (averaging over a macroscopic area). This indicates multilayer formation or 3D aggregation and correlates well with the reported AFM measurements, which showed micelle formation on the surface. It is also apparent that the influence of NaOH in the hydrolysate does not affect the chromophores on the molecule.

The irradiation of the silane quartz wafers was carried out first with two different light sources: a UV hand lamp at 254 nm and 364 nm with an irradiance of 610 μW·cm^{-2} and 400 μW·cm^{-2}, respectively and a UV crosslinker at 254 nm and 365 nm (irradiance of 3.03

and 2.77 mW·cm^{-2}, respectively).
Upon irradiation with both 254 nm light sources the local maximum is shifted to a higher wavelength and looses absorbance (Fig. 5.20). Irradiation with the less powerful UV hand lamp shows a gradual decrease of absorbance; whereas, irradiation with the crosslinker does not show any change in absorbance in the first 6 s but then upon irradiation with 30 s, the spectrum shows a sharp decrease of absorbance and a shift to longer wavelengths. After 700 s, irradiation with the TLC lamp, nearly all absorbance has vanished.
The kinetic spectra (Fig.5.20c,d) show an expected decrease of the azide chromophore for the local maximum at around 320 nm. As for the generation of the new local maximum around 360nm, the compound seems to transform into an intermediate product ca. 260 nm before a new absorption band is visible at 360 nm. In addition to this intermediate product irradiation with the UV hand lamp seems to generate a second "transitional product" at 340 nm which arises after irradiation for 70 s but which is then converted into the final product with λ_{max} ca. 360 nm upon further irradiation. The shift towards higher wavelengths is also characteristic for azophenyl or azepine formation.

When irradiating the silane quartz wafer with 365 nm, all of the absorbance at ca. 320 nm had disappeared after ca. 600 s (Fig. 5.21a,b). Both spectra showed new absorption bands at ca. 360 nm and ca. 260nm. The latter is characteristic of aryl amines that can have formed upon irradiation of the azide, with an absorption maximum at ca. 250nm. In both spectra the new absorption bands are of a lower absorbance intensity than the original one at 320 nm.

From azidobiphenyls it is known that upon photolysis in the presence of ketones, 60% of carbazole and 40% azobiphenyl is produced; whereas without ketones present, the yield for carbazoles is much higher [Swenton 70, Lehman 73]. Ketones are known to act as triplet sensitisers and this indicates that triplet energy is transferred to the azide, which then fragments into a nitrogen and a triplet nitrene. The carbazole must have formed from the singlet nitrene. The triplet nitrene on the other hand, which must have been formed from the triplet excited state of the azide, leads to the azo compound (Fig.5.22). Triplet quenchers, such as piperylene, reduce the amount of azobiphenyl to less than 1%. Swenton and co-workers concluded that this could not be due to conversion of the triplet nitrene to a singlet, for it had been established that triplet aryl nitrenes were of lower energy than singlets. Hence, piperylene must catalyse intersystem crossing to the more stable singlet azide since the ground state of the azide, unlike that of nitrenes, is a singlet. Lehman and co-workers presented evidence that triplet nitrenes and a ground state of the azide gave rise to an azobenzene, which would be feasible since, in contrast to an excited state azide, the ground state azide would be present in relatively high concentrations [Swenton 70, Lehman 73].

Since, as part of this thesis, no triplet quenchers or sensitisers were present during photolysis, it is assumed that the triplet nitrene extracts a hydrogen atom from another molecule (*i.e.* substrate, product, or surroundings), thereby becoming an amino radical,

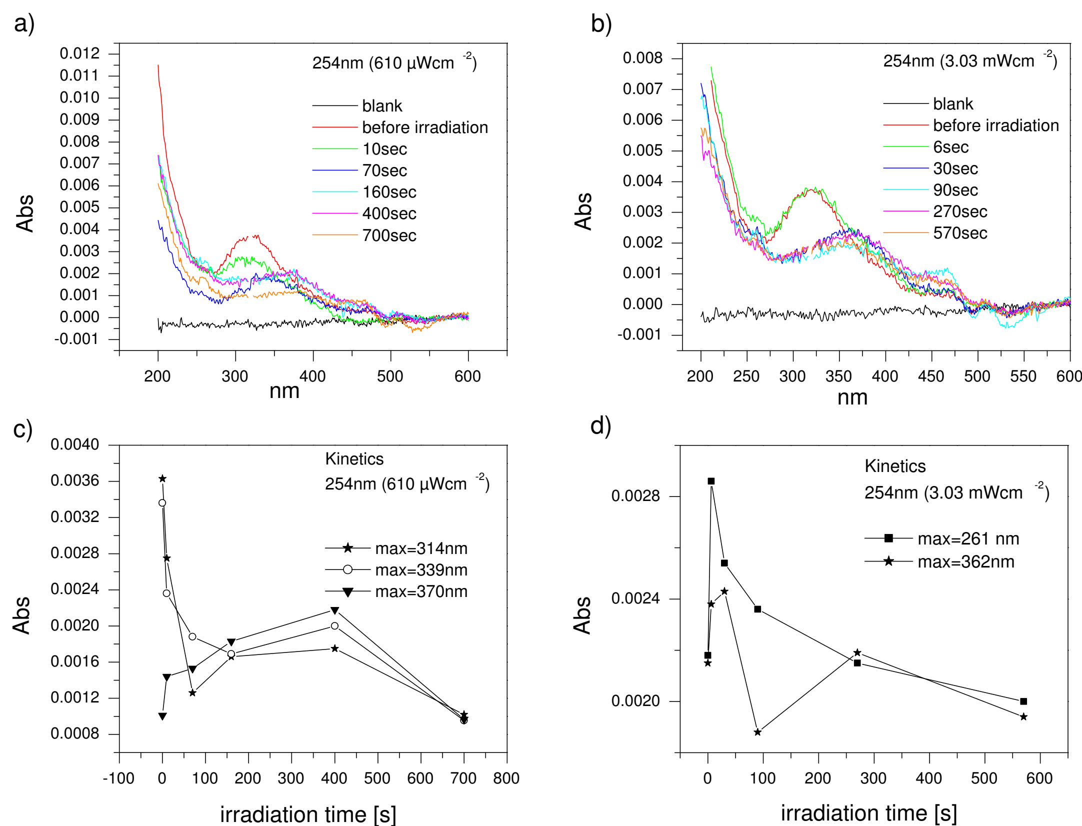

Figure 5.20: *Irradiation of ANTSP with 254 nm using a) a UV hand lamp, b) UV crosslinker; c) kinetic curve w.r.t. different absorption maxima in (a); c) kinetic curve w.r.t. different absorption maxima in (b).*

which may lead to an azo compound in 2 ways:

1. Dimerisation to a hydrazobenzene, followed by an oxidation (by aryl nitrene) to an azo compound (Fig. 5.23a).
2. Abstraction of a second hydrogen, becoming an amine, which can react with more nitrene to generate hydrazobenzene with further oxidation to azobiphenyl (Fig. 5.23b).

The fact that upon irradiation of ANTSP with both wavelengths new absorption bands at ca. 260 nm and 360 nm form favours the route suggested in Fig. 5.23b. Substituted aryl amines give a main absorption band at ca. λ_{max} = 260 nm and azobiphenyls at λ_{max} = 250. However, electron withdrawing substituents, such as the nitro group, in the *para* position to the azide, increase the reaction rates of all intermediates involved and the selectivity for functional

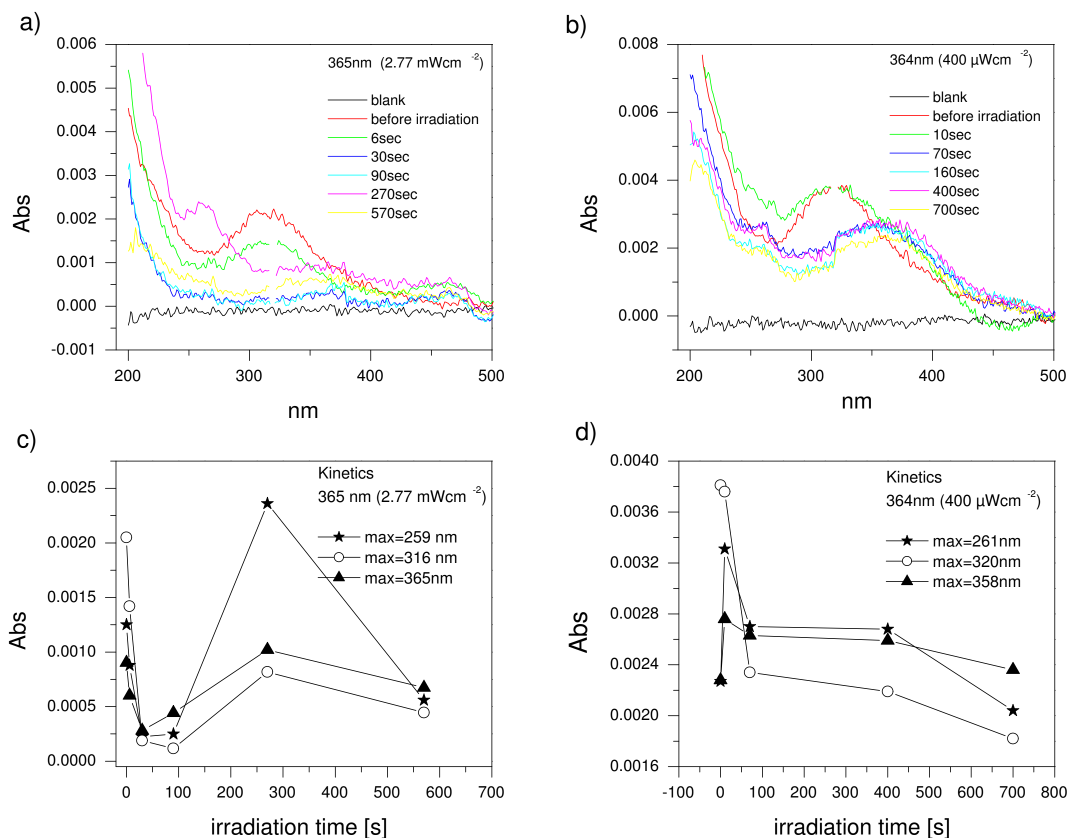

Figure 5.21: *Irradiation of ANTSP with 365 nm using a) a UV hand lamp, b) UV crosslinker; c) kinetic curve w.r.t. different absorption maxima in (a); c) kinetic curve w.r.t. different absorption maxima in (b).*

groups decreases [Reiser 70]. The lifetime of triplet aryl nitrenes (as a measure of the rate of hydrogen-atom abstraction) is greatly decreased by electron-withdrawing *para* substituents, but insertion reactions from the singlet nitrene are favoured.

Another enigmatic reaction of aryl azides is the one that leads to the incorporation of one of the azide nitrogens into the ring, expanding it to an azepine when nucleophiles are present (Fig. 5.24). Sundberg and co-workers carried out the experiments in the presence of piperylene, a triplet quencher, and concluded that azepine formation must occur *via* a singlet nitrene [Sundberg 74]. This conclusion was supported by Tsui and co-workers. Because they did not believe that nitrene reacted with amines to form azepines directly, they suggested that singlet aryl nitrenes equilibrate to azirines. These azirines are capable of forming azepines with nucleophiles, such as amines [Tsui 76]. Since azepines also have their main absorption

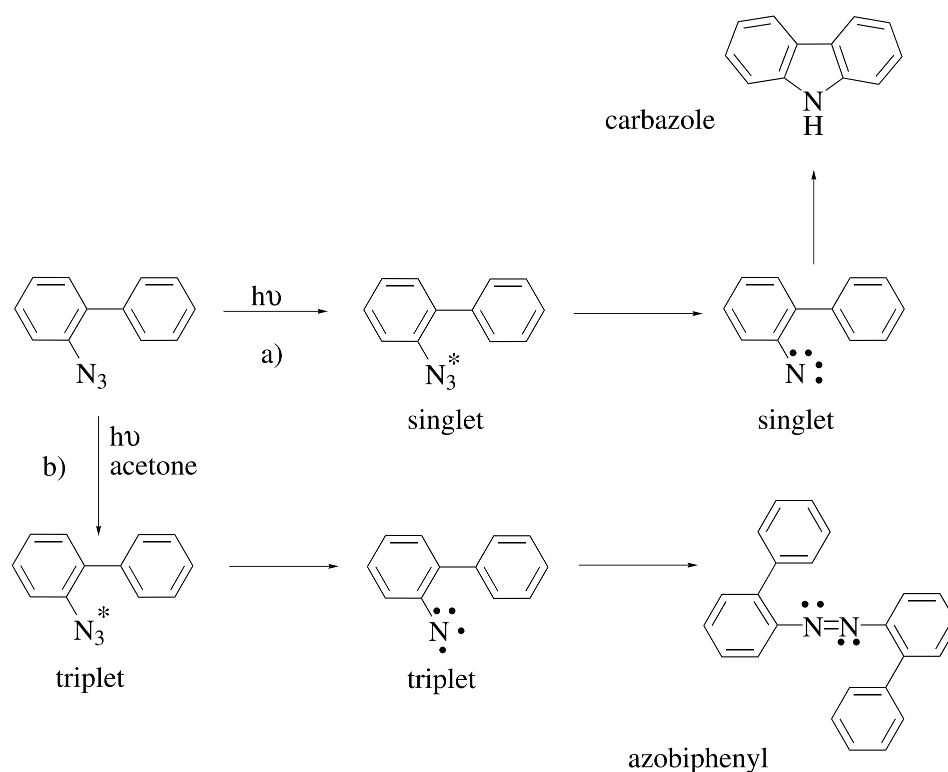

Figure 5.22: *a) Conversion of azidobiphenyl to singlet azide with further reaction to carbazole; b) in the presence of a ketone, azidobiphenyl is converted to triplet nitrene which forms an azophenyl [Smith 84].*

band between 350 and 400 nm, they could have formed during irradiation of ANTSP, even though no direct nucleophiles had been present during photolysis.

The static water contact angle measured before and after irradiation showed a huge shift towards hydrophilicity after irradiation. The average contact angle before irradiation was 71°; whereas, after irradiation with 254 nm in UV-crosslinker, the angle was 48° and with 365 nm the angle was 51°. This clearly shows that the wettability of the surface has changed and that a more polar group must have formed on the surface (*e.g.* an amine), which is emphasised by the formation of an absorption at ca. 260 nm upon irradiation with 365 nm wavelength light.

5.5 Site-Selective Patterning of Azidosilanes on Silica Surfaces

Silicon wafers were modified with ANTSP and irradiated through a mask at 365 nm. Water condensation patterns and colloidal assembly were then performed on the wafers in order to

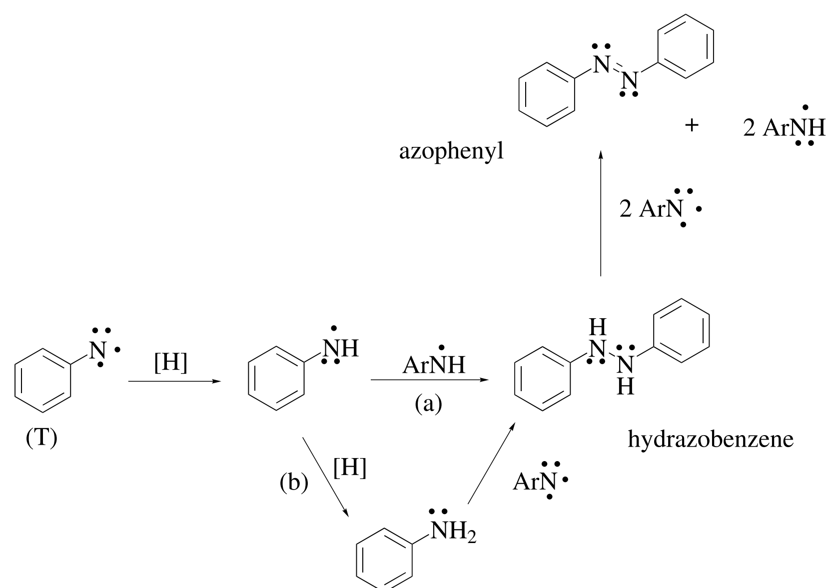

Figure 5.23: *Triplet nitrene undergoes H-abstraction with a) further dimerisation with aminoradical to give hydrazobenzene, b) second H-abstraction and further reaction with aryl nitrene to give hydrazobenzene that can then be oxidised to an azo compound [Smith 84].*

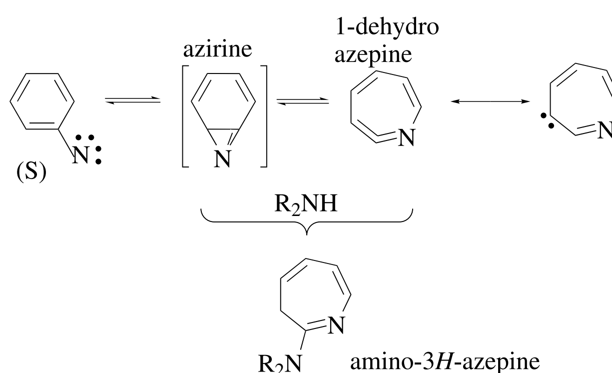

Figure 5.24: *Incorporation of singlet azide nitrogen into the ring to form azirine, which can either be converted into azepine or react with a nucleophile to give an amino azepine directly [Smith 84].*

verify the irradiation. Hydrophilic and polar water molecules form a breath pattern on the substrate, from which the hydrophilic and hydrophobic regions can be distinguished. The different wettability properties of the irradiated and non-irradiated regions are expected to modify the shape of the condensed water droplets on the substrate, which represents the underlying pattern. Charged colloidal particles should self-assemble onto the more polar irradiated areas and not onto the nonpolar non-irradiated regions on the wafer surface.

The colloidal particles used for the assembly process onto the azide-silane monolayers con-

sisted of polybutylmethacrylic acid (PBMA-COOH) bearing a parking area[4] of 203 Å^2 per COOH, higher charged polystyrene particles with carboxylic acid functionalities (98 Å^2 per COOH, (PS-7)) and polystyrene particles with hydroxypropylcellulose (PS-cell) bearing no charge. Another polymer cast on the surface was polystyrene dissolved in THF (PS film) also bearing no charge.
Three different light sources were used for irradiation: a Hg pressure lamp (22 mW·cm^{-2}, 365 nm), UV crosslinker (3.03 mW·cm^{-2}, 365 nm), and an Ar laser (400 mW·cm^{-2}, 365 nm). Irradiation of the substrate with the Hg lamp and with the UV crosslinker was performed in

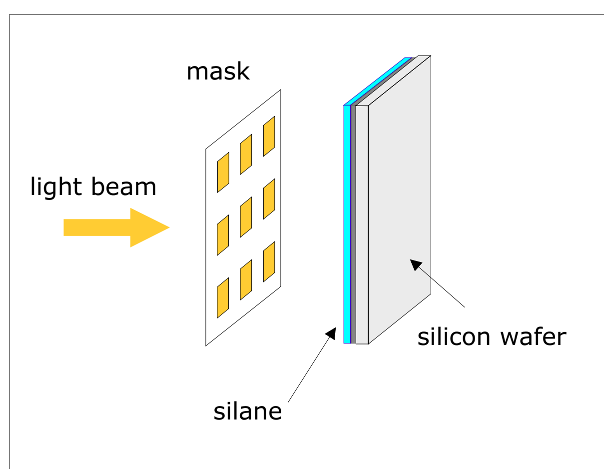

Figure 5.25: *Illustration of the vertical irradiation of SAM through gold mask.*

a vertical fashion, with the wafer being placed flat against the surface and gold mask placed directly on top of it. When irradiating with the laser, the beam of light was horizontal, and the wafer and gold mask had to aligned vertically (Fig.5.25). After irradiation the wafer was cleaned again with THF in an ultrasonic bath.

5.5.1 Experimental Results

The experimental procedure for patterning of the ANTSP layers start with the irradiation of a wafer that has been coated with ANTSP. A condensation pattern arising from the different areas of wettability should be visible under the light microscope, proving the transformation of the azide head group into a more hydrophilic group. The next step is to assemble the colloidal particles, as well as the polymer film, on a substrate with SAMs of ANTSP and then irradiate through a mask. The results obtained are then compared with colloidal assembly experiments carried out after irradiation of the azide.

[4]parking area = area per surface charge

5.5.1.1 ANTSP Without Particles

An ANTSP modified wafer was irradiated and a breath pattern was visible under the microscope, verifying the change of wettability upon irradiation of the azide silane. In order to

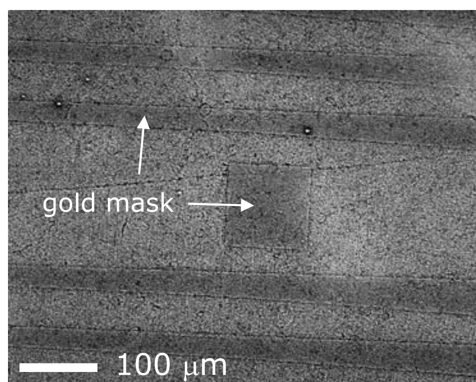

Figure 5.26: *Optical microscopic image (**D**ifferential **I**nterference **C**ontrast) of breath pattern of ANTSP modified silicon wafer that had been irradiated through a mask with the Hg lamp for 10 minutes (365 nm, 22 mWcm^{-2}).*

confirm that the change in wettability of the azide is not an artefact, but indeed a result of a the photochemically induced transformation of the aromatic azide, the same irradiation experiment was performed with an aminopropyltriethoxysilane (APTS) modified substrate. No condensation pattern was observed in this case.

5.5.1.2 Selective Irradiation Experiments on ANTSP Monolayers with Time-Dependent Colloidal Particle Deposition

Charged Polystyrene (PS-7) colloids were allowed to assemble on ANTSP modified silicon wafers *via* the drop-coating method. The colloidal particles were added as 0.2 wt% suspension in Milli-Q water using a pipette and either left on the wafers to evaporate in air or removed again with the pipette by suction of the solution from the wafers after a certain time. The wafers were then irradiated with the Hg lamp at 365 nm for 3 and 7 minutes, respectively, and rinsed with Milli-Q water afterwards.

The colloid suspension was deposited onto two wafers *P1* and *P2* with a pipette and the suspension was left to evaporate in air. *P1* was then irradiated through the mask for 3 minutes and *P2* for 7 minutes. After washing, the optical microscope showed only patches of colloids without a pattern transferred. It seemed that the dried colloids on the wafer had built multilayers that were too thick for the light beam to irradiate the silane that was underneath them.

Another two wafers *P3* and *P4* were also covered with the colloidal suspension, which was removed by suction with a pipette after 30 minutes. After rinsing, *P3* was irradiated for 3 minutes and *P4* for 7 minutes and a pattern was visible on *P4*, whereas, with *P3* again only patches of colloids were visible.

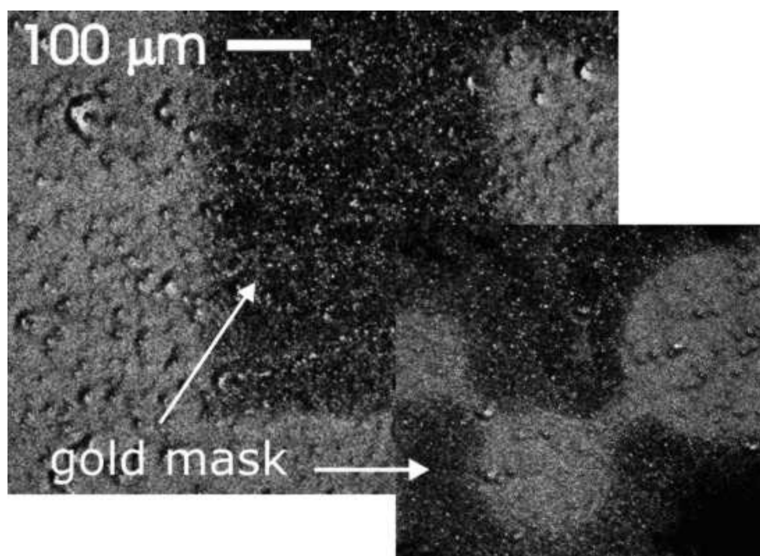

Figure 5.27: *Optical microscopic image (DIC) of irradiated and non-irradiated ANTSP after attempted PS-7 particle assembly; image shows P4 after 30 min incubation with colloidal suspension and 7 min irradiation.*

A further two wafers P5 and P6 were coated with the colloids for 1 hour before removing them by pipette, rinsing with water, and irradiating them for 3 and 7 min, respectively. A weak pattern was visible under the optical microscope on both wafers.
When the colloidal suspension was left on wafers *P7* and *P8* for 2 h and then irradiated for 7 and 3 min, respectively, a pattern was visible on *P8* only, which had been irradiated for 3 minutes. *P7* only showed patches of polymer and the colloidal layer also appeared very thick.

In summary, even though some patterns were visible after 3 and 7 min irradiation, no general consensus could be formed regarding the irradiation times. The worst pattern was visible when the colloids that had been allowed to dry in air rather than pipetting them away. As for the wafers with the colloids that had been removed by suction after deposition, the longer the colloids were allowed for deposition the better the pattern was after irradiation. A summary of all deposition times is given in Table5.1.

The wafers that showed a pattern under the optical microscope were further investigated with the electron microscope and with AFM, but only single colloids and not a real pattern could

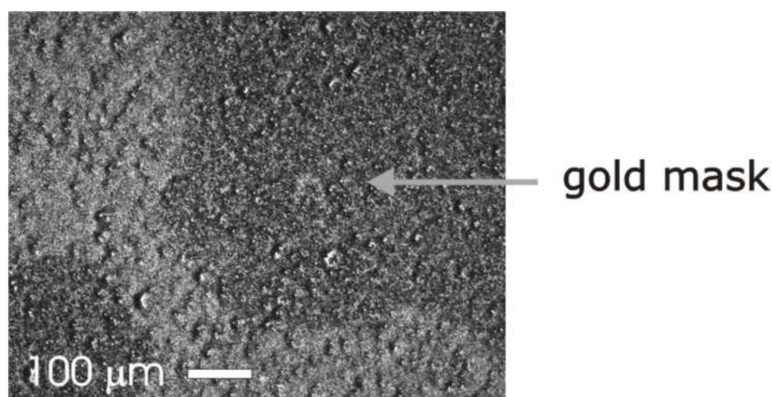

Figure 5.28: *Optical microscopic image (DIC) of irradiated and non-irradiated ANTSP after attempted PS-7 particle assembly; image shows P8 after 2 h incubation with colloidal suspension and 3 min irradiation showing P8 with 2 h colloidal assembly and 3 min irradiation.*

	deposition time	irradiation time	pattern
P1	16 h	3 min	no
P2	16 h	7 min	no
P3	30 min	3 min	no
P4	30 min	7 min	yes
P5	1 h	3 min	no
P6	1 h	7 min	no
P7	2 h	7 min	no
P8	2 h	7 min	yes

Table 5.1: *Time dependent PS-7 colloidal deposition, using the drop-coating method*

be detected. Consequently, either hardly any colloids had been adsorbed from the start, or the particles were not covalently bound and therefore had been mostly washed off. The pattern observed under the microscope is thus a result of the imaging contrast due to differences in hydrophilicity on the surface.

5.5.1.3 Selective Irradiation Experiments on ANTSP Layers with Charge-Dependent Colloidal Particle Deposition

The same irradiation experiments were then conducted with a polymer film and polymer particles of different charge. End functionalised core-shell particles used for deposition on the SAM of ANTSP were: PBMA-COOH (203 Å^2 per charge), PS-7 (98 Å^2 per charge), PS cellulose (no charge) in aqueous ethanol suspensions and a pure PS-film dissolved in THF. The colloids and PS-film were deposited using the dip-coating method.

Wafers *P1* and *P5* were coated with PBMA-COOH particles for 1 h and then irradiated for 2 and 5 min, respectively. No colloids could be detected on *P1* but the condensation pattern (Fig.5.29a) clearly indicated a change of wetting behaviour after irradiation. DIC microscopy of *P5* showed a very weak pattern after irradiation (Fig.5.29b).

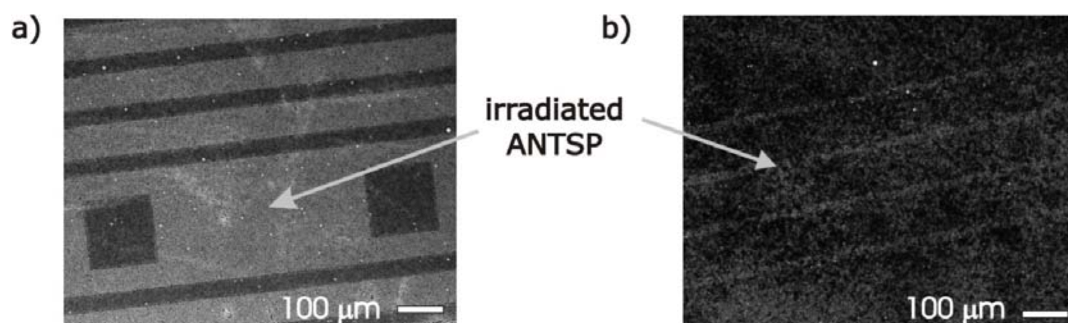

Figure 5.29: *Optical microscopic image (DIC) of irradiated and non-irradiated ANTSP with assembled PBMA-COOH particles; a) condensation image of P1 with 1 h colloidal assembly and 2 min irradiation; b) P5 with 1 h colloidal assembly and 5 min irradiation.*

P2 and *P6* were coated with PS-7 (bearing a lower charge than PBMA-COOH) for 1 h and then irradiated 2 and 5 min, respectively. On both wafers, a colloidal pattern was clearly visible with darkfield microscopy (Fig. 5.30). When the uncharged PS-cellulose colloidal

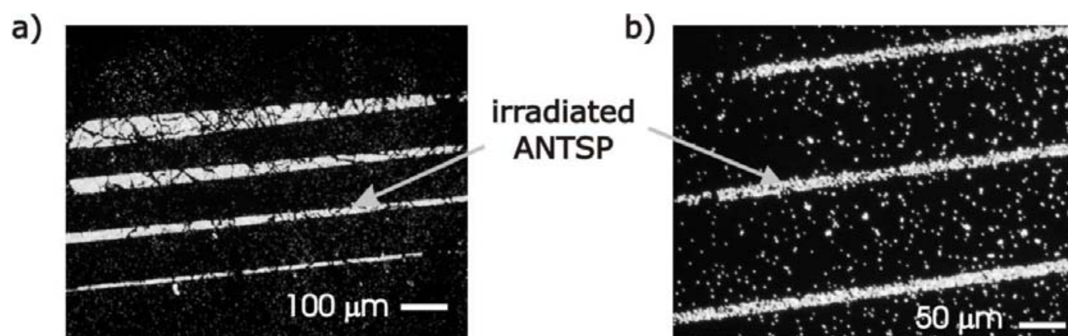

Figure 5.30: *Optical microscopic image (darkfield) of irradiated and non-irradiated ANTSP with assembled PS-7 particles; a) P2 with 1 h colloidal assembly and 2 min irradiation; b) P6 with 1 h colloidal assembly and 5 min irradiation.*

suspension was deposited onto wafers *P3* and *P7* for 1 h and then irradiated for 2 and 5 minutes, respectively, only a very weak pattern was visible (Fig.5.31). With *P3*, a pattern was only visible with a breath pattern.

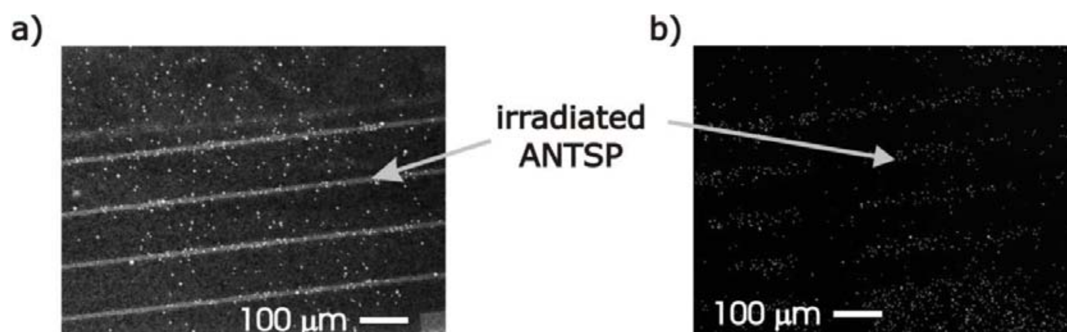

Figure 5.31: *Optical microscopic image (dark field) of irradiated and non-irradiated ANTSP with assembled PS-cellulose particles; a) Condensation image of P3 with 1 h colloidal assembly and 2 min irradiation; b) P7 with 1 h colloidal assembly and 5 min irradiation*

To further confirm that the uncharged polymer did not deposit on the irradiated ANTSP regions, a pure polystyrene film with a molecular weight of ca. 190000 $gmol^{-1}$ was dissolved as a 0.5% solution in THF and wafers *P4* and *P8* were dip-coated in the solution for 1 h and then irradiated for 2 and 5 min, respectively. On both wafers, no polymer deposition was visible under the microscope, only a breath pattern could be detected, again confirming the successful irradiation of ANTSP. Particle and polymer deposition are summarised in Table5.2.

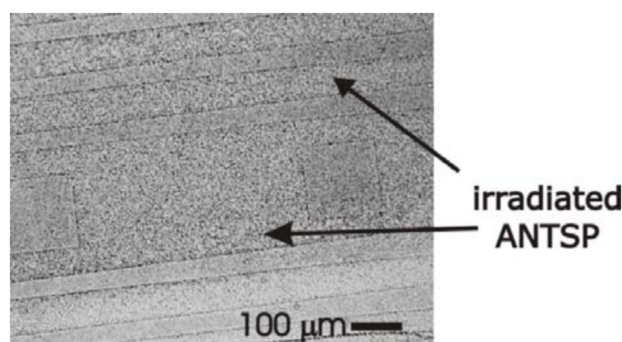

Figure 5.32: *Optical microscopic image (darkfield) with breath pattern of irradiated and non-irradiated ANTSP with deposited PS film; image shows P4 with 1 h deposition and 2 min irradiation.*

It is visible from the experiments above that the best deposition of colloidal particles occurred with the most charged latex particles, namely the polystyrene bearing carboxylic acid functions on the surface (PS-7). The lack of colloidal particles on some of the irradiated areas and of the PS-film indicate that no covalent bonding occurred upon irradiation. Therefore, the attachment of the PS-7 particles onto the irradiated regions of the surface is believed to occur *via* electrostatic forces.

	particles/polymer	deposition time	irradiation time	pattern
P1	PBMA-COOH	1 h	2 min	breath pattern
P2	PS-7	1 h	2 min	yes
P3	PS-cellulose	1 h	2 min	breath pattern
P4	PS-film	1 h	2 min	breath pattern
P5	PBMA-COOH	1 h	5 min	faintly visible
P6	PS-7	1 h	5 min	yes
P7	PS-cellulose	1 h	5 min	breath pattern
P8	PS-film	1h	5 min	breath pattern

Table 5.2: *Charge dependent particle deposition, using the dip-coating method.*

5.5.1.4 Colloidal Assembly After Irradiation

Another irradiation experiment was undertaken with ANTSP modified silicon wafers. The wafer was first irradiated through a mask with an Ar laser and then colloidal particles and a polymer film were allowed to self-assemble on the wafers. The polymer deposition time was also allowed to vary from 6 to 60 min in order to investigate a possible time dependence. Different wafers prepared with different reaction conditions were analysed.

Substrate 1 (10 min hydrolysis, 3.5 h silane deposition) was irradiated for 2 min with the laser. A PS film was deposited immediately onto the wafer and left for 60 minutes. The pattern that was then visible under the microscope (Fig. 5.33) showed dewetting of the more hydrophilic irradiated regions. As a result, the polymer molecules adsorbed onto the non-irradiated areas, where the aryl azide should still be intact, hence no major interaction should occur between the polymer film and the azide. It is assumed that the formed nitrene has already reacted with other species in the environment prior to the deposition on the film and therefore no covalent bonding to the PS film had occurred. When the experiment was repeated with the same conditions (substrate 2), but this time only allowing the polymer to deposit on the surface for 6 min instead of 60 min, the same inverted pattern could be observed (Fig.5.33a), but with a lower selectivity contrast. This demonstrated that the deposition time of the polymer indeed has an influence on the final selectivity.

When carrying out the experiments with different hydrolysis times of ANTSP (Fig. 5.34) using PBMA-COOH particles, again the inverted pattern was obtained. It is also visible that selectivity has changed. Wafer *FK1 P1*, where ANTSP had been hydrolysed for only 10 min, showed a lower selectivity than wafer *FK2 P1*, where ANTSP had been hydrolysed for 40 min. The longer the hydrolysis times the more hydrolysed are the ethoxysilanes, which leads to a higher density of silane groups in the SAM. Therefore more aryl azide can be irradiated,

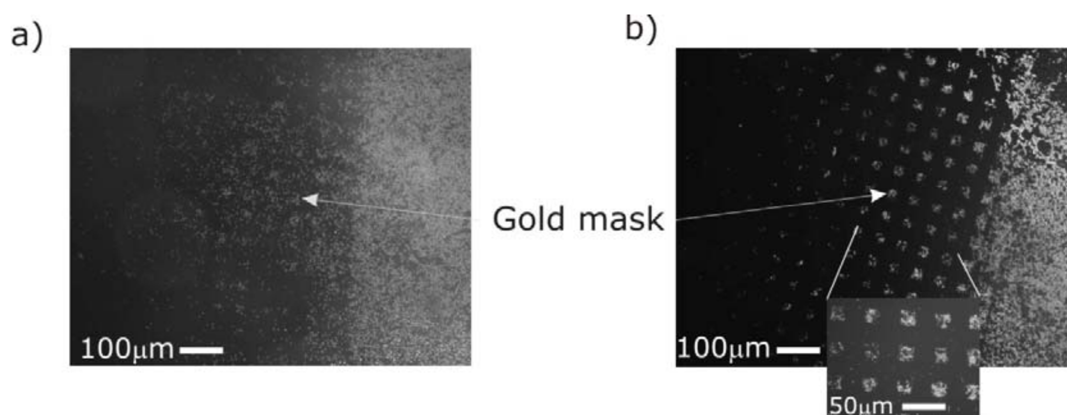

Figure 5.33: *Optical microscopic image (DIC) of irradiated and non-irradiated ANTSP showing the differences in selectivity w.r.t. the deposition time; a) Substrate 1 with 6 minutes PS deposition and b) Substrate 2 with 60 min PS deposition; on both pictures PS had adsorbed onto non-irradiated regions where the gold mask had covered the substrate.*

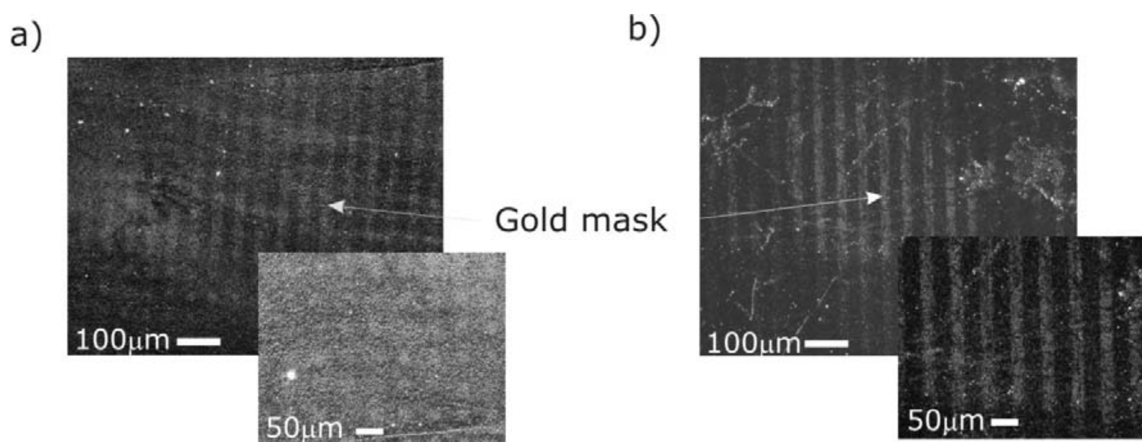

Figure 5.34: *Optical microscope image (DIC) of irradiated and non-irradiated ANTSP with assembled PBMA-COOH particles, showing the differences in selectivity w.r.t. the hydrolysis time; a) FK1 P1 with 10 minutes hydrolysis and b) FK2 P1 with 40 minutes hydrolysis.*

thus forming more hydrophilic silane groups onto which the particles can be assembled. If the density of ANTSP is low from the start, then less colloidal particles can assemble on the irradiated areas, as indicated by lower selectivity. It has also become obvious that the longer the polymer particles are assembled onto the irradiated regions, the better the selectivity.

5.5.1.5 ANTSP and NR_4^+ Patterns with Polymer Film

In order to create more complex laterally structured silanes and to investigate further the driving force for polymer deposition on the ANTSP region, silicon wafers were patterned with photolithography. N-Trimethoxysilylpropyl-1-N,N,N-trimethylammoniumchloride (NR_4^+) was deposited onto the wafers according to the procedure in Chapter 7.2.1. After removal of the remaining photoresist, ANTSP was then deposited onto the substrate allowing 30 minutes hydrolysis in THF without water and 2 h silane deposition. Before the wafers were coated with polymer, the breath pattern of the pure ANTSP/NR_4^+ was recorded with the light microscope. As expected, it is visible from Fig. 5.35 that the ammonium regions are much more hydrophilic than the ANTSP regions. The wafers were then spin-coated with a

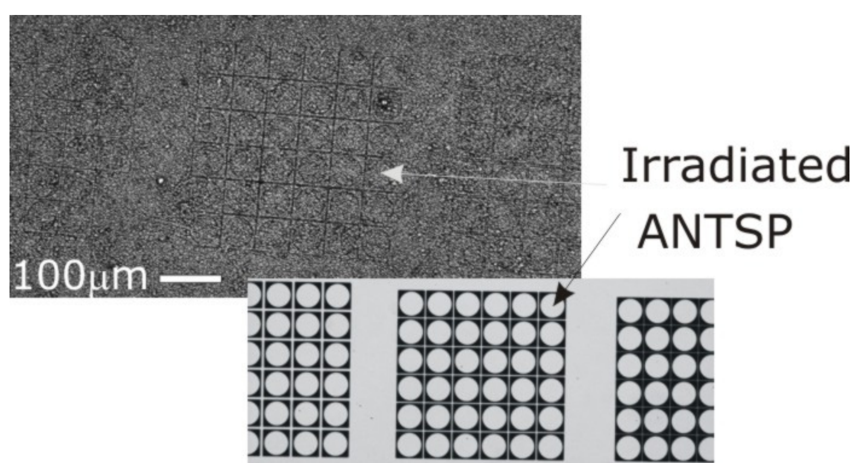

Figure 5.35: *Optical microscope image (DIC) of breath pattern of ANTSP/NR_4^+ on silicon wafer; smaller image shows the gold mask used: areas protected by the gold mask bear ANTSP silane, whereas non-protected regions comprise the NR_4^+ silane.*

1% solution of polystyrene film in THF and then irradiated with a UV Hg-lamp (365 nm) for 20 s.

After irradiation, the wafers were cleaned in an ultrasonic bath and a pattern was recorded showing an adsorption of the PS-film onto the ANTSP regions. The polymer that had been cast onto the positive charged ammonium regions was removed during sonification. Thus, the polystyrene molecules must have bound to the ANTSP regions on the surface due to covalent bonding or due to strong adhesion, since they would have been otherwise removed. The charged NR_4^+ groups on the surface do not interact with the uncharged polystyrene molecules. The driving force of the polymer deposition must be the formation of a covalent bond with ANTSP or the interaction with the resulting surface functionality. In contrast to the deposition of the PS-film as described in Fig. 5.32, the polymer was spin-coated onto the wafer rather than dip-coated into the THF solution. Since the PS-film was still visible

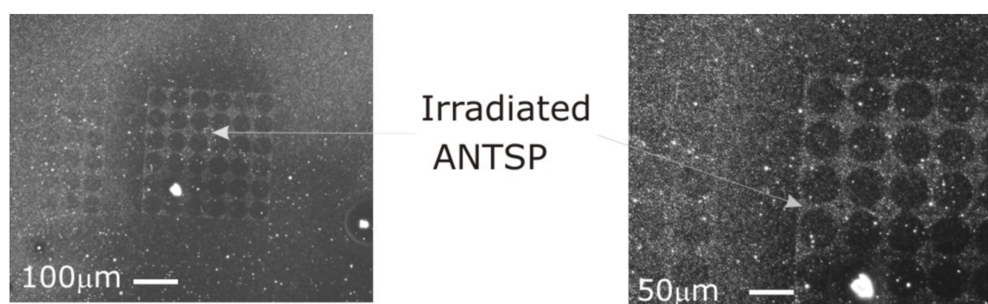

Figure 5.36: *Optical microscopy image (DIC) with assembled PS film on ANTSP/NR_4^+ pattern with PS present on ANTSP regions after irradiation.*

with the optical microscope after irradiation, the uniform distribution of this technique allows consistent coverage of the surface with the polymer film. Consequently, this technique is preferred for future deposition experiments.

5.6 Summary

It has been possible to synthesise a compound (ANTSP), which can be used to modify silicon dioxide surfaces due to its ethoxysilane anchoring group. Its head group can further react upon light irradiation due to the azide moiety on the aromatic ring. Hydrolysis conditions were optimised in order to minimise micelle cluster formation, arising from the reactive alkoxysilane group. Kinetic experiments with varying concentrations of the catalyst were performed to study the hydrolysis efficiency of the catalyst.
Cluster formation that had occurred during hydrolysis was further investigated with dynamic light scattering. This confirmed that upon addition of catalytic amounts of NaOH the hydrodynamic radius increases. UV-spectroscopy was then applied to monitor the disappearance of the chromophores during irradiation of ANTSP, thus indicating that the nitrene had further reacted to give an hydrazobenzene or azobenzene compound upon irradiation with 254 nm. Upon irradiation with 365nm the absorption band around 250 nm that occurred together with the absorption band ca. 360 nm, also indicated the formation of an arylamine.
When polymer particles were deposited on the surface and then irradiated through a mask, the best pattern was obtained with the most charged colloidal particles (PS-7), indicating attractive electrostatic interactions between the particles and the irradiated ANTSP region. An increase in hydrophilicity after irradiation was clearly visible in the condensation pattern under the optical microscope and by contact angle measurements.

Chapter 6

Wavelength Dependant Patterning of Mixed Silane Layers

6.1 Introduction

As described in Chapter 5, light is a particular convenient medium to generate a lateral pattern on a surface, especially if specific chemical reactions can be induced on the surface by irradiation. in this context, photosensitive protecting groups provide a perfect tool for generating chemical patterns on the surface. In order to increase the complexity of the patterns on a surface, a mixture of silanes carrying different photoreactive protecting groups can be assembled on the substrate.
This approach allows the introduction of different types of functional groups across the same surface by co-adsorbing two different silanes simultaneously. Upon irradiation the head groups are removed and the initial activity of the functional groups is restored. It is thus possible to control the photolysis and the resulting deprotection, and therefore the lateral pattern bearing different chemistries can be introduced any time. The advantage of this technique is that reactive groups and patterning tools are brought to the surface in a one-step process, thus reducing the number of processing steps that are needed for conventional photolithography. No spinning-on of the photoresist is required, after irradiation no developing step is necessary in a developer solution and no removing of the photoresist is needed anymore. Using this approach it is even possible to simultaneously bring two different silanes onto a surface, bearing head groups that would not be compatible if assembled in their respective unprotected state. For example, amino and carboxy functionalised head groups assembled next to each other on a surface would form strong hydrogen bonds, imparting the surface a salt character that is hard to modify. Moreover, this salt character leads to the formation of ”small separated islands” on the wafer surface that make further reaction of the functional head groups with another molecule nearly impossible. It is even possible to assemble functional groups on

the surface that are usually not compatible with alkoxysilanes, such as carboxylic acid or hydroxyl groups. These groups hydrolyse the alkoxysilane in the presence of water (due to catalytic H^+), which leads to condensation and subsequent polymerisation of the compound. By introducing a protected form of the carboxylic acid, water traces will not effect the silane and no polymerisation can occur before the silane is covalently bound to the silica surface.
Light directed chemical synthesis is only limited by the number of synthesis sites that can be addressed with the appropriate resolution, and the high degree of miniaturisation is only limited by the spatial addressability, such as the diffraction of light. Experiments conducted by Jonas and co-workers showed the successful site-selective cleavage of a photo-protected silane that had been synthesised prior to adsorption, and which formed well defined monolayers. Upon irradiation, the protecting group was cleaved off with an Argon laser at 364 nm to yield the free reactive primary amine groups. The existence of the groups was proven by reaction with a fluorescent label [Jonas 02a].

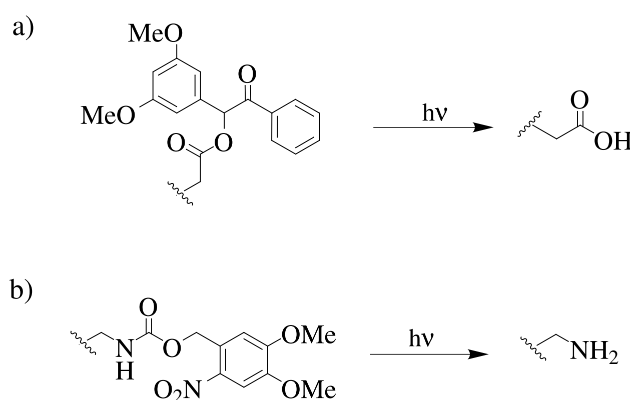

Figure 6.1: *Schematic representations of a) benzoin protecting group for carboxylic acids, and b) NVoc protecting group for amines.*

A further refinement of this method involves modification of the surface with a mixture of alkoxysilanes bearing orthogonal protecting groups. This means that it is possible to selectively remove one of the protecting groups in presence of the other in any chronological sequence. The irradiation is based on the different photochemical properties of the protecting groups, such as the reactivity of the compound and the required chromophore excitation (wavelength). As part of this thesis two orthogonal protecting groups are used: a nitroveratryloxycarbonyl (NVoc) group to protect an amine functionalised silane and a 3’,5’-dimethoxybenzoin (Bnz) group for protection of a carboxylic acid functionalised silane. The NVoc group can be deprotected at wavelengths $\geq$350 nm and the benzoin group at 254 nm [Bochet 00, Blanc 02]. The irradiation scheme with both the protected amine and carboxylic acid functional groups on a silica surface is shown in Fig. 6.2. They can either be deprotected separately (Fig. 6.2a,b) or in a two-step site-selective irradiation through a mask (Fig. 6.2c). This will generate a lateral pattern of regions with different deprotected functional groups, without the need for additional patterning or surface modification processes. Areas of either only free COOH, only free NH_2, both free NH_2 and COOH or still photo-protected silane will be present on the irradiated surface. If, after deprotection, the entire surface is exposed to a solution (or

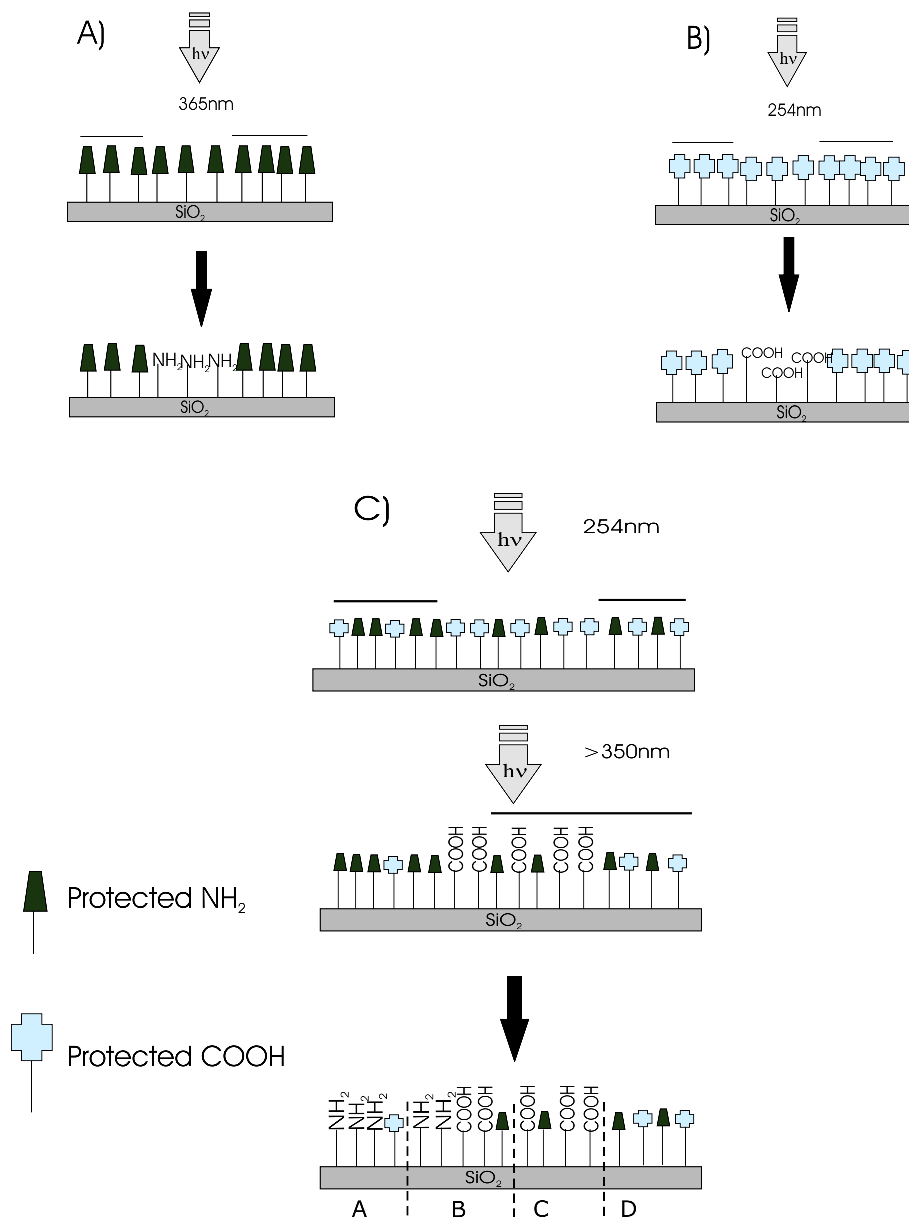

Figure 6.2: *Concept of the chemical surfaces patterning procedure by site-selective activation of the protected functionalities. a) and b) SAMs of photo-protected silanes were irradiated through a mask, which selectively removes the photolabile protecting groups from irradiated regions. c) If the surface is modified with two different photoremovable protecting groups, illumination through a second mask with a different wavelength activates a different region. As a result 4 different areas are obtained consisting of either only free NH_2 (A), free COOH (C), both liberated groups (B) or non-irradiated regions (D). The irradiated areas can then further react with any number of targets that can be immobilised by this technique.*

suspension) of the molecules (or particles) that need to be adsorbed, reaction will occur only in regions that were activated by light in the preceding step.

This chapter will describe the synthesis of a benzoin protected carboxylic acid silane. The use of this silane for surface modification and patterning of silica surfaces will be illustrated. In addition, mixed layers of this silane and an NVoc-protected amino silane will be fabricated and used for site-selective adsorption of colloids and for immobilisation of oligodeoxynucleotides (ODNs). The orthogonality of these two silanes will also be demonstrated.

6.2 The Concept of Orthogonal Protecting Groups

The concept of orthogonal protecting groups originates from peptide synthesis that is based on appropriate combination of protecting groups together with an efficient method for the activation of the carboxy group prior to reaction with the amino component [Albericio 00]. This means that the N^{α}-amino group of one of the amino acids and the C-terminal carboxyl group of the other should both be blocked with suitable protecting group so that formation of the desired peptide (amide) bond can occur by activation of the free carboxyl group. The most widely used protecting groups for NH_2/COOH protection are *tert*-butoxycarbonyl (Boc)/benzyl (Bzl) and 9-fluorenylmethoxycarbonyl (Fmoc)/*tert*-butyl (*t*-Bu) as protection schemes. The disadvantage of the Boc/Bzl combination is that even though the Boc group is removed by milder acids, *i.e.* trifluoroacetic acid (TFA) and Bzl is removed by stronger, *i.e.* HF, the long exposure of the peptide chain to TFA during the removal of the Boc group might also lead to the premature cleavage of the Bzl group. On the other hand Fmoc and *t*-Bu are removed by two completely different mechanisms (β-elimination and acidolysis, respectively) and can therefore be removed at any order in presence of the other group [Wade 00, Ritzen 00, Zhu 00, Bloomberg 93].
A major drawback associated with these protecting groups in organic syntheses is the fact that introduction and cleavage requires two synthetic steps, which reduce the overall yield remarkably. Moreover, the synthetic plan becomes even more complicated when the protecting groups are incompatible with certain solvents. This means that optimum conditions for each cleavage have to be tailored to each individual protecting group in order to not destroy the other groups. Photolabile protecting groups can overcome this problem since the only reagent that they require for cleavage is light.

A prerequisite for a photochemical removal of a protecting group is a chromophore that is sensitive to light but relatively stable to the most common chemical reagent encountered in the ground state manifold [Pillai 80]. The wavelength of the light chosen should be

such that it will only be absorbed by the protecting group and will not affect other parts of the molecule. Moreover, photo-deprotection should not harm the protected molecule and the resulting photoproduct should be easily removed. Another factor of great importance is the lifetime of the excited state, which is responsible for the deprotection reaction. That means, the longer the excited state before cleavage occurs, the more the chances are for undesirable quenching processes to arise, which in turn reduces the efficiency of the cleavage reaction. This of course, would hinder the removal of the photo-protecting group and might labilise the quenching species [Becker 91].

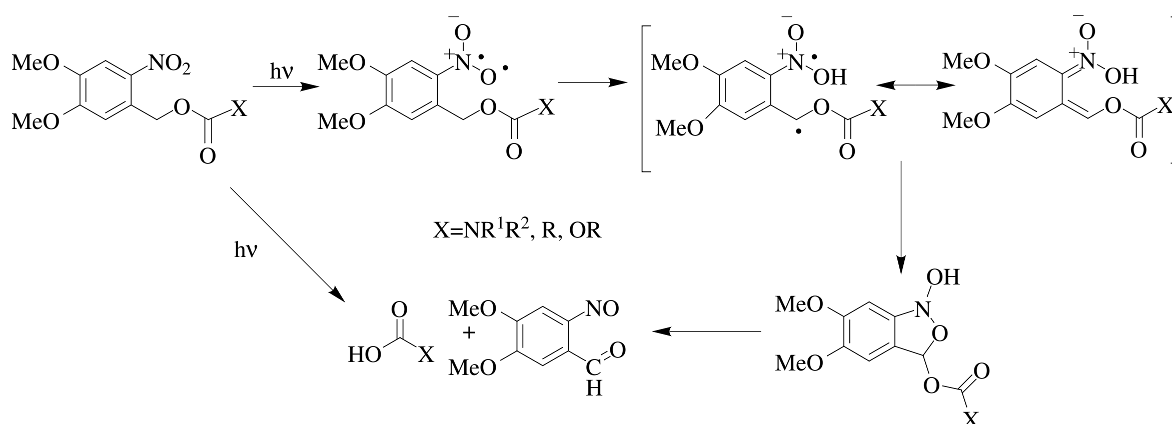

Figure 6.3: *Photolytic cleavage of NVoc-protected carbonyl compounds.*

Since photolytic cleavage is the consequence of the absorption of a photon by the compound, the excitation of the chromophore present can lead to highly reactive diradical species. Hydrogen abstraction in the γ-position is very common among these species and its mechanism was first identified by Norrish in 1935 [Bochet 02]. Among these so-called "Norrish type II" reactions are protecting groups bearing carbonyl moieties, such as carbamates, carbonates and esters that are converted into an acetal derivative, which spontaneously collapses into an aldehyde and the desired functional group. The most popular carbamate protecting group is the nitroveratryloxycarbonyl group (NVoc) used for protection of the amine group, which decarboxylates to give an aldehyde, the free amine and CO_2. However, NVoc protection can also be used for photoprotection of alcohols and carboxylic acids [del Campo c].

The photo-mechanism of NVoc deprotection is shown in Fig. 6.3, where the primary photochemical process is an intramolecular hydrogen-abstraction from the benzyl C-H bond in *ortho*-position by the excited nitro group. An electron distribution then follows to form an azinic acid (*aci*-nitro group), which rearranges to the nitroso group. The only problem associated with the NVoc group is the side reaction of the formed aldehyde photoproduct with the released amine group to give an imine. This can be overcome by either introducing a scav-

enger molecule, such as semicarbazide hydrochloride to the reaction mixture, which captures the aldehyde or to substitute the benzylic methylene group with another *o*-nitrophenyl group which releases a ketone upon photolysis that is less prone to imine formation than aldehydes. Other useful carbonyl photoprotecting groups include the nitrobenzylcarbonyl group (NBoc) used particularly for protection of hydroxy groups in carbohydrates or α-ketoesters as photo liberators of aldehydes and ketones in fragrances [Cameron 91, Rochat 00].

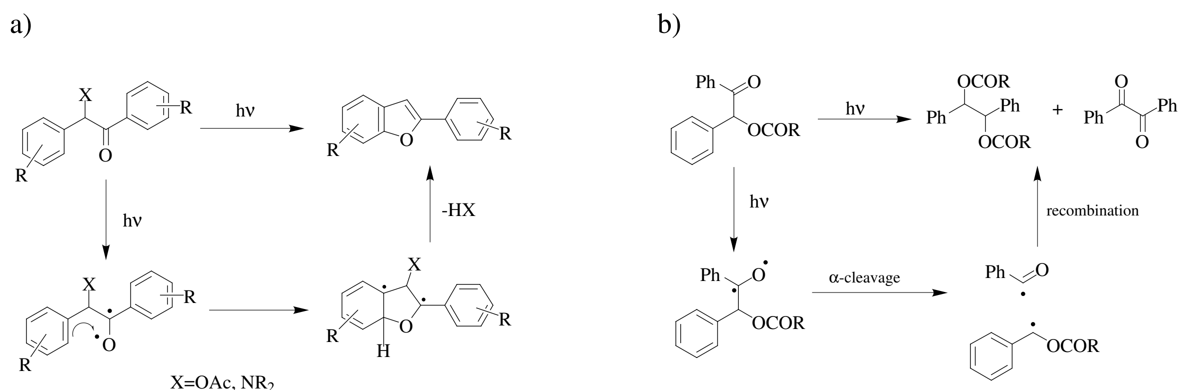

Figure 6.4: *a) Photolytic cleavage of benzoin ester* via *diradical mechanism in presence of substituents to yield benzofuran and liberated fragment; b) α-cleavage of benzoin ester bearing no substituents.*

Benzoin ester (Bnz) have also become very popular as photoprotecting groups due to their application in *e.g.* caged phosphates, such as cAMP (caged adenosine monophosphate) and ATP (adenosine triphosphate) and their use as a protecting groups for both carboxylic acids and amines [Corey 65, Stowell 96]. In 1964 Sheehan and co-workers showed that it was possible to cyclise benzoin acetate into 2-substituted benzofuran and to release the carboxylic acid group by irradiation with a high pressure mercury lamp with a Pyrex filter [Sheehan 64, Sheehan 71]. The carboxylic acid was thereby released with a high quantum yield (Φ=0.64) thus making it attractive for the protection of carboxylic acids. They also found out that substitution of the benzylic ring significantly increased the rate of reaction and that 3',5'-dimethoxybenzoin led to a fast and smooth cyclisation upon photolysis. The advantage of using the dimethoxybenzyl moiety as a photo-protecting group has also been used by other groups [Chamberlin 66, Cameron 91, Bochet 00] and they found out that the reaction occurred within 10^{-10} s after the absorption of light, indicating a short-lived n-π* singlet excited state. The extremely short-lived excited state makes the Bnz group attractive for intercellular biologically active substances (*i.e.* protected phosphates). The benzofuran photoproduct is non-polar and inert and can therefore be readily separated from acid or polar compounds.

The first suggested mechanism is based on a diradical process (Fig. 6.4a), whereas a few years later a new mechanism was proposed based on the Paterno-Büchi-type reaction where oxe-

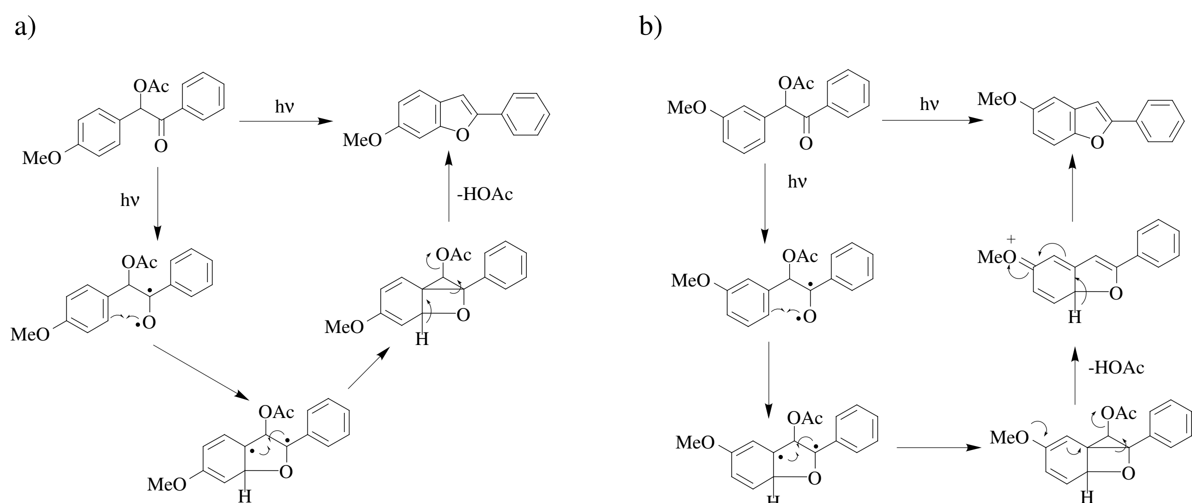

Figure 6.5: *Both mechanisms occur* via *Paterno-Büchi type reaction with a) bearing the methoxy substituent in the* para-*position and b) bearing the methoxy substituent in the meta-position of the benzoin ester.*

tane is formed from a photo-induced reaction of an olefin and a ketone (Fig. 6.5) *via* a [2+2] cycloaddition [Sheehan 71]. The substituents on the benzoin play a major role in determining the photolysis mechanism. Whereas 4,4'-dimethoxybenzoin only gave trace amounts of benzofuran, 3'5'-dimethoxybenzoin leads to a very smooth cyclisation, releasing the acid moiety in high yields. On the other hand, if no substituents are present the mechanism occurs *via* an α-cleavage of the diradical (Norrish type I reaction), resulting from the carbonyl excitation (Fig. 6.4b), which does not lead to the formation of benzofuran and the desired free acid moiety [Lewis 75, Lipson 96].

6.3 Synthetic Details

NVoc protected samples were all provided by A. del Campo, Max Planck Institute for Polymer Research in Mainz.
The synthesis of the organosilane bearing a Bnz protected carboxylic acid head group was carried out *via* a benzotriazole-mediated conversion of benzaldehyde to a benzoin protected undecenoyl ester bearing a double bond on the α-position for further hydrosilylation. This procedure involves first the activation of benzaldehyde with benzotriazole to yield an acyl anion equivalent **38** that can then be easily lithiated and trapped with the electrophilic dimethoxybenzaldehyde during acid work-up [Katritzky 95]. After esterification of the aryl ketone the last step involves the hydrosilylation of the double bond with triethoxysilane to yield the desired silane.

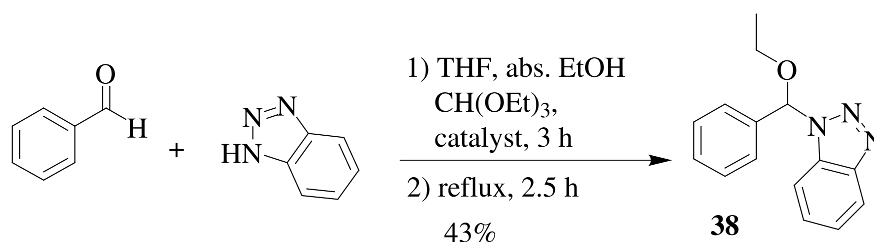

Figure 6.6: *Synthesis of benzotriazole activated benzaldehyde starting from benzaldehyde, benzotriazole, absolute ethanol, triethylorthoformate and a catalytic amount of sulfuric acid*

When the reaction was carried out using benzaldehyde, benzotriazole, absolute ethanol and triethylorthoformate (Fig. 6.6), it became clear that the reaction time was an important parameter in the activation of benzaldehyde with benzotriazole. It was observed that reaction times longer than 3 h lead to a thermal composition (back reaction) of the formed product into its reactants. Purification of the crude *via* column chromatography on silica afforded the pure product only in a 20% yield since most of the obtained product fractions again contained the benzaldehyde starting material indicating decomposition at room temperature and/or decomposition due to the slightly acidic silica gel. The yield could be improved to 44% by using flash column chromatography, but after removing the solvent of the pure product fractions *in vacuo*, the benzotriazole and benzaldehyde spots were again faintly visible on the TLC plate. As reported before by Katriztky *et al.* an alternative route for the preparation of **38** is the reaction between the corresponding acetal and benzotriazole in refluxing toluene [Katritzky 95].

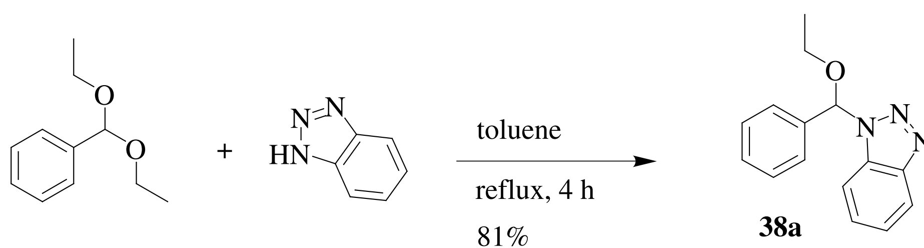

Figure 6.7: *Synthesis of benzotriazole activated benzaldehyde starting from benzaldehyde diethylacetal and benzotriazole.*

The reaction was therefore repeated according to Fig. 6.7. After purification, two spots were visible on the TLC plate having an R_f = 0.54 and R_f = 0.40, respectively. Both showed the same m/z of 253 = 100% with FD-mass spectrometry, indicating the formation of two stereoisomers during the reaction. Indeed when considering the sp^3 carbon in the diacetal compound, benzotriazole can undergo both a backside and front side attack since it is not sterically hindered to yield a chiral molecule. ^{1}H NMR confirmed that both products were the benzotriazole activated benzaldehyde. In order to delineate the

sensitivity of the product at room temperature both product isomers were spotted onto TLC plates and monitored every 20 min. It was clearly visible that decomposition into benzotriazole and benzaldehyde occurred after only 90 min at room temperature. The product was therefore stored in the dark under argon and below -10 °C to minimise decomposition.

The next step was an acyloin formation to yield the benzoin product (Fig. 6.8). In order for the condensation to occur lithiation of **38a** with n-BuLi at -78 °C and quenching with the electrophile had to occur very fast in order to avoid partial decomposition of the resulting anion intermediate and hence low yields. Even though the product was stored

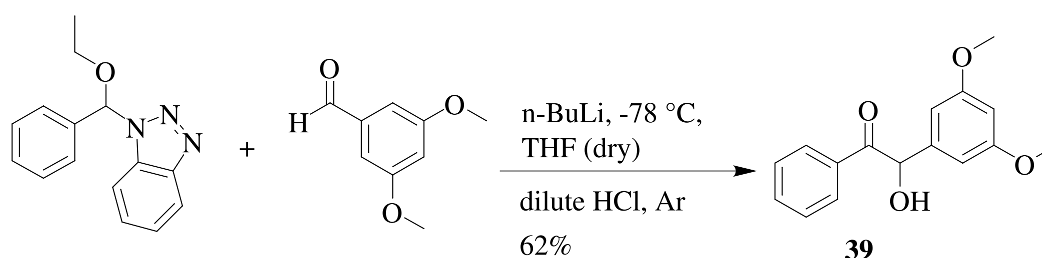

Figure 6.8: *Synthesis of 3',5'-dimethoxybenzoin.*

under argon and below -10 °C it was readily seen that its colour had changed from yellow to dark red. FD-mass spectrometry confirmed the decomposition of the product. Therefore the next reaction step had to be carried out as soon as the pure benzoin compound had been isolated. This step involved the acylation of the alcohol moiety **39** with both butenoic acid and undecenoyl chloride (Fig. 6.9).

Acylation of the alcohol was straightforward and afforded **40** and **41** in quantitative yields. However, esterification with butenoic acid in presence of diisopropylcarbodiimide lead to the formation diisopropylurea. Unfortunately column chromatography could not remove all of the urea traces and smaller impurities. Even though their presence was only 2-3% in the final product, these impurities were enough to block the Pt-catalyst's action in the following hydrosilylation (Fig. 6.10). Esterification of **39** with triethylamine and undecenoyl chloride also lead to the formation of side-products but after 3 successive column chromatographies with 3 different eluent compositions the pure compound could be isolated and hydrosilylation occurred without formation of the saturated benzoin ester to yield the desired product **43**.

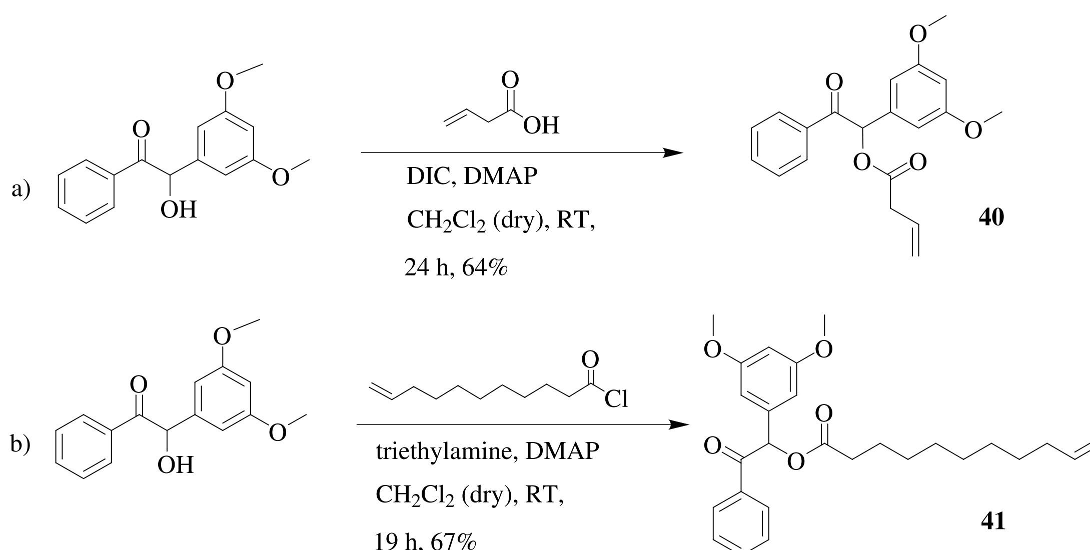

Figure 6.9: *Esterification of 3',5'-dimethoxybenzaldehyde with a) butenoic acid and diisopropylcarbodiimide and b) undecenoyl chloride and triethylamine, both in the presence of dimethylaminopyridine.*

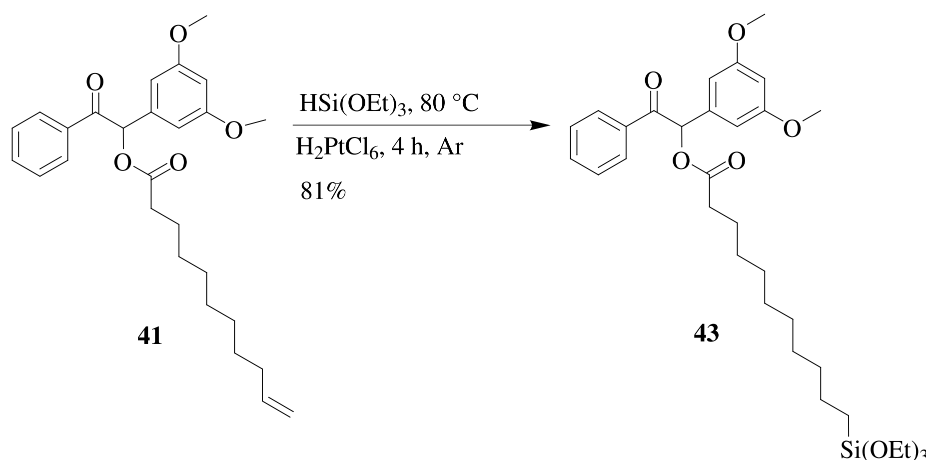

Figure 6.10: *Hydrosilylation with hexachloroplatinic acid and triethoxysilane.*

6.4 Surface Modification and Characterisation

The hydrolysis and condensation kinetics of the Bnz silane in solution were analysed using solution ^{1}H NMR in the presence of catalytic amounts of HCl and NaOH. Disappearance of the ethoxy group on the Si-atom and formation of the new ethanol can thus be easily monitored and quantified.

As visible in Fig. 6.12a, hydrolysis of the alkoxy group in the presence of 1N HCl occurs very fast and almost reaches completion after 100 min. The appearance of multiple peaks in the ^{1}H NMR spectrum (Fig. 6.12b) in the region of ca. 0.45 ppm corresponds to the α-methylene group at the Si-atom. They reflect the formation of intermediate products

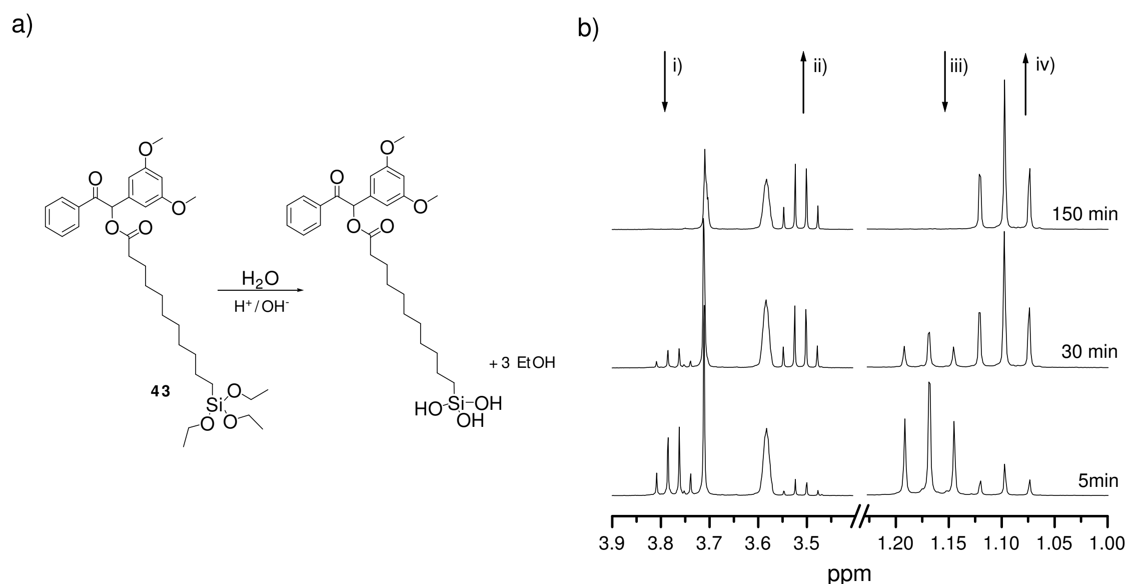

Figure 6.11: *a) Hydrolysis of ethoxysilane **43** with water and catalyst; b) ^{1}H NMR spectra of hydrolysis: i) decrease of ethoxy CH_2, ii) increase of EtOH CH_2, iii) decrease of ethoxy CH_3, iv) increase of EtOH CH_3.*

(mono-, di- and trisilanol) during hydrolysis. It can be seen that after ca. 370 min the signal looses intensity and the remaining Si-CH_2 peak is broader than the initial one (at t = 0). These features may indicate that condensation between the silanol species in solution is taking place.

The same kinetic experiments were carried out using 1N NaOH. Fig. 6.13a-c shows the hydrolysis experiments of benzoin using first 2 μl NaOH, then 5 μl and then 10 μl NaOH as the catalyst in a 1ml d_8-THF silane solution. From Fig. 6.13a (i) it is visible that after 40 h only ca. 20% of the ethoxy groups have been hydrolysed when 2 μl NaOH were added, whereas kinetic experiments carried out with 2 μl HCl as the catalyst, showed much higher hydrolysis levels. When 3 more μl 1N NaOH were added to the solution, a slight increase in hydrolysis rate is visible. Fig. 6.13b (i) shows 15% more transformation of alkoxy to ethanol than before. Addition of 5 more μl 1N NaOH to the same solution leads to a complete hydrolysis of the alkoxysilyl groups. After 60 h of hydrolysis a broadening in the Si-CH_2 peak is noticeable in Fig. 6.13c (ii), as a result of the silanol condensation process.

Even though benzoin hydrolysis with HCl as the catalyst occurred much faster than with

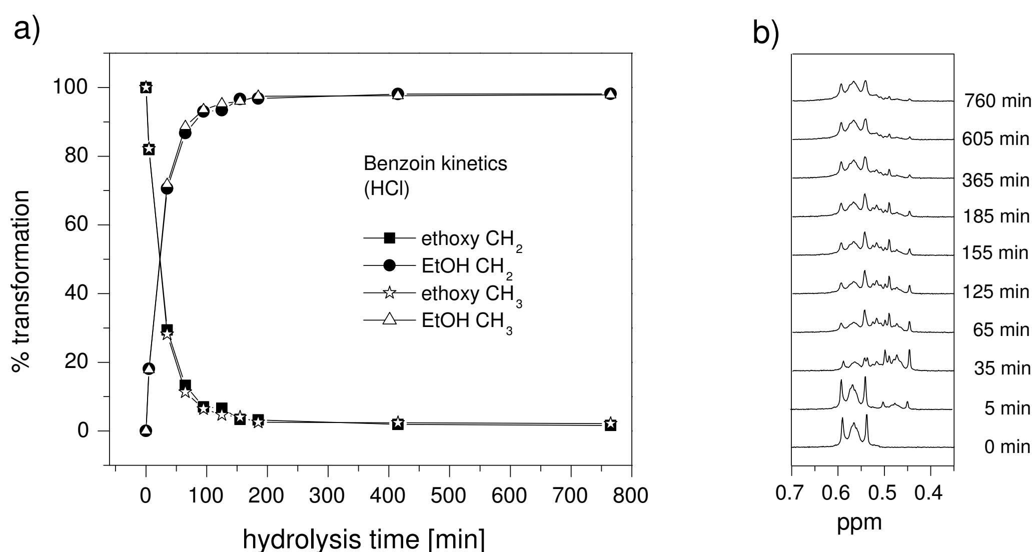

Figure 6.12: *a) Kinetic experiments for monitoring the hydrolysis of benzoin using 2 μl 1N HCl as a catalyst in a 1ml d_8-THF silane solution. % calculations are based on increase of ethanolic CH_2 and CH_3 and decrease of ethoxy CH_2 and CH_3 in the liquid ^1H NMR spectrum of the hydrolysing benzoin solution in d_8-THF, b) ^1H NMR chemical shift of Si-$\boldsymbol{CH_2}$ during hydrolysis.*

NaOH, NaOH was used for further hydrolysis experiments. Considering the NVoc silane that was going to be used for mixed silane layer deposition, NaOH has to be preferred. This is due to the fact that catalytic amounts of HCl during hydrolysis may cleave the NVoc carbamate group, as observed by del Campo [del Campo a].

6.5 Time Dependant Irradiation and UV Measurements

In order to photo-selectively cleave the protecting groups, appropriate parameters had to be found to optimise time and wavelength for the deprotection. The kinetics of the photocleavage of the silanes was monitored by UV-spectroscopy of layers with photo-protected silane on quartz wafers that had been irradiated with different light sources. The benzoin possesses a chromophore adsorption at around 250 nm, which can be assigned to n-π* transition of the carbonyl moiety, as shown in the UV spectra of the silanes (Fig. 6.15). NVoc bears the carbamate group that acts as a chromophore and absorbs at ca. 220 and ca. 250 nm for the N-H and carbonyl moiety, respectively, whereas the nitro group on the methoxy-substituted benzene ring adsorbs at around 360 nm.

From Woodward and Patchornik it was known that the nitroveratryl (NVoc) group for amine protection could be irradiated with wavelengths longer than 320 nm [Patchornik 70]. The photolysis liberates the desired free amine, carbon dioxide and an *ortho*-nitrosobenzaldehyde

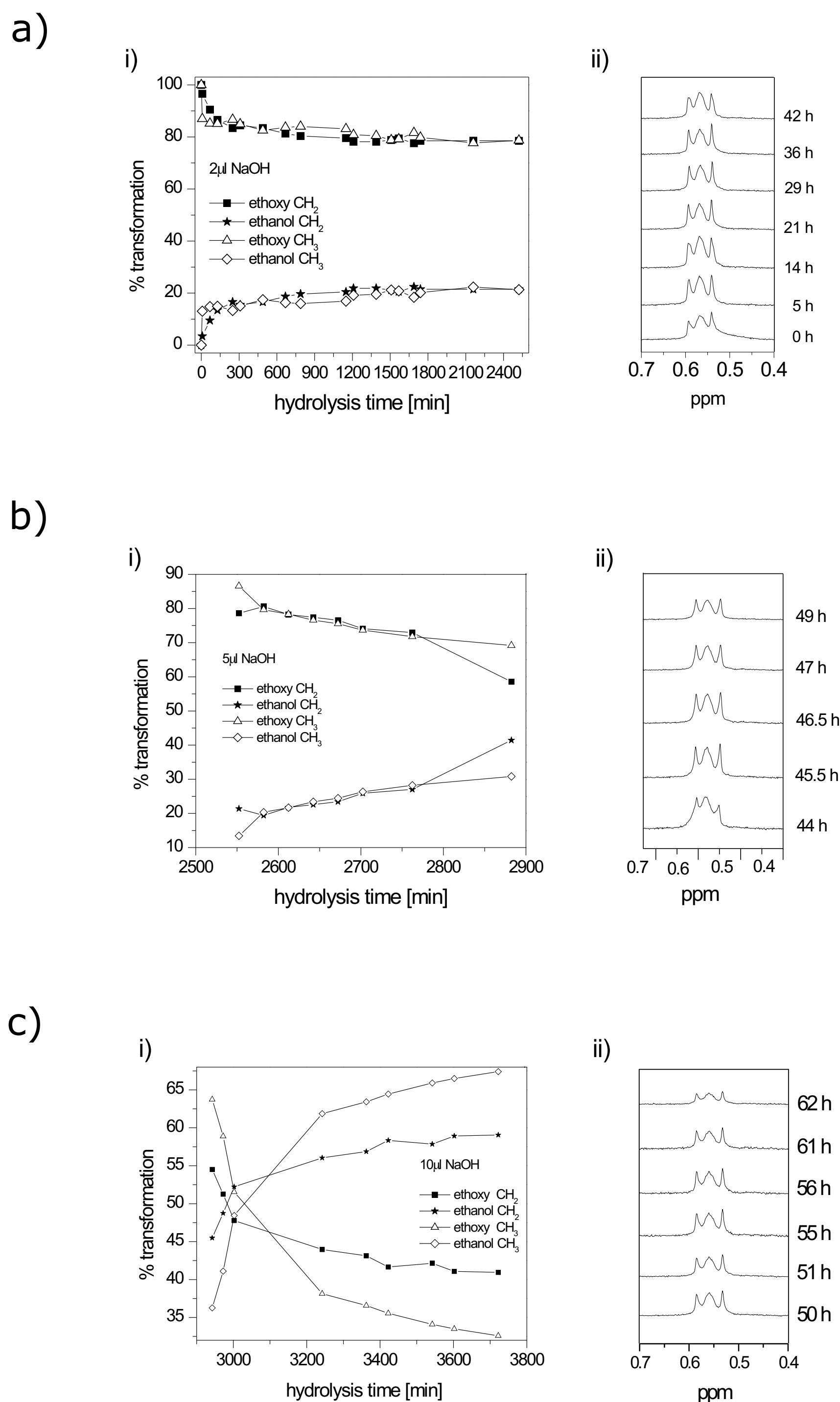

Figure 6.13: *a) Kinetic experiments for monitoring the hydrolysis of benzoin using NaOH as a catalyst. % calculations are based on increase of ethanolic CH_2 and CH_3 and decrease of ethoxy CH_2 and CH_3 in liquid ^1H NMR spectrum of the hydrolysing benzoin solution in d-THF, b) ^1H NMR chemical shift of Si-$C\boldsymbol{H}_2$ during hydrolysis.*

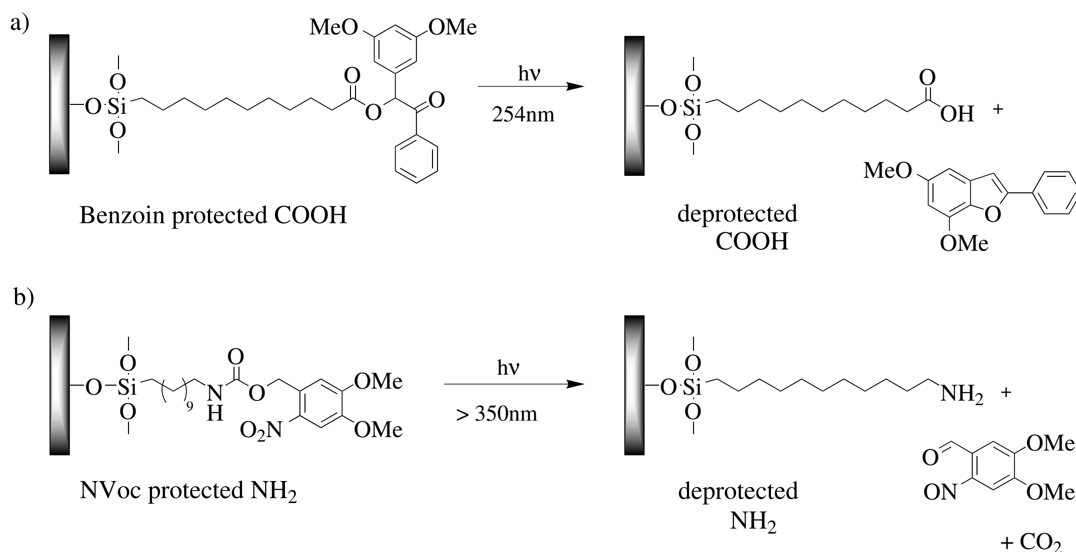

Figure 6.14: *Irradiation and deprotection of a) Bz protected COOH to yield free carboxylic acid and a benzofuran photoproduct and b) NVoc protected NH_2 at ≥350 nm to yield the free amine and a nitrosobenzaldehyde derivative.*

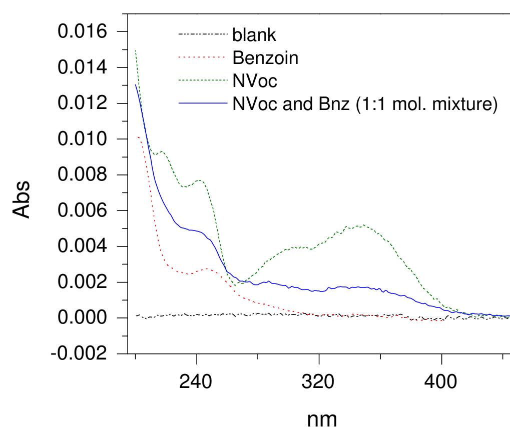

Figure 6.15: *UV absorption spectra of benzoin protected silane, NVoc protected silane and a 1:1 molar mixture of both silanes on a quartz substrate.*

derivative (Fig. 6.14). On the other hand, the benzoin moiety is known to be very reactive, when irradiating at low wavelengths (ca. 250 nm) [Chamberlin 66, Cameron 91, Bochet 00]. The irradiation sources used in this work consisted of a UV hand lamp at 254 nm lamp (610 μW·cm^{-2}) and at 365 nm (400 μW·cm^{-2}), a UV crosslinker with both 254 nm and 365 nm light bulbs and an irradiance of 3.03 and 2.77 mW·cm^{-2}, respectively and an Ar laser at 365 nm (continuous wave, 400 mW·cm^{-2}). Quartz substrates containing only benzoin silane

and only NVoc silane were irradiated first with the different irradiation sources in order to delineate the relative reactivity of each protecting group, thus optimising the conditions for substrate irradiation with both protecting groups on the surface. After irradiation the samples were cleaned in an ultrasound bath to remove the formed photoproducts.

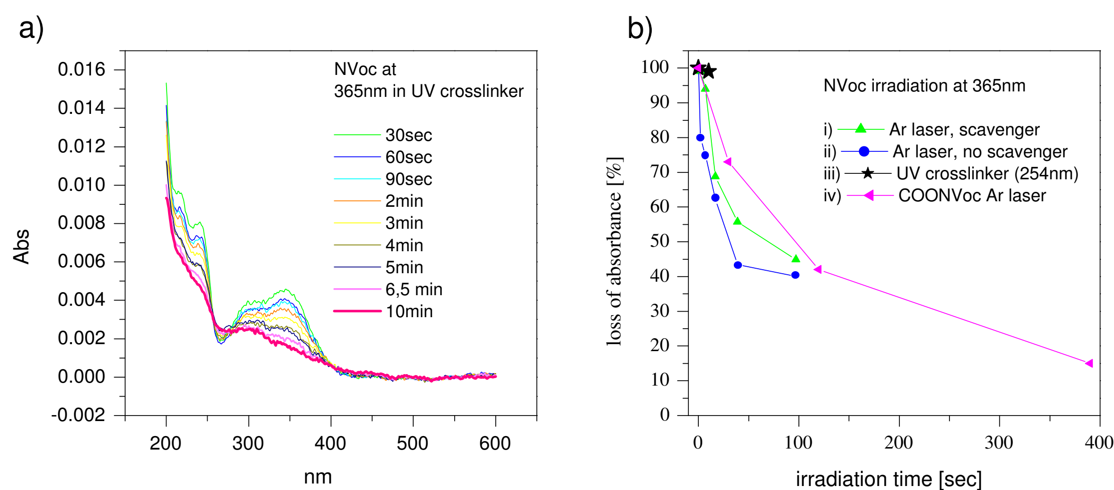

Figure 6.16: *Cleavage of NVoc photo-protecting group: a) visible as loss of absorbance at λ_{max}=345m due to irradiation of NVoc silane with UV crosslinker at 365 nm (3 mWcm^{-2}); b) comparison of different light sources for deprotection at 365 nm, measured as loss of absorbance of the chromophore at λ_{max} = 345 nm.*

The kinetics of the deprotection reaction of the NVoc by irradiation at λ = 365 nm (3.03 mW·cm^{-2}) are shown in Fig. 6.16a. It is clear that nearly all the NVoc is deprotected after 10 min. It is also visible that not all of the intensity is lost, indicating the formation of an imine after to the reaction of the aldehyde photoproduct with the free primary amine group. The imine λ_{max} is around 270 nm and from the spectra it is visible that even though the overall intensity of the NVoc is decreasing upon irradiation, the local maximum around 290 nm shows a higher intensity compared to the local maximum around 360 nm than before irradiation. This problem has been overcome in the literature by adding scavenger molecules to the substrate, such as hydrazine, hydroxylamine hydrochloride or semicarbazide hydrochloride. The latter was then added in a new deprotection experiment. However, it was observed that the NVoc's residual absorption in the presence and absence of a scavenger molecule (ii) did not fall below 40% (Fig. 6.16b). It is assumed that some of the head groups are imbedded into the polymerised silanol matrix and that the steric hindrance neither allows the scavenger molecule to penetrate this matrix nor does it allow the potential scavenger product to diffuse out again. Therefore some of the cleaved NVoc chromophores are still

present inside the matrix even after extensive washing.
When a NVoc protected carboxylic acid silane was irradiated at 365 nm, no imine formation occurred since deprotection does not lead to an aldehyde photoproduct. This result corroborates the hypothesis of the imine formation in NVoc protected amine layers.

Irradiation of benzoin protected silane occurs much faster as visible in Fig. 6.17a. Using a standard UV hand lamp with 610 μW·cm^{-2} and a UV crosslinker with 3.03 mW·cm^{-2} irradiance it was possible to deprotect the silane within 220 and 45 s, respectively. The

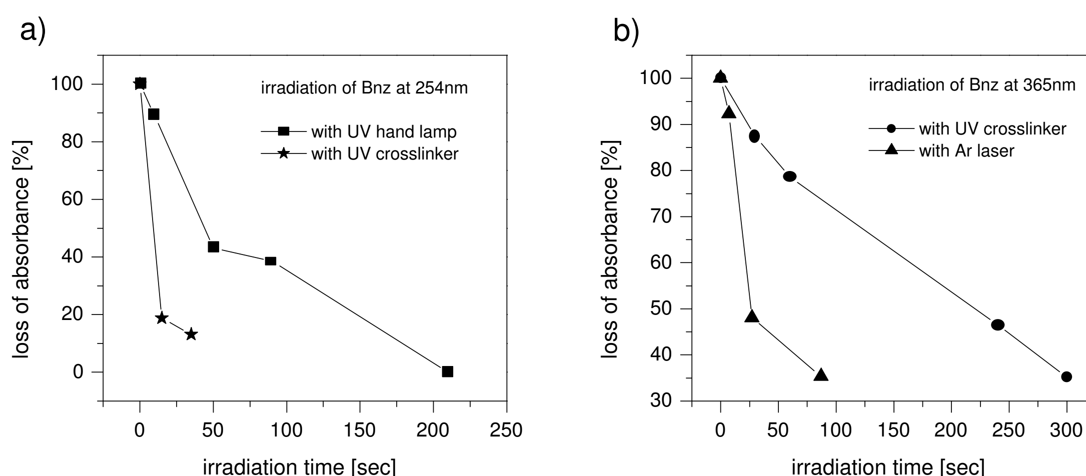

Figure 6.17: *Irradiation of Bnz protected silane at a) 254 nm using a UV hand lamp and a crosslinker and b) at 365 nm using a UV crosslinker and an Argon laser; in both figure loss of absorbance is measured at λ_{max} = 245 nm.*

shorter wavelength makes the irradiation more energetic and therefore the Bnz protecting group is cleaved off much quicker than the NVoc group, where the longer wavelength makes the light beam less energetic. However, the benzoin group is also cleaved by irradiation at 365 nm (Fig. 6.17b). When irradiating the Bnz group at 365 nm using a UV crosslinker (2.77 mW·cm^{-2}) a nearly complete removal of the chromophore group is visible within 300 s. Irradiation with the much more powerful Argon laser at 365 nm leads to an even faster removal of the chromophore within 100 s.

Even though the benzoin group did not remain completely stable under irradiation conditions with 365 nm UV light, it could still be shown that the chromophores in the Bnz group further decreased on a mixed Bnz/NVoc substrate upon irradiation with 254 nm UV light, after it had already been irradiated with 365 nm. In Fig. 6.18 most of the NVoc group is deprotected after 5 min with 365 nm light. The NVoc's absorbance maxima are 230, 250 and 360 nm for the

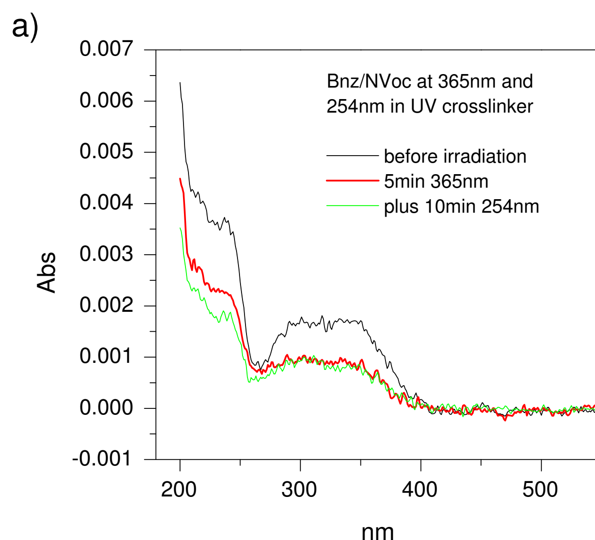

Figure 6.18: *Irradiation of a mixed Bnz/NVoc substrate: a) at 365 nm in a UV crosslinker to deprotect the amine groups and b) further irradiation of the same sample with 254 nm in UV crosslinker to deprotect the carboxylic acid groups.*

amide, methoxy, and the nitro group on the aromatic ring, respectively and their decrease is clearly visible. A decrease of the benzoin chromophore at ca. 250 nm can also be seen. When irradiation the same sample for further 10 min at 254 nm the benzoin chromophore looses more in intensity whereas the NVoc group remains stable.
From the liquid UV spectra (Fig. 6.19) it is visible that the absorbance of the benzoin silane is tailing off until about 380 nm. Even though the main absorption maximum lies around 250 nm it is therefore possible for the benzoin chromophore to absorb at higher wavelengths. Even though light at 365 nm is less energetic, benzoin is able to absorb enough photons in order to undergo a photochemical reaction that results in the removal of the protecting group.

It was therefore necessary to find an optimum wavelength that would both cleave the NVoc protecting group but not affect the Bnz group. The optimum wavelength was therefore assumed to lie between 400 and 420 nm, thus still guaranteeing an absorbance by the NVoc chromophores but no absorption of the benzoin chromophores.

The best irradiation source was found in form of a pulsed Titanium:Sapphire (Ti:Sa) laser guaranteeing both a monochromatic and parallel light at 411 and 420 nm. NVoc protected silane was then irradiated from 2 s to 5 min at 411 nm (8 KHz, 100 mWcm^{-2}),

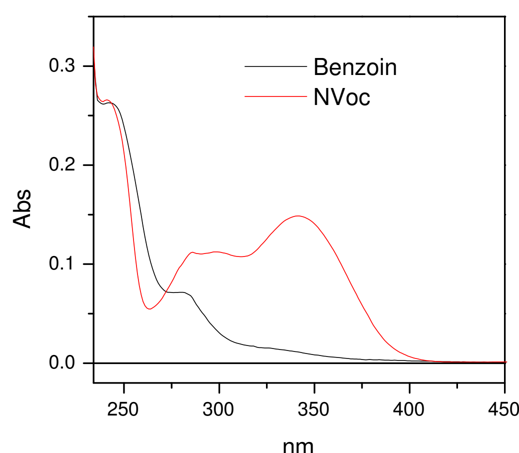

Figure 6.19: *Liquid UV spectrum of Bz and NVoc in THF showing the absorption maximum of benzoin tailing off until 380 nm.*

but hardly any deprotection was visible. This was surprising since irradiation of the NVoc group in the UV crosslinker at 365 nm with an intensity of only 3 mW·cm^{-2} took 10 min for deprotection. Therefore it was expected that the much more powerful Ti:Sa laser would remove the protecting group much faster than the UV crosslinker. It was concluded that this must be due to the less energetic nature of the light beam at 411 nm. Furthermore, with an extinction coefficient of 8516 Lmol^{-1}cm^{-1} for the NVoc group, chromophores absorb less light anyway, so that above 400 nm deprotection takes even longer.

Since Blanc and co-workers [Bochet 02] also deprotected their NVoc groups at 420 nm, irradiation experiments were then undertaken at 420 nm (200 mWcm^{-2}) with longer irradiation times. Indeed it was possible to remove more than 60% of the NVoc protecting group after 90 min (Fig. 6.20). Irradiation of the benzoin moiety under the same conditions left the protecting group intact, with a maximum loss of absorbance w.r.t. the absorption maximum at ca. 250 nm of 10%. In an effort for avoiding such long irradiation times, a new set of experiments was undertaken where irradiation of the NVoc group was carried out at 411 nm but using double the power, namely 200 mWcm^{-1}, thus still guaranteeing an absorption by the NVoc chromophore, but with the anticipation of leaving the benzoin moiety untouched. After already 15 min, the absorption maximum of the NVoc chromophore at ca. 350 nm has indeed decreased by about 50% (Fig. 6.21a), whereas the benzoin absorption at ca. 250 nm has hardly been reduced and does not decrease further after irradiation of 1 hour (Fig. 6.21b). NVoc removal continues upon further irradiation and levels out at ca. 45%.

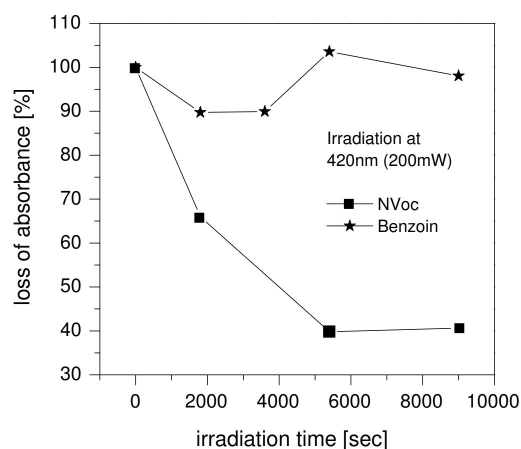

Figure 6.20: *Deprotection of the NVoc and Bnz group at 420 nm using Ti:Sa laser with an irradiance of 200 mWcm^{-2}; measured from the loss of absorbance at λ_{max} = 245 nm.*

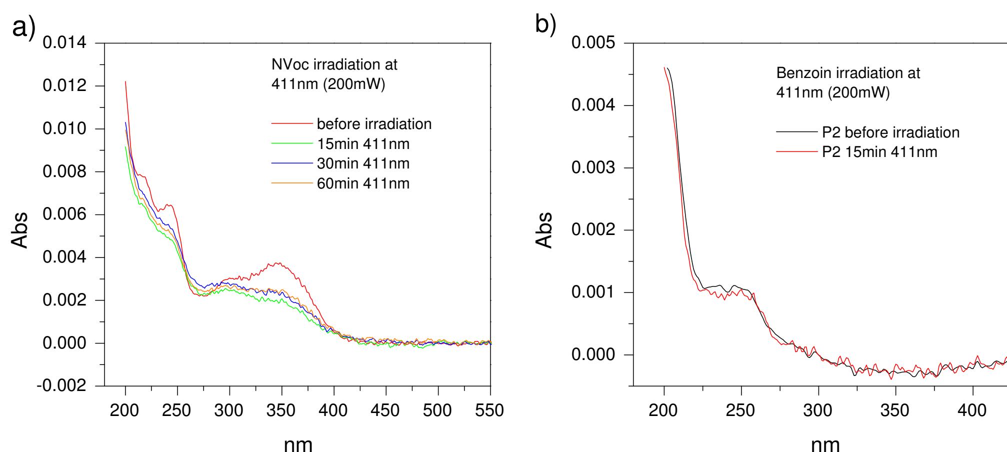

Figure 6.21: *Deprotection of the NVoc and Bnz group at 411 nm using Ti:Sapphire laser with an irradiance of 200 mWcm^{-2}.*

Since it was clear that the best irradiation source for deprotection of the NVoc silane was the Ti:Sa laser at 411 nm, the wafers were then irradiated through a gold mask in order to generate a pattern on the wafer surface. Yet, a problem that had not been anticipated was encountered when irradiating quartz wafers through a gold mask with 254 nm in the UV crosslinker. From

experiments carried out in the following section (Chapter 6.7), it became clear that irradiation of the quartz wafers through a gold mask in the UV crosslinker led to a deprotection of all photolabile protecting groups on the surface. When looking at the UV crosslinker setup it becomes clear why this is the case: The UV crosslinker used is a device that has five UV tubes fitted to the top inside the box and the sample to be irradiated is placed flat on the bottom of the crosslinker with the mask on top of it. Upon irradiation, the non-parallel light of the light bulbs then penetrates the quartz surface mainly were the surface is not covered by the gold mask, but also from all sides, and is reflected on the bottom of the crosslinker. Upon reflection inside the quartz wafer, the light therefore deprotects the remaining photolabile groups from underneath when passing through the wafers again.
A new irradiation source was therefore required that could yield a parallel light of 254 nm. Again the solution was found in form of the Ti:Sa laser, but this time with a frequency tripling in order to create 254 nm. Even though the irradiance of the laser output was in the same magnitude as the irradiance in the UV crosslinker (which was 3 $mWcm^{-2}$), new irradiation test had to be undertaken to guarantee optimum deprotection and to make sure that the NVoc group was not affected by this new laser light.

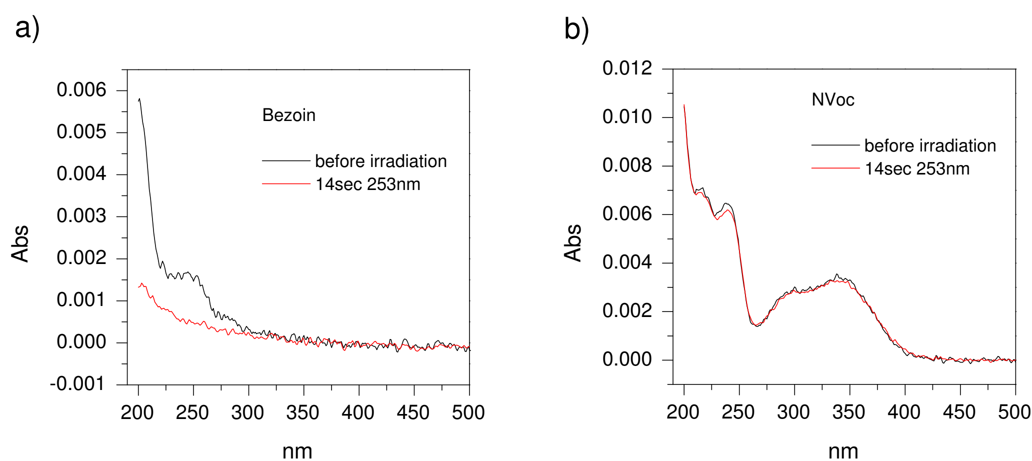

Figure 6.22: *Deprotection of the NVoc and Bnz group at 253 nm with an irradiance of ca. 5 $mW \cdot cm^{-2}$ using Ti:Sa laser.*

A quartz wafer with SAMs of only benzoin protected silane and a quartz wafer with SAMs of only NVoc protected silane were therefore irradiated with the laser and their UV spectra were recorded. It is visible from Fig. 6.22a that nearly all benzoin is deprotected after 14 s whereas the NVoc silane (Fig. 6.22b) is not affected at all by this wavelength.

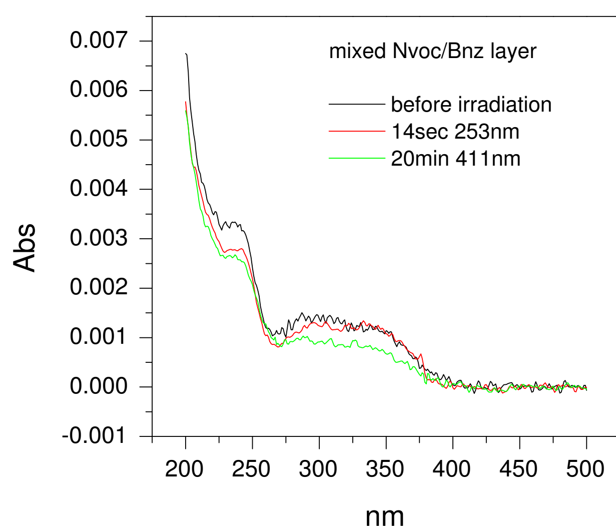

Figure 6.23: *Deprotection of mixed NVoc/Bnz substrate with 253 nm first and then 411 nm using Ti:Sa laser.*

In order to finally prove the concept of orthogonality a quartz wafer bearing SAMs of both NVoc and Bnz protected silane in 1:1 molar mixture was then irradiated first with 253 nm and then with 411 nm using the Ti:Sa laser. Upon irradiation with 253 nm (5 mWcm^{-2}), the absorption maximum of the Bnz groups at ca. 240 nm should therefore decrease, whereas the absorption maximum of the NVoc at ca. 345 nm should remain stable and *vice versa*, when irradiating the sample again with 411 nm.
A decrease of the absorption maximum of the Bnz groups at ca. 245 nm is indeed visible when irradiating with 253 nm, whereas the λ_{max} of NVoc at 335 nm remains stable (Fig. 6.24). The slight decrease at around 300 nm in the UV spectrum is again due to the removal of the benzoin groups. Upon irradiation with 411 nm for 20 min, it is also visible that the benzoin moiety remains stable, whereas the absorption maximum of the NVoc at ca. 345 nm has been decreased by more than 30%.

Using the data obtained from these measurements, the wafers were then site-selectively irradiated through a gold mask to generate a complex structure on the surface. First, substrates modified with a single silane layer, were irradiated with the appropriate wavelength through a mask and then a mixed silane substrate was irradiated with λ_1 through a mask with alternating gold stripes and again with λ_2 through the same mask that had been rotated around 90° in order to create a square pattern (Fig. 6.24).

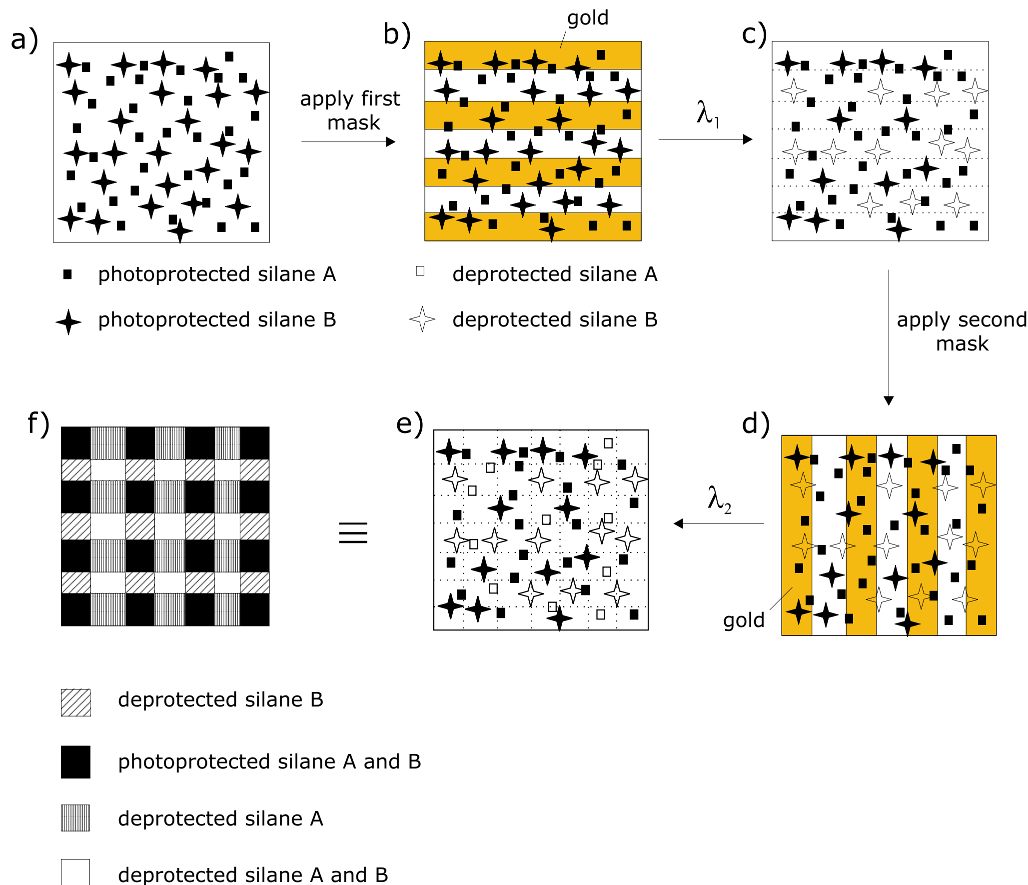

Figure 6.24: *Deprotection scheme of mixed silane substrate with 2 different wavelengths: two photoprotected silanes are assembled on wafer surface (a), first mask is applied (b) and first silane is irradiated at λ_1 (c), after applying second mask (d) the second silane is deprotected with λ_2 (e), which leads to formation of a squared pattern on the surface bearing different silane compositions (f).*

The silane substrates used for irradiation experiments with the gold mask consisted of:

1. NVoc protected amine silane (NH_2), *irradiated for 30 s at 365 nm through gold mask with Ar laser*
2. NVoc protected NH_2 and NVoc protected COOH (as a binary mixture), *irradiated for 30 s at 365 nm through gold mask with Ar laser*
3. NVoc protected carboxylic acid silane (COOH), *irradiated for 30 s at 365 nm through gold mask with Ar laser*
4. Bnz protected COOH, *irradiated for 40 s at 245 nm through gold mask with UV crosslinker*

5. Bnz protected COOH and NVoc protected NH_2 (as a binary mixture), *irradiated first at 411 nm with Ti-Sapphire laser through gold mask with the stripes aligned vertically and then at 254 nm with the UV crosslinker through the same mask with the stripes aligned horizontally*

The successful deprotection can then be demonstrated by colloidal particle assembly and by fluorescence labelling of the now liberated free functional groups, and subsequent observation of the pattern under the microscope.

6.6 Colloidal Assembly on Site-Selectively Irradiated Wafers

After a Bnz/NVoc modified silicon wafer had been irradiated through a mask at 254 nm with a UV crosslinker, the particles were deposited on the surface *via* the drop-coating method. Colloidal adsorption experiments were carried out using PBMA-COOH particles at pH 7.

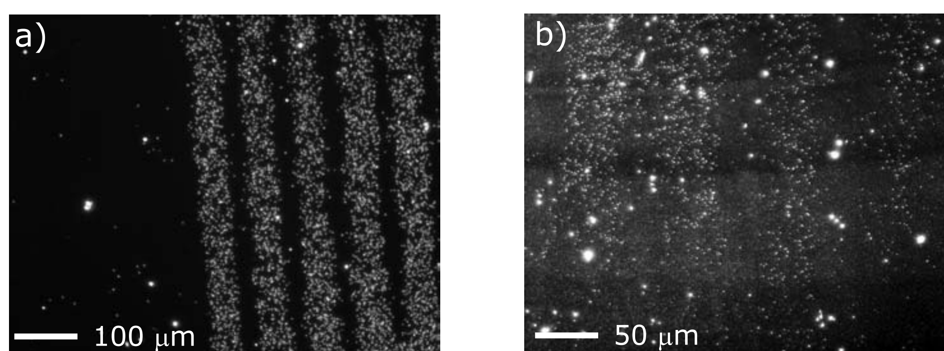

Figure 6.25: *Optical microscopic images (darkfield) of colloidal adsorption at pH 7 on Bnz/NVoc modified silicon wafers: a) wafer irradiated at 254 nm in UV crosslinker, with PBMA-COOH adsorption; b) wafer irradiated at 411 nm and 253 nm using Ti:Sapphire laser, with PS-10 adsorption.*

Considering the pK_A of carboxylic acid group (which is ca. 5), the COOH groups on the surface and on the particles are partly dissociated, leading to the exertion of H-bonds between the groups. Fig. 6.25a shows indeed, the colloidal particles have adsorbed onto the deprotected COOH regions of the substrate.
When irradiating another Bnz/NVoc modified silicon wafer first at 411 nm and then at 254 nm with a Ti:Sapphire laser, a faint pattern could be detected after adsorption of colloidal PS-10 particles at pH 7 (Fig. 6.25b).
These adsorption experiments clearly indicate the successful irradiation of photo-protected silane layers on a silica surfaces.

6.7 Fluorescence Labelling

Since the irradiation experiments were supposed to yield active COOH and NH_2 groups, their presence had to be verified. A common and well known method is fluorescence staining with fluorophore dyes. If the fluorescence labelling showed the presence of a pattern on the substrates, it would be clear that the irradiation had worked correctly and that the irradiated functional groups were indeed active on the surface.

6.7.1 Fluorescent Dyes

Two fluorophores were used, namely Alexa Fluor 488 and Alexa Fluor 546. The green fluorescent dye Alexa Fluor 488 (AF 488) exhibits a fluorescence spectrum with an excitation and emission maximum of ca. 491 and 515 nm, respectively. It is water soluble hence requiring no organic solvents, and stable between pH 4 and pH 10. Since it is more stable than fluorescein more time can be allowed for observation and image capturing. AF 488 can be used for both amine and carboxylic acid coupling. Amine coupling occurs with AF 488 succinimidyl ester, which forms an amide bond between the fluorophore and the surface. Carboxylic acid coupling, on the other hand occurs with AF 488 hydrazide sodium salt that forms a substituted hydrazone with the EDC/NHSS activated carboxylic acid group on the surface.

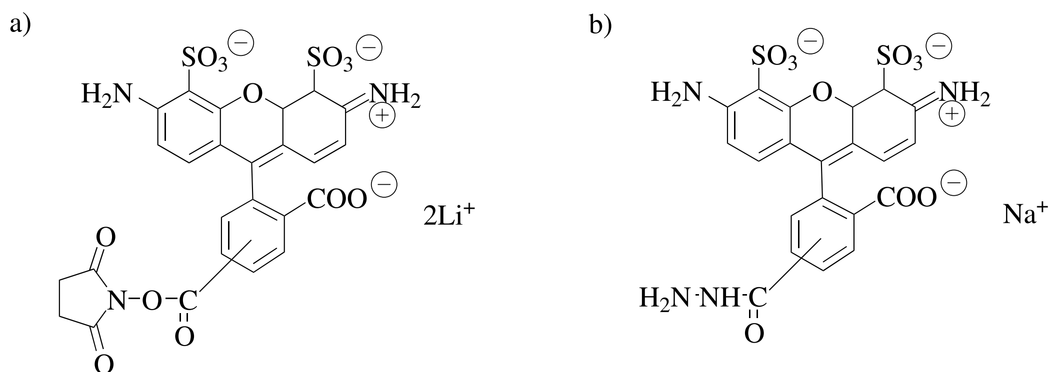

Figure 6.26: *a) Alexa Fluor 488 succinimidyl ester for amine coupling b) Alexa Fluor 488 hydrazide sodium salt for carboxylic acid coupling.*

Alexa Fluor 546 (AF 546), which emits in the orange range of the spectrum, provides good contrast to AF 488. It exhibits an excitation and emission maximum of ca. 553 and 569 nm, respectively and it is photostable. Just as AF 488 it is pH insensitive and water soluble. AF 546 was used in its succinimidyl form for coupling with the amine surface. The fluorescence

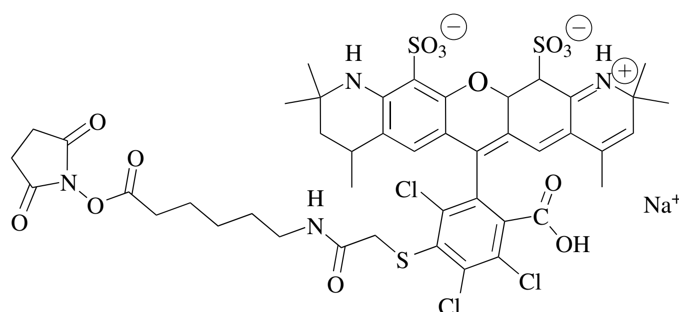

Figure 6.27: *Alexa Flour 546 succinimidyl ester for amine coupling.*

markers were then coupled to the free amine and carboxylic acid groups on the wafers surface according to Chapter 7.4.

6.7.2 Results

Fluorescence staining was tested on irradiated NVoc-NH_2 modified substrates and on irradiated NVoc protected NH_2/COOH mixed layers.
NVoc protected NH_2 was incubated with AF 488 succinimidyl ester in DMSO overnight. After washing with water, a pattern was visible under the fluorescence microscope (Fig. 6.28a). Since the Alexa Fluor dyes are known to be insensitive to pH the experiment was repeated with AF 546 succinimidyl ester in DMSO but washing afterwards with a phosphate buffer saline (PBS) solution of pH 7.2. Thus, the background fluorescence could be reduced, which resulted in a better contrast of the fluorophore pattern to the surface background (Fig. 6.28b). The pattern observed clearly showed the presence of the fluorophore but also showed the inverted pattern on the surface. Inverted pattern means that the fluorescent dye has adsorbed preferentially onto the non-irradiated areas of the wafer, where usually no reaction should have occurred since no free amine groups were present in these areas. The gold-covered parts of the mask are scratched during normal handling and leave a fingerprint on the pattern that permits the identification of irradiated and non-irradiated regions. The scratches in the mask result in a deprotection of the underlying photolabile groups and thus to a coupling of the dye with these irradiated areas. In a “true” pattern these scratches would be visible as bright “threads” between irradiated regions that have coupled with the bright fluorophore. However, if the dye couples only with non-irradiated regions , then the scratches appear dark against the fluorophore background, thus telling the observer that the pattern is inverted.

A binary mixture of NVoc protected NH_2 and NVoc protected COOH (*irradiated for 30 s at 365 nm through a gold mask with Ar-laser*) was then incubated sequentially with both AF 488 hydrazide sodium salt and AF 546 succinimidyl ester (Fig. 6.29). Since both functional

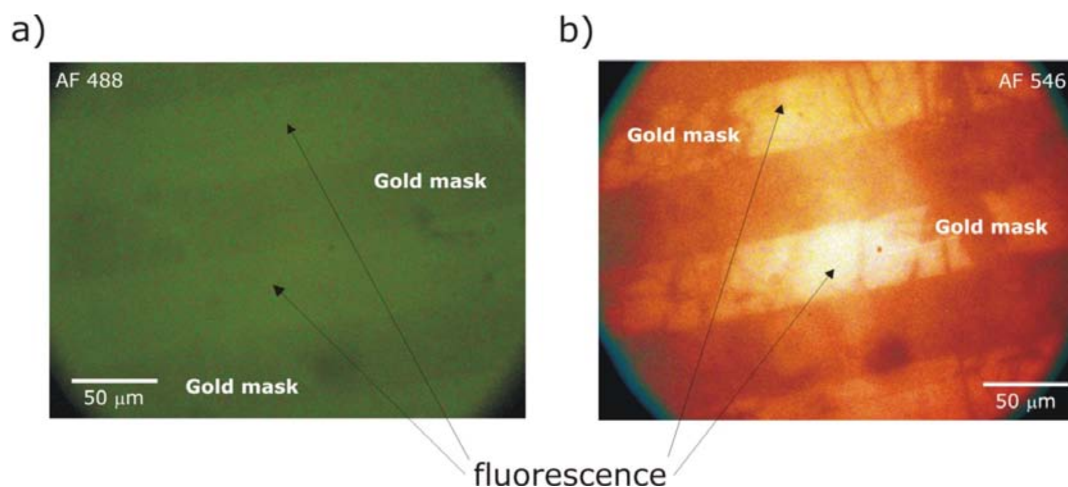

Figure 6.28: *optical microscope pictures of two substrates that were stained with a) AF 488 for coupling with carboxylic acid groups, after washing with H_2O and b) AF 546 for coupling with amine groups, after washing with buffer solution (inverted pattern). The term* gold mask *denotes the regions where the gold mask has been during irradiation.*

groups were liberated in the same region upon deprotection (since both groups were carrying the same NVoc photolabile protecting group), the two fluorophores were expected to be visible in the same regions under the microscope.
The binary layer was first stained with the AF 488 hydrazide salt for carboxylic acid coupling and then with the AF 546 succinimidyl ester for amine coupling. The hydrazide storage solution was diluted with PBS buffer at pH 7.2 and after incubation with AF 546 an inverted pattern was observed showing non-specific adsorption of both fluorophores onto the non-irradiated NVoc groups.
When labelling the binary layer with the same fluorophores the other way round, the desired pattern was faintly visible under the fluorescence microscope, showing successful specific coupling with the deprotected amine and carboxy groups. Unfortunately, the pattern was too weak to be recorded by the camera.
Since both dyes seemed to have coupled or adsorbed everywhere on the wafer surface, non-specific adsorption of the hydrazide dye AF 488 (that should only couple with COOH groups) onto the amine groups was investigated by incubating the amine surface with AF 488 hydrazide sodium salt in buffer overnight. The wafers were washed afterwards with a phosphate buffer at pH 8.6 in order to remove any unspecifically bound NHSS. Chemically hydrazine cannot couple with amine groups, but nevertheless, a weak fluorescence pattern could be detected, again on the non-irradiated and non-deprotected regions, indicating definitely non-specific binding.
In the next step NVoc protected COOH (*irradiated for 30 s at 365 nm through a gold mask with Ar-laser*) was incubated with AF 546 succinimidyl ester (that is used for amine coupling) in order to test any non-specific binding of the succinimide fluorophore with the carboxylic

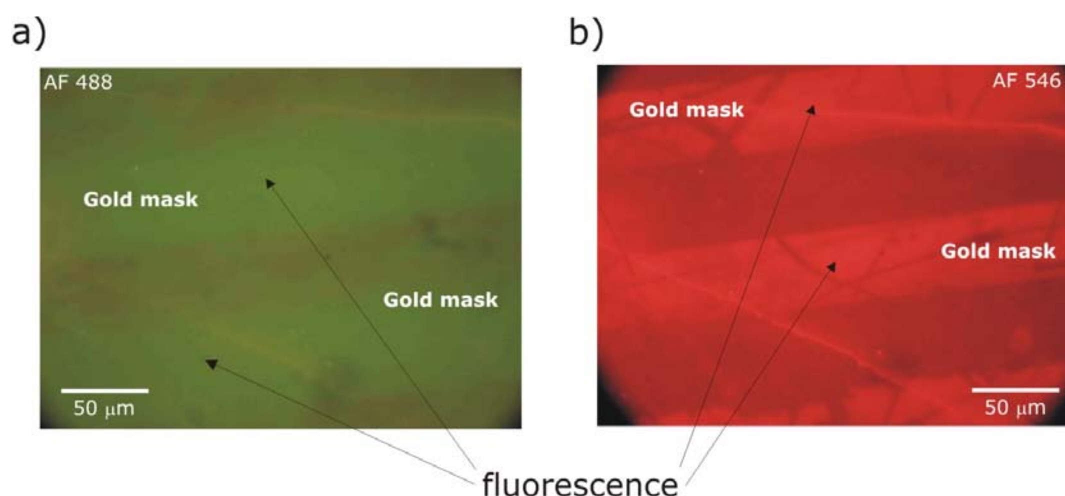

Figure 6.29: *optical microscope pictures of quartz wafers bearing both photoprotecting groups on the surface: a) AF 488 stained carboxylic acid groups, b) AF 546 stained amine groups. The term* gold mask *denotes the regions where the gold mask had been during irradiation.*

acid groups. Even though no coupling should occur between the carboxylic acid and the succinimide in DMSO a faint fluorescence pattern could be detected on the non-irradiated benzoin sites. The inverted pattern is a result of non-specific binding between AF 546 and the non-irradiated benzoin moiety.

After benzoin protected COOH was irradiated through a gold mask at 254 nm in a UV crosslinker (3mW$\cdot$cm^{-2}) for 24 s and labelled with AF 488, bright fluorescence was observed all over the wafer but no pattern. This gave reason to believe that no pattern had been present from the start (*i.e.* irradiation with the UV crosslinker led to a complete deprotection of all benzoin head groups due to internal reflection inside the quartz wafer).
Moreover, when staining a non-irradiated Bnz substrate with AF 488 hydrazide salt, fluorescence was visible after washing, indicating non-specific adsorption to the benzoin head group.

When quartz wafers bearing both Bnz protected COOH and NVoc protected NH_2 (as a binary mixture) were labelled with the two fluorescence dyes, no squared pattern as described in Fig. 6.24 could be observed (Fig. 6.30).
First, AF 488 hydrazide salt was coupled to the COOH groups and then AF 546 succinimidyl ester was allowed to react with the amine groups. A horizontal pattern was visible with both fluorescence filters. Both filters showed the same amount of fluorescence intensity on the same stripes. Since only horizontal stripes are visible in Fig. 6.30a and b, horizontal deprotection of the NVoc groups must have been successful whereas vertical deprotection of the Bnz moiety did not result in any pattern on the surface. Irradiation with the UV crosslinker at 254 nm must have removed all photolabile benzoin groups. As a result free

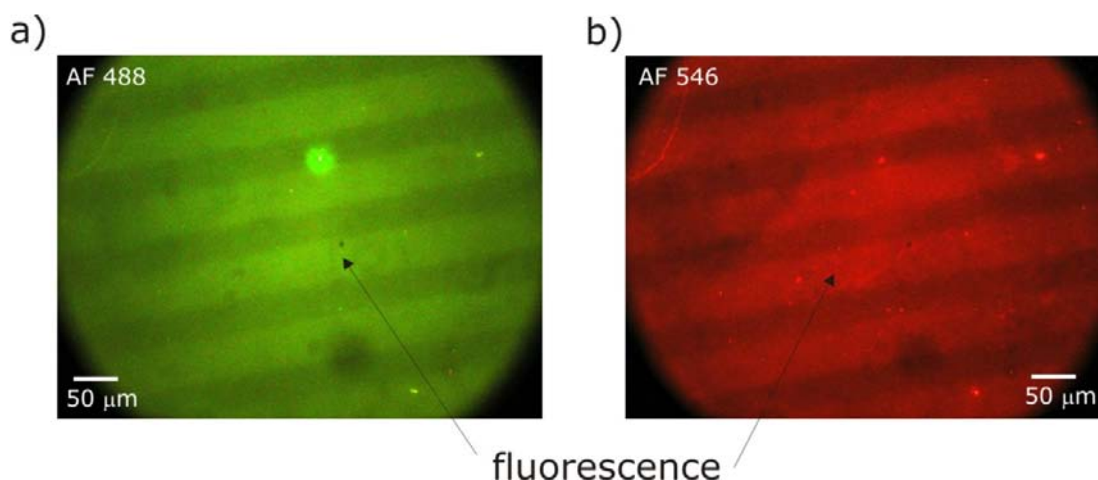

Figure 6.30: *Optical microscope pictures of mixed amine/carboxy layer stained with a) AF 488 for carboxylic acid groups, b) with AF 546 for amine groups.*

COOH groups are present all over the wafer, also on those areas where the NVoc had first been irradiated with 365 nm through the mask. Consequently, two types of stripes appeared on the surface: one stripe bearing only free COOH groups and one stripe consisting of both amine and COOH functionalities. Therefore a fluorescence pattern was observed showing regions onto which both fluorescence marker have coupled with both surface functionalities, and regions where the AF488 hydrazide only reacted with the carboxy groups. This resulted in a pattern with more and less fluorescence on the surface.

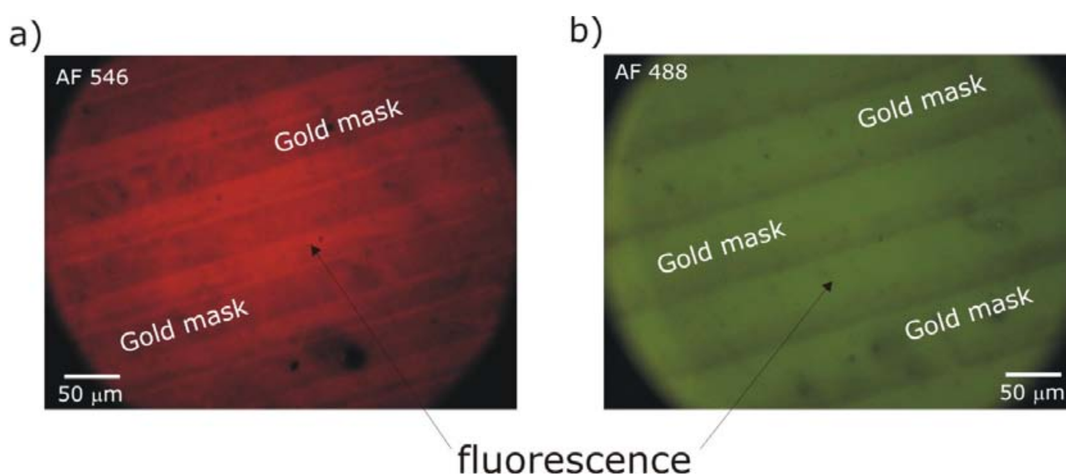

Figure 6.31: *Optical microscope pictures of mixed amine/carboxy layer stained with a) AF 546 for amine groups, b) with AF 488 for carboxy groups.*

When the same kind of wafer was stained the other way round, with first AF 546 succinimide

and then AF 488 hydrazide, again no squared pattern was visible, as visible in Fig. 6.31. In both cases a) and b), the quartz substrates had been irradiated first with 411 nm through a horizontally striped mask in order to deprotect the amine groups and then at 254 nm in the UV crosslinker through a vertically striped mask. A cross pattern was expected to be observe under the microscope. But again when coupling the mixed silane layer vice versa with the fluorescent dyes the same horizontal stripes were visible under the microscope.
The reason for this is the same as before, namely the complete deprotection of the benzoin moiety in the UV crosslinker. In between the labelled amine and carboxy stripes (Fig.6.31a, b) plenty of background fluorescence is visible that results from the complete deprotection of the benzoin moiety on the rest of the wafer.

6.8 Attachment of ODNs on Patterned Surfaces

After irradiating quartz wafers bearing either Bnz, NVoc or both protected silanes on the surface, the liberated functional groups were detected using oligonucleotide immobilisation with further hybridisation using the fluorescent labelled complementary strand. Thus, if immobilisation and hybridisation had occurred correctly, the fluorescence pattern should be visible with fluorescence or confocal microscopy (Fig. 6.32).
For coupling the oligonucleotide with an NH_2 group on the surface, an amine-terminated single-stranded 25-mer thymine oligodeoxynucleotide (NH_2-C_6-spacer-5'-$_dT_{25}$-3')[1] was used with glutaraldehyde as the coupling agent for immobilisation. The complementary adenine strand having the fluorescent marker (fluorescein) attached to the 5'end (5'-$_fA_{25}$-3') was then used for hybridisation. For coupling with the carboxylic acid group the same single-stranded oligodeoxynucleotide (NH_2-C_6-spacer-5'-$_dT_{25}$-3') could be used by immobilisation with NHSS and EDC. The same complementary fluorescence marker 5'-$_fA_{25}$-3' was then used again for hybridisation. When carrying out immobilisation experiments with mixed silane layers, two different ODNs (ssC_{25} and ssT_{25}) were used, and hybridised with their Cy3 and Cy5 labelled complementary sequence.

6.8.1 Substrate Preparation

Coupling of the amide surface group with glutaraldehyde resulted in an imine bond. After incubation with $ssNH_2$-C_6-spacer-5'-$_dT_{25}$-3', a second imine bond was formed that was later reduced back into an a more stable amine bond using $NaBH_3CN$. The substrate was then left in a 80 °C warm water bath (18 MΩ·cm) for 1 minute to denature any none-specifically bound oligonucleotide base pairs.

[1] C denotes the base cytosine and G denotes the base guanine

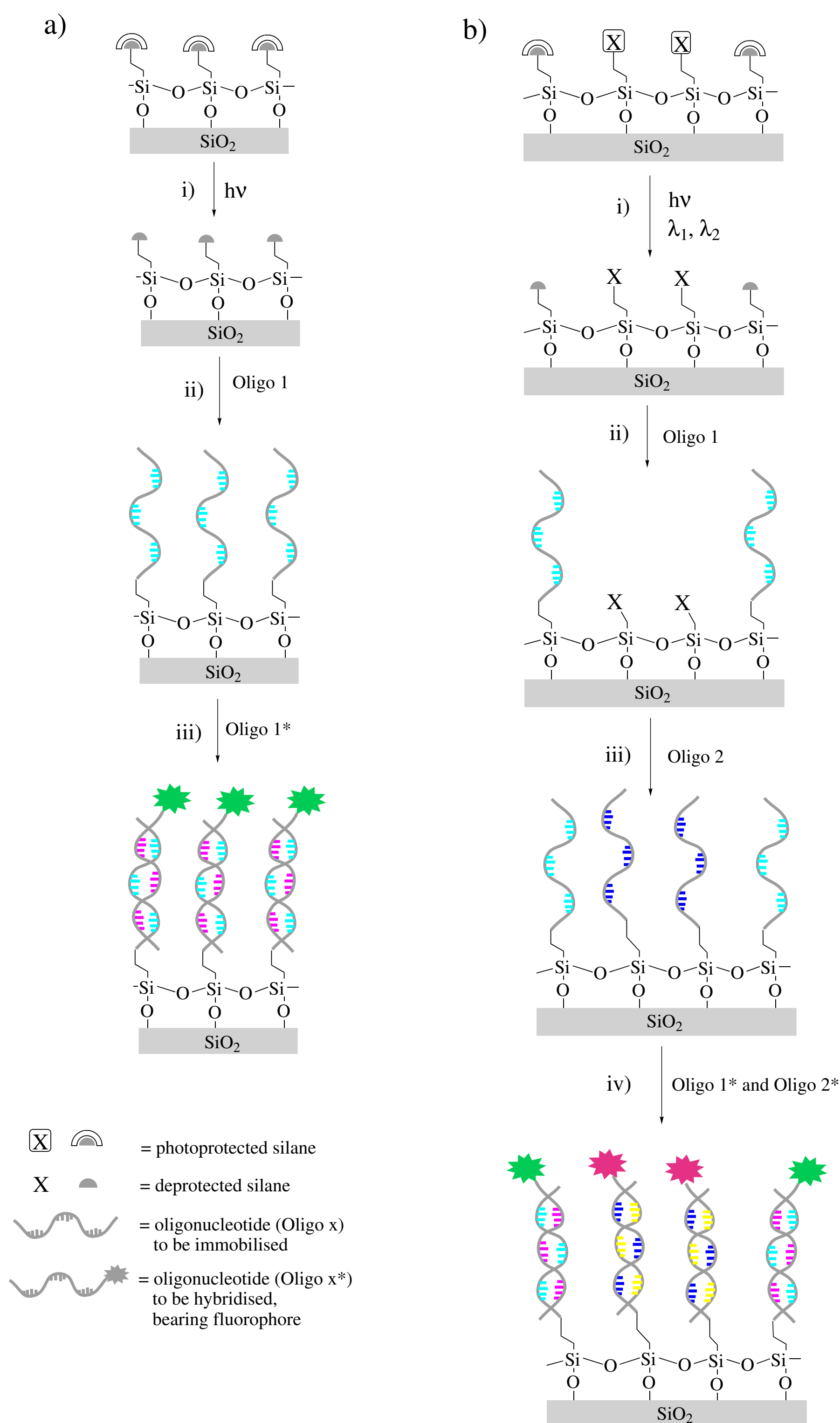

Figure 6.32: *Scheme of oligonucleotide immobilisation and further hybridisation; a) SAM of single photo-protected silane: irradiation (i), immobilisation of oligonucleotide onto free functional groups (ii), hybridisation with fluorescent labelled complementary strand; b) SAM of mixed photo-protected silanes: irradiation with both wavelengths (i), immobilisation of first oligonucleotide (ii), immobilisation of second oligonucleotide (iii), hybridisation with 1:1 mixtures of both fluorescent labelled complementary strands (iv).*

For immobilisation of the oligonucleotide onto the carboxylic acid surface groups, the substrate was placed into a buffer solution (pH 7.2) for 30 min to equilibrate the pH for the coupling with the COOH groups on the surface. Coupling agents NHSS and EDC were spotted on the substrate to activate the carboxylic acid functions. After incubation with ssNH_2-C_6-spacer-5'-$_dT_{25}$-3' an amide bond was formed.
When two different oligonucleotides were immobilised on a substrate bearing both amine and carboxylic acid groups on the surface, the first oligonucleotide was immobilised onto the primary amine groups on the surface (e.g. ssT_{25}) and then the second oligonucleotide (e.g. ssC_{25}) was then immobilised onto the carboxy functionalities on the surface (as illustrated in Fig. 6.32b).
The reason for first coupling with the amine groups and then with the COOH moiety is the use of $NaBH_3CN$: When coupling glutaraldehyde with the amine, the resulting imine is reduced to an amine bond in a reductive amination with the use of $NaBH_3CN$. If coupling of the oligonucleotide to the surface had first been carried out with the COOH groups on the surface, an amide bond would have been formed. However, reaction of $NaBH_3CN$ with an amide bond can lead to formation of a secondary amine bond or maybe to a cleavage of the amide bond. Therefore, immobilisation of the oligonucleotide onto the carboxy groups was carried out after immobilisation onto the amine groups.

6.8.2 Results

ssNH_2-C_6-spacer-5'-$_dT_{25}$-3' was attached to a NVoc-deprotected NH_2 layer and then used for hybrid capturing of 5'-$_fA_{25}$-3'. It was possible to detect a weak pattern under the fluorescence microscope, which showed the successful hybridisation with the complementary fluorescence labelled oligonucleotide. Unfortunately the fluorescence was too weak to be recorded by the camera attached to the microscope.
The amino-modified oligonucleotide was also immobilised onto NVoc protected COOH *via* coupling with NHSS and EDC. After hybrid capturing with the fluorescein labelled complementary oligonucleotide, the pattern under the microscope showed the correct pattern (Fig. 6.33).

Similar experiments performed with Bnz-COOH wafers, irradiated with the Ti:Sa laser at 253 nm, showed an inverted pattern after the hybrid capture (Fig. 6.34). Fluorescence inside the non-irradiated squares is clearly visible, when immobilised 5'-$_dT_{25}$-3' was hybrid captured with Cy5-labelled 5'-$_fA_{25}$-3'. Nevertheless, this confirmed that irradiation of quartz wafers under these conditions generates regions with different adsorption properties.

The protocol for immobilising the amine terminated oligonucleotide onto carboxy functionalities was altered this time, according to Whitesides and co-workers [Lahiri 99], and an ad-

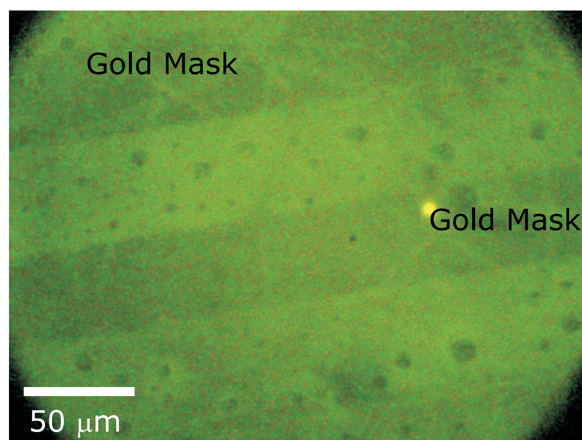

Figure 6.33: *Optical microscope picture of NVoc protected COOH silane after irradiation with 365 nm Ar-laser 488 nm; picture shows fluorescence of FTIC-labelled DNA on COOH terminated silane.*

ditional washing of the surface at pH 8.6 was introduced in order to deactivate non-reacted NHSS ester.

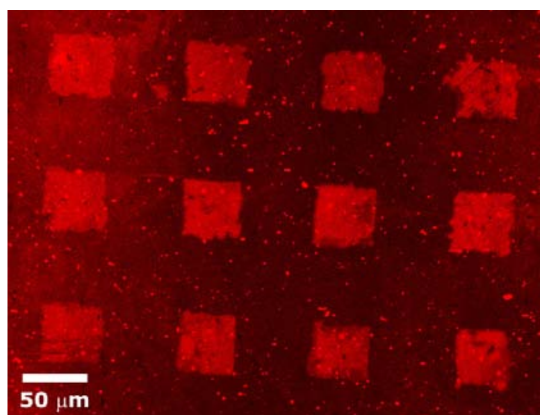

Figure 6.34: *Confocal microscope picture of Cy5 labelled DNA on quartz wafer bearing COOH terminated silane. Fluorescence is visible inside the squares, where the gold mask had been for irradiation.*

Oligonucleotides can be envisioned as polyanionic chains, capable of interacting electrostatically with the charged surface. They can form H-bonds *via* their bases with NH_2 or COOH on the surface. Van der Waals interactions between the aromatic rings of the bases and the NVoc or Bnz moieties are also possible. These interactions may be responsible for the non-specific adsorption of the ODNs onto the non-irradiated areas of the support.

Non-specific adsorption is a frequent problem when immobilising biomolecules onto

surfaces. A common way to reduce it, is to coadsorb competing molecules (such as Albumin or other proteins) that show high affinity for the surface and act as blocking agents. However, the coadsorption of these molecules makes it difficult to identify which mechanism and forces are involved in the process and therefore they are not used in these experiments.

Using a substrate modified with a binary mixture of NVoc protected NH_2 and NVoc protected COOH for immobilisation, an inverted pattern could be detected under the microscope (Fig. 6.35). The image shows that the Cy5 fluorophore of the A_{25}-mer, coupled to the amine

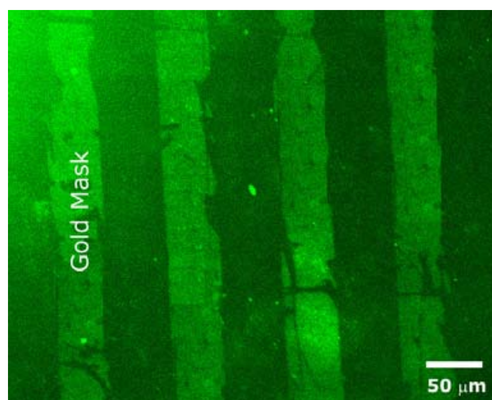

Figure 6.35: *Confocal microscope picture of mixed NVoc protected NH_2 and NVoc protected COOH layer after deprotection; Fluorescence only visible with Cy5 labelled DNA on quartz wafer bearing NH_2 terminated silane*

groups, could be detected with a much higher intensity than the Cy3 fluorophores, which are conjugated to the COOH groups. This can be due to the fact that both photoprotection groups are right next to each other in the same area. Steric crowding may lower the yield of the immobilisation of the nucleotide that is attached to the surface (in this case, the oligonucleotides attached to the COOH groups). Moreover Cy5 has an extinction coefficient of 200,000 $Lmol^{-1}cm^{-1}$ whereas Cy3 has an extinction coefficient of 133,00 $Lmol^{-1}cm^{-1}$ [Sims 74, Waggoner 89], which might lead to a domination of the Cy5 fluorophore over Cy3.

A mixed silane quartz wafer bearing Bnz protected COOH and NVoc protected NH_2 was irradiated with a striped gold mask according to Fig. 6.24, with the mask being aligned vertically for NVoc deprotection and horizontally for Bnz irradiation.
Coupling of the T_{25} oligonucleotide with the amine group on the surface was carried out first and then the C_{25} oligonucleotide was immobilised onto the carboxy groups on the surface. The complementary oligonucleotide strands A_{25} and G_{25} containing the fluorophores Cy5 and Cy3, respectively were then hybrid captured to the immobilised strands and fluorescence was detected with the confocal microscope (Fig. 6.36).

Fig. 6.36a,b shows the confocal microscope pictures of both fluorophores, as detected with

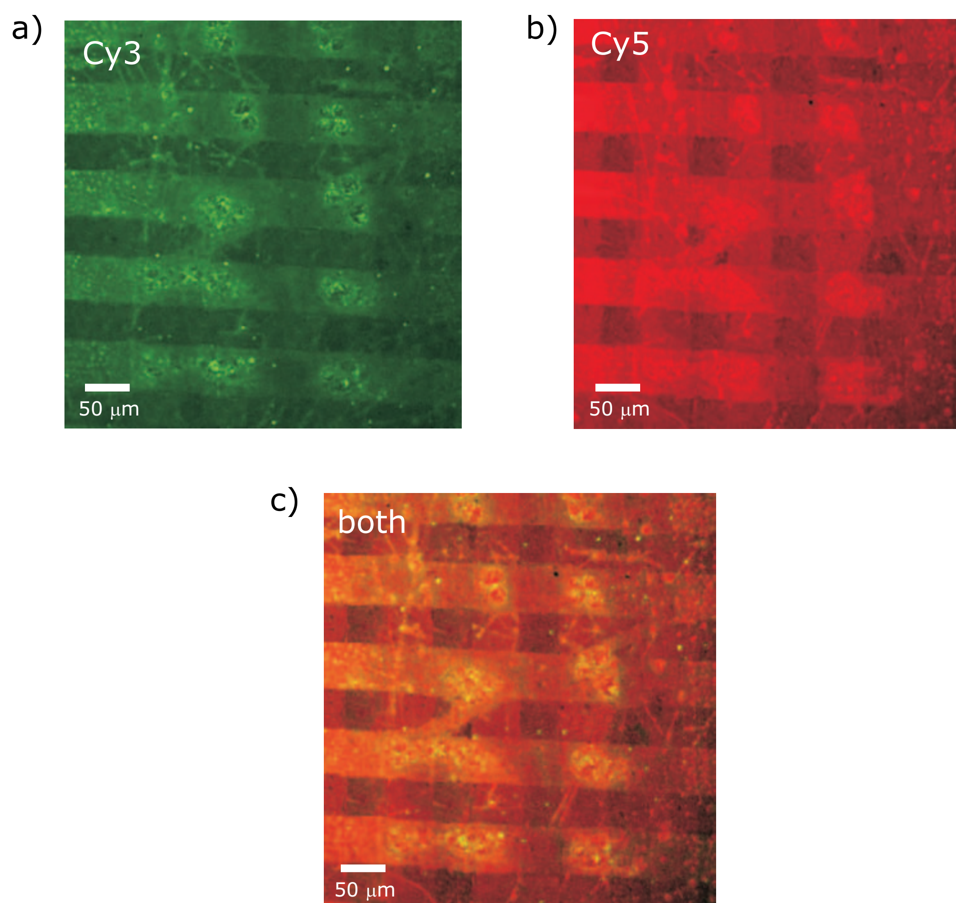

Figure 6.36: *Confocal microscope picture of a) Cy3 (excitation: 543 nm, emission: 570 nm) and b) Cy5 (excitation: 633 nm, emission: 670 nm) labelled DNA strands that have coupled to the COOH and NH_2 groups, respectively; c) shows combined images of both Cy3 and Cy5.*

their respective emission filters. Cy3 and Cy5 are denoted in green and red, respectively. Picture Fig. 6.36c shows the combined images from the confocal microscope of Cy3 and Cy5. In all three pictures the horizontal stripes refer to the irradiation with 253 nm for deprotection of the benzoin and the vertical stripes correspond to the irradiation at 411 nm for deprotection of the NVoc groups.

The single picture of Cy3 shows clearly the desired pattern of horizontal fluorophore stripes. The image of Cy5 on the other hand shows them as well, but with the vertical stripes being also faintly visible. The vertical stripes seem to lie beneath rather than "beside" the fluorescence pattern of Cy3. Therefore fluorescence resulting from the Cy5 on the amine groups is hindered and its intensity is diminished. Non-specific adsorption of Cy5 onto the horizontally irradiated Bnz regions is apparent in Fig. 6.36b. Nevertheless, the square regions on the wafer containing only labelled amine, only labelled COOH, both labelled groups together and non-labelled groups at all, are visible in Fig. 6.36c, thus proving the intact existence of both functional

groups next to each other on the wafer surface after irradiation, and proving the orthogonality of the deprotection step.

6.9 Discussion and Summary

It has been shown that alkoxysilanes bearing carboxylic acid end groups could be synthesised by optimising known reactions pathways for acyloin formation. By doing so, it was possible to synthesise a benzoin protected silane which could be used to in the chemical modification of silica surfaces. The photolabile benzoin group is a well-suited protecting group since it is easily cleaved off with UV light at 254 nm, which results in free carboxylic acid groups covalently bound to the surface and a stable benzofuran photoproduct that can then be easily removed from the surface upon washing. When modifying the surface with a 2-component mixture of orthogonal photosensitive silanes, it was then expected to selectively remove one of the protecting groups in the presence of the other in any chronological sequence. Therefore another alkoxysilane bearing an nitroveratryloxycarbonyl (NVoc) group for protection of a primary amine was allowed to form a surface layer in a 1:1 molar mixture with the benzoin silane. The NVoc group can be removed at wavelengths above 350 nm, resulting in the liberated free amine groups and a nitrosobenzaldehyde photoproduct that can easily be removed by washing the wafer in THF afterwards. The formed benzaldehyde can form an imine with the liberated primary amine on the surface, which lowers the effective photolytic transformation. However, adding a scavenger molecule did not make an improve.
Before orthogonal deprotection could be carried out, the irradiation conditions were optimised in order to guarantee the complete removal of one protecting group without damaging the other. Different irradiation experiments were therefore conducted at different wavelengths and with different irradiation sources. From the UV measurements it became clear that irradiating the mixed substrates with a frequency doubled Ti:Sa laser at 411 nm for 15 min, and then with a frequency tripled Ti:Sa laser at 253 nm for 20 s, guaranteed orthogonal deprotection.

After a site-selective irradiation of the mixed silane layer through a mask successful deprotection was then demonstrated by allowing fluorescent dyes to react with the liberated functional groups, which could be detected under the fluorescence microscope. Fluorescent pattern could be detected in most cases, although non-specific interactions of the dye with the non-irradiated regions lead to inverted pattern in some cases.
Further labelling experiment were carried out by immobilising oligonucleotide strands to the functional group *via* coupling agents, and then hybrid capturing these strands with the complementary fluorescence labelled oligonucleotides. Successful hybridisation and therefore successful patterning of the surface could be observed with the confocal microscope. Again, in this case some patterns showed an inversion of the fluorescence pattern. Nevertheless,

specific fluorescence labelling could be demonstrated, thus making these wafers attractive as model systems for possible DNA microarrays.

Chapter 7

Experimental Section

7.1 General

All chemicals and solvents were purchased from ABCR (D-76189 Karlsruhe), Acros Organics (B-2440 Geel), Fisher Scientific UK Ltd. (GB-Loughborough, Leics. LE11 5RG), Fluka Chemie AG (D-82024 Taufkirchen), Merck KGaA (D-64271 Darmstadt), Proligo Primers & Probes (F-75011 Paris), Riedel-de-Haen (D-30926 Seelze) and Sigma-Aldrich Chemie GmbH (D-89555 Steinheim), with *p.a.* purity, and were used as received (unless stated otherwise). Solvents were dried over molecular sieves (4 Å) or with known literature procedures.

Chromatography:
Preparative column chromatography and flash column chromatography were carried out using Merck silica gel (63-200 μm) and (43-63 μm), respectively. Analytical thin layer chromatography was carried out using Merck silica gel G/UV_{254} using a UV lamp and potassium permanganate to visualise the components. Preparative thin layer chromatography was carried out with TLC plates (20$\times$20 cm, 2 mm layer thickness, SIL G-200 UV_{254}) purchased from Macherey-Nagel, Germany.

IR-Spectra:
Infra-red spectra were recorded on a Perkin Elmer Paragon 1000 FT-IR spectrometer. The wavenumbers are given in cm^{-1} and the following abbreviations are used: br-broad, s-strong, w-weak.

Mass spectra:
Mass spectra were recorded with Electron Impact (EI) and Field Desorption (FD) using a TRIO-2000 and ZAB 2-SE-FPD from VG-Instruments.

Melting Point:
Melting points were determined with a semi-automatic melting point apparatus B-545 (Büchi) and are uncorrected.

UV/Vis Spectra:
UV/Vis Spectra were recorded on a Perkin Elmer L9 UV/Vis NIR spectrometer, and the axis were denoted with wavelength (nm) and relative absorbance (Abs).

Scanning Electron Microscopy:
Low voltage scanning electron microscope (LVSEM) images on native samples (non-sputtered) were recorded with a LEO Gemini 1530 at acceleration voltages of 0.2-1.0 keV.

Confocal Microscopy:
The microscope used was a commercial LSM setup manufactured by Carl Zeiss (Jena, Germany) consisting of the module LSM 510 and the inverted microscope model Axiovert 200. The types of laser included an Argon laser (457, 488, 514 nm with an output power of 3, 10, 15 mW, respectively), a green He/Ne laser (543.5 nm, 1 mW) and a red He/Ne laser (632.8 nm, 5 mW). Two objective lenses were used; namely a ZEISS Plan-Neofluar (with 20x magnification and an numerical aperture of 0.5), and a ZEISS C-Apochromat (with 40x magnification and an numerical aperture of 1.2).

Contact Angle Measurements:
For contact angle measurement a Drop Shape Analysis System DSA 10 by Krüss, Germany was used, combined with a CCD camera for image capturing.

AFM Images:
For the investigations presented in this thesis, all images were recorded under ambient conditions using a MultiMode Atomic Force Microscope or a Dimension 3100, connected to a NanoScopeIIIa controller. The microscopes were operated in tapping and in contact mode. The substrates to be investigated had a size of 1×1.5 cm and were sucked onto the wafer holder by a vacuum pump.

NMR Measurements:
Solution ^{1}H and ^{13}C NMR spectra were recorded on a Bruker Spectrospin 250 and a AMX 300 spectrometer. All measurements occurred at room temperature, are referenced to TMS (δ = 0 ppm) and calibrated using the deuterated lock-signal w.r.t. the solvent. The chemical shifts are given in parts per million and the coupling constants in Hertz. The following abbreviations are used: s-singlet, t-triplet, q-quartet, m-multiplet, br-broad. The numbering of the molecular images in Section 7.5 are arbitrary and only meant to aid in peak assignment.

Optical Microscopy:
Optical microscopy images (DIC and darkfield) were recorded on a Zeiss Axioscope with

reflected light microscopy (HBO lamp) using a digital camera (Zeiss AxioCam) that was attached to the microscope.

DLS Measurements:
DSL measurements were carried out on a ALV 5000 instrument, using a Kr-Ion laser at λ = 647.1 nm.

Kinetic Experiments:
The conditions in the NMR tube were the same as in a real hydrolysis experiment. This means that a 1% solution of the silane in deuterated THF was made up to which the catalyst was added just before the NMR measurement. It was thus possible to calculate the % transformation of the ethoxy CH_2 and CH_3 peaks in liquid ^{1}H NMR spectrum into ethanolic CH_2 and CH_3 peaks, that form upon hydrolysis of the ethoxy anchor groups around the silicon atom.

7.2 Silane Deposition on Silica Surfaces

Silicon wafers (25 $\times$ 13 mm), provided by *Wacker Siltronic* with a 1.6 nm native oxide layer, were placed into a fresh Piranha solution (conc. H_2SO_4/30%H_2O_2 (3:7) v/v) for 1 h for cleaning and then rinsed with copious amounts of deionised Milli-Q water (R=18MΩ*cm). The wafers were then stored for further use in Milli-Q water, and when needed they were blow dried in a stream of nitrogen.

7.2.1 Solution Phase Silanisation

Aminopropyltriethoxysilane (APTS), N-trimethoxysilylpropyl-1-N,N,N-trimethylammonium chloride (NR_4^+), ANTSP were prehydrolised as a 1 wt% solution in Milli-Q water for 30 min. After filtration of the mixtures through a 0.2 μm PTFE (Teflon) filter, the clean substrates were then immersed into the silane solution for 30 min. After deposition the substrates were gently rinsed with Milli-Q water and then tempered for 1 h at 95 °C in a vacuum oven. They were finally sonicated in an ultrasound bath to remove any unspecifically adsorbed silane and then blow dried for further use.
Bnz and NVoc silane were both prehydrolised for 16 h as a 2 wt% solution in THF. The clean substrates were immersed into the silane solution for 6 h and the wafer were then rinsed with THF, baked at 95 °C in a vacuum oven and finally sonicated for 2$\times$3 min in THF.

7.2.2 Vapour Phase Silanisation

Clean substrates were exposed to vapours of the silane by placing them in a closed container, and then washing with the appropriate solvent.
OTE: 2 ml of OTE were added to the bottom of the vessel and after evacuation (0.02 mbar) for 15 min, the whole container was heated to 95 °C in an oil bath for 2 h. After silanisation the substrates were successively cleaned with dichloromethane, cyclohexane, acetone, and Milli-Q water in an ultrasound bath for 2 × 3 min, respectively.
HMDS: 2 ml of HMDS was added to the container, and silane deposition was allowed to take place at room temperature and ambient pressure for 15-30 min. The substrates were rinsed afterwards with a 1:1 mixture of acetone/dichloromethane and finally with cyclohexane (all 2×3 min).

7.2.3 Photolithography

The steps involved during the lithography process all had to be optimised to guarantee the desired pattern. For instance, when spinning on the resist the velocity of the coating had to be approximately 4000 rounds per minute (rpm) for 60 s. Longer coating times or less rpm did not result in a satisfactory pattern. The same holds for the irradiation time: when irradiating the resist for too long, the pattern on the wafer were nearly always destroyed during development. The best irradiation time was therefore found at 4 s at 365 nm with a Hg lamp (22 mW·cm^{-2}). Photolithographic patterning was carried out using a positive tone photoresist (Microposit S 1805) that was diluted 1:1 with a thinner (Microposit ma-T 1041) and spin-coated onto the wafer at 4000 rpm for 60 s. After baking in a vacuum oven at 95 °C for 1 h the wafers were irradiated through a gold mask with a UV mask aligner (Hg pressure lamp, 365 nm, 22 mW·cm^{-2}) for 4 seconds. They were then developed in a developer solution (Microposit MF CD26) for 30 seconds and then rinsed twice again with Milli-Q water.

Removal of the photoresist is crucial to the modification steps that follow since silanes can only react where free silanol groups on the surface are available. When removing the resist after silane deposition in the last step, a commercially bought photoresist remover was used. Unfortunately, the removal was not very clean and some photoresist was left on the wafer surface. Wiping off the remaining resist with Kim-Wipes that had been soaked in dichloromethane only resulted in scratches on the remaining photoresist and on the surface of the wafer, which was visible under the optical microscope. A new solution was found in removing the resist in an ultrasound bath by successive washing with dichloromethane, acetone, methanol and water. By doing so it was possible to remove all the photoresist without scratching the surface.

7.2.4 Formation of Structured Silane Layers

OTE/SiOH: The clean photolithographically patterned substrates were modified with OTE by vapour phase deposition. After silanisation, the substrates were sonicated successively in dichloromethane (3×2 min), acetone (3×2 min), methanol (1×3 min) and Milli-Q water (1×3 min).
HMDS/NH_2: The clean substrates were first modified with HMDS according to Section7.2.2. After removal of the photoresist by sonication with cyclohexane (2×3 min), acetone (2×3 min), dichloromethane (3×2 min), methanol (1×3 min) and Milli-Q water (1×3 min), they were then immersed into an aq. APTS solution according to section 7.2.1.
NH_2/SiOH: The clean photolithographically patterned substrates were modified with APTS by solution phase deposition according to section 7.2.1.
NH_4^+/SiOH: The clean photolithographically patterned substrates were modified with N-trimethoxysilylpropyl-1-N,N,N-trimethylammoniumchloride by solution phase deposition according to section 7.2.1.

7.3 Colloid Deposition on Silicon Wafers

The latex particles used as part of this thesis were synthesised according to the literature [Krüger 01, Fustin 03] and consisted of three types of COOH-functionalised polymer, namely polybutylmethacrylate (PBMA), crosslinked polybutylacrylate (xl-PBA) and polystyrene (PS). PBMA-COOH was prepared by a ”seeded” semi-continuous emulsion polymerisation under monomer-starved conditions in a three-step procedure. First, the colloid seed was prepared by batch polymerisation, followed by a PBMA polymerisation to give the core to which a shell of methacrylic acid (MAA) was introduced in an additional semi-continuous step. After purification *via* ultrafiltration with a Milipore centrifugal filter, the diameter was determined by dynamic light scattering and gave a diameter of 225 nm. The surface charge induced by the carboxylic acid functions was determined by polyelectrolyte titration, from which it is possible to calculate the surface area per charge (called “parking area”). For PBMA-COOH the value obtained was 203 $Å^2$charge^{-1}. Crosslinked PBA-COOH was also synthesised in seeded semi-continuous emulsion polymerisation starting from poly-*n*-butylmethacrylate seed in batch process and then using butylacrylate, methacrylic acid and allymethacrylate as crosslinkers. Adding methacrylic acid again in the second step led to a higher surface charge and therefore to a smaller parking area (44 $Å^2$charge^{-1}). The size obtained by light scattering was 155 nm. The polystyrene particles used were all synthesised in a batch polymerisation, where only the content of acrylic acid was altered, giving differently charged colloidal objects. PS-7 particles were synthesised in a batch polymerisation with 7% of acrylic acid and 0.5% sodium styrene sulphonate (NaSS) as a co-monomer making it a hydrophilic particle with a parking area of 98 $Å^2$/COOH. PS-10 particles only contained 0.2%

NaSS, with a parking area of 527 Å^2/COOH.

7.3.1 Colloidal Deposition on Patterned Silane layers

Particle deposition on NH_4^+/SiOH, NH_2/SiOH, NH_2/HMDS layers, using PS-7, PS-10, PS-cell, PBMA were carried out as 0.2 wt% suspension , with an incubation time of 30 min, unless stated otherwise. The substrates were then rinsed in Milli-Q water and gently blow dried in a stream of nitrogen.

7.3.2 Colloids Deposition on ANTSP layers

For all colloidal suspensions, the stock suspension was diluted with ethanol to give a 0.2 wt% suspension. The polystyrene film was cast onto the wafers as a 0.2 wt% suspension in THF. The clean substrates were immersed into the colloidal and polymer suspension for 1 h, unless stated otherwise, and were then taken out of the suspension and gently blow dried in a stream of nitrogen. Spin-coating of the particles onto the wafers occurred with 2000 rpm for 30 s.

7.4 Fluorescence Labelling

7.4.1 Buffer Preparation

Phosphate-Buffered Saline (PBS):
NaCl (8 g), KCl (0.2 g), NA_2HPO_4 (1.44 g), KH_2PO_4 (0.24 g) were dissolved in 800 ml of Milli-Q water. The pH was adjusted with HCl and further water was added to make up a 1 L solution, that was autoclaved.

Sodium Citrate Buffer (20×SSC):
NaCl (175.3 g) and sodium citrate (88.2 g) were dissolved in 800 ml Milli-Q water. The pH was adjusted to 7.2 with a few drops of conc. HCl. The volume was then adjusted to 1 L and the solution was autoclaved.

Phosphate Buffers (Gomori Buffers):
To a solution of 1 M $NaHPO_4$ (98 ml) was added 1 M NaH_2PO_4 (2 ml) and the resulting solution was adjusted to 1 L. After autoclaving, the solution was stored at room temperature[1].

[1] All buffer solutions were prepared according to [Sambrook 01]

7.4.2 Amine Coupling

1 mg of Alexa Fluor 488 and 546 succinimidyl ester was dissolved in 1 ml of dry DMSO. 100 μl were then taken out of this stock solution and diluted again to 1 ml with DMSO. 2 drops of this reacting solution was deposited onto the quartz substrates and left overnight. The substrate was then washed with water, dried in a stream of nitrogen and preserved from light.

7.4.3 Carboxylic Acid Coupling

1 mg of Alexa Fluor 488 hydrazide sodium salt was dissolved in 1 ml of Milli-Q water and stored below -18°C preserved from light and moisture. 2 drops of aqueous 0.2 M EDC and 2 drops of 0.05 M aqueous NHSS was deposited onto the quartz substrate and left to incubate for 2 h. The solution was then washed off with water, and 2 drops of the hydrazide storage solution plus 2 drops of phosphate buffer (1 M) were added to the substrate and left to incubate overnight.

The irradiated quartz substrates containing amine and carboxylic acid functionalities were blow dried with nitrogen before fluorescence staining in order to remove any dust particle that could have been deposited.

7.4.4 Oligonucleotide Immobilisation and Hybrid Capturing

Amine Coupling

The quartz surface was covered with a 1% glutaraldehyde solution in SSC buffer (1x), pH 7.2 for 3 h, in order to form an imine bond with the primary amine on the surface, and was then washed 5 times with SSC buffer, pH 7.2. 70 μl of ssNH_2-C_6-spacer-5'-$_dT_{25}$-3' (5.12 μM in SSC buffer, pH 7.2) were than spotted on the surface and left for 20 h. The substrate was again washed with buffer, pH 7.2 and then covered with a 25% solution of $NaBH_3CN$ in SSC buffer (1x) for 30 minutes in order to reduce the imine bond back into a more stable amine bond. The substrate was then washed with Milli-Q water and left for 1 minute in a 80 °C warm water bath to denaturalise any none-specifically bound oligonucleotide base pairs. A solution of 5.12 μM complementary 25-mer adenine oligonucleotide (5'-$_fA_{25}$-3') in SSC (1x) was added to the surface and allowed to hybridise for 3 h.

Carboxylic Acid Coupling

The substrate was placed into a PBS buffer solution for 30 minutes to equilibrate the pH for coupling. 2 aliquots of 0.05M NHSS and 0.2M EDC in PBS were spotted on the substrate

Name	Sequence [5'-3']	Molecular Weight [g/mol]	Conc. [μM]
Cy5dA25	5'-(Cy5)A_{25}-3'	8306	335
Cy3dG25	5'-(Cy3)G_{25}-3'	8676	340
NH_2G5dC25	5'-(NH_2)gggggC_{25}-3'	8993	507
Oligo 1	5'-(NH_2)(CH_2)$_6$$T_{25}$3'	7607	2519
Oligo 2	5'-(FTIC)-A_{25}-3'	8313	319
Oligo 3	5'-(NH_2)$C_6$$T_{25}$-3'	9458	238

Table 7.1: *Summary of all ODNs used.*

and left for another 30 minutes in order to activate the carboxylic acid groups. The substrate was then washed again with PBS and incubated with ssNH_2-C_6-spacer-5'-$_d$$T_{25}$-3' (5.12 μM in PBS buffer) for 20 h. A 5.12 μM solution of the complementary oligonucleotide (5'-$_f$$A_{25}$-3') in PBS was then added to the substrate and left to hybridise for 45 minutes.

The 25-mer adenine strand was present with two respective fluorophores: one oligonucleotide was bearing fluorescein isocyanate (FTIC), which is excited at 488 nm and emits above 510 nm, and another A_{25}-mer had the fluorophore Cy5 attached to its 5' end. The G_{25}-mer used for hybrid capturing the C_{25} strand had the fluorophore Cy3 attached to its 5' end, which was excited at 550 nm and emitted at around 590 nm. Cy3 and Cy5 are common fluorophores in molecular biology and complement each other well.

7.5 Synthesis of compounds

7.5.1 2-Amino-5-nitrobenzoic acid

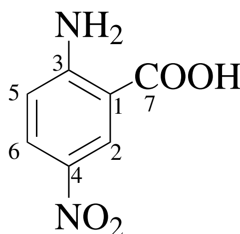

2 [182.13]

A solution of 2-cyano-4-nitroaniline (4.00 g, 0.025 mol) in aq. NaOH (1.90 g pellets in 5.90 g H_2O, 25%, 2 mol) was heated under reflux for 6 h, until no further ammonia evolved, as visible from the inflation of a ballon that had been attached to the flask. The resulting red-coloured solution was cooled with ice whilst acidifying the mixture with aq. sulfuric acid (25%). The

precipitate was collected and recrystallised from ethanol to yield 60% of the desired product as an yellow powder. Thin layer chromatography gave a characteristic streak round R_f = 0,26 using chloroform/methanol (8:1).
Melting point: 230 °C
^{1}H NMR (250 MHz, d_6-acetone) δ [ppm] = 7.20 (d, 1 H, J = 9.1 Hz, H_{ar}), 7.63 (sb, 1 H, COOH), 8.42 (dd, 1 H, J = 9.1 Hz and 2.8 Hz, H_{ar}), (d, 1 H, J = 2.8 Hz, H_{ar}).
^{13}C NMR (63 MHz, d_6-DMSO) δ [ppm]: 114.5 (1-C_{ar}), 118.8 (5-C_{ar}), 126.8 (2-C_{ar}), 130.4 (6-C_{ar}), 139.3 (4-C_{ar}), 166.5 (3-C_{ar}), 170.3 (COOH).
IR (KBr) [$\tilde{\nu}$/cm^{-1}]: 3650 (s), 1626 (m), 1582 (s), 1303 (s). FD-MS [m/z]: 182.9 (100%, M^+).

7.5.2 2-Azido-5-nitrobenzonitrile

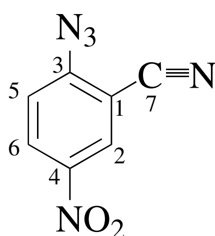

4 [189.13]

To a cooled solution of 2-amino-5-nitronitrile (5.26 g, 32 mmol) in 83 ml of conc. HCl was added a solution of $NaNO_2$ (5.40 g, 78 mmol, 3.3 eq.) in cold H_2O (25 ml) and stirred for 3 h at 0 °C, thereby changing the colour from yellow to dark red. A solution of NaN_3 (6.50 g, 0.1 mol, 5.2 eq.) in cold H_2O (10 ml) was then added at 0 °C and stirred overnight. The solution was then poured onto ice and the precipitate was collected as a yellow powder. The crude compound was then purified by plug chromatography. To do this, a slurry consisting of silica gel and dichloromethane/acetone (1:1) was poured into a sintered funnel of 10 cm diameter attached to a vacuum pump. At the same time as the solvent was removed with help of the vacuum, the crude product was added portion-wise to the silica gel in the funnel. Thus, the reactants were adsorbed onto the silica gel and the product was present in the filtrate. After removing the solvent *in vacuo*, the desired product was obtained as a red powder in a 82% yield.
^{1}H NMR (250 MHz, d_6-DMSO) δ [ppm]: 7.75 (d, 2 H, J = 8.2 Hz, H_{ar}), 8.52 (dd, 1 H, J = 8.2 Hz and 1.8 Hz, H_{ar}), 8.79 (d, 1 H, J = 1.8 Hz, H_{ar}).
^{13}C NMR (63 MHz, d_6-DMSO) δ [ppm]: 103.0 (1-C_{ar}), 114.2 (5-C_{ar}), 121.3 (CN), 129.3 (6-C_{ar}), 129.7 (2-C_{ar}), 143.6 (CN_3), 149.7 (CNO_2).
IR (KBr) [$\tilde{\nu}$/cm^{-1}]: 2238 (m), 2143 (s), 1538 (s), 1519 (s), 1481 (s). FAB-MS [m/z]: 188.9 (60%, M^+).

7.5.3 5-Azido-2-nitrobenzoic acid

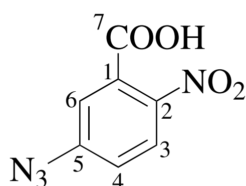

6 [208.13]

To a cooled solution of 5-amino-2nitrobenzoic acid (0.3 g, 1.65 mmol) in 10 ml of conc. HCl was added a solution of $NaNO_2$ (0.37 g, 5.36 mmol, 3.2 eq.) in cold H_2O (2.5 ml) and stirred for 3 h at 0 °C. A solution of NaN_3 (0.56 g, 8.62 mmol, 5.2 eq.) in cold H_2O (10 ml) was then added at 0 °C and stirred overnight. The solution was then poured onto ice and the precipitate was collected as a yellow powder (0.34 g, 82%).
Melting point: 165 °C
^{1}H NMR (250 MHz, d_6-DMSO) δ [ppm]: 7.43 (m, 2 H, H_{ar}), 8.07 (dd, 1 H, J = 6.6 Hz und 2.5 Hz, H_{ar}), 14.02 (sb, 1 H, OH).
^{13}C NMR (63 MHz, d_6-DMSO) δ [ppm]: 120.0 (4-C_{ar}), 122.1 (5-C_{ar}), 126.5 (2-C_{ar}), 131.0 (3-C_{ar}), 143.7 (6-C_{ar}), 145.6 (1-C_{ar}), 166.0 (COOH).
IR (KBr) [$\tilde{\nu}$/cm^{-1}]: 3855 (br), 2114 (s), 1715 (s), 1585 (s), 1519 (s), 1354 (s).

7.5.4 N-Hydroxylsuccinimidyl-5-azido-2-nitrobenzoate

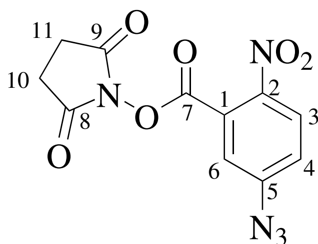

9 [305.20]

To a stirred solution of 5-azido-2-nitrobenzoic acid (0.5 g, 2.4 mmol) in dry THF (10 ml) was added at 0 °C a solution of N-hydroxysuccinimide (0.4 g, 3.5 mmol, 1.5 eq.) in THF (5 ml), followed by a solution of DCC (0.722 g, 3.5 mmol, 1.5 eq.) in THF (2 ml). The resulting mixture was stirred under nitrogen for 6 h and then filtered. The solvent was removed *in vacuo* to give 1.23 g of a crude brown-yellow viscous material. The compound was purified by column chromatography (chloroform/ethyl acetate (49:1)) to give 0.73 g (88%) of the target material

as a yellow powder.
Melting point: 130°C
^{1}H NMR (250 MHz, d_6-DMSO) δ [ppm]: 2.86 (s, 4 H, CH_2CH_2), 7.37 (d, 1 H, J = 2.5 Hz, 6-C**H**$_{ar}$), 7.48 (dd, 1 H, J = 8.9 Hz und 2.5 Hz, 4-C**H**$_{ar}$), 8.20 (d, 1 H, J = 8.9 Hz, 3-C**H**$_{ar}$).
^{13}C NMR (63 MHz, d_6-DMSO) δ [ppm]: 25.3 (CH_2CH_2), 120.0 (N_3C**C**HCCO), 122.8 (N_3**C**CH), 124.9 (CO**C**), 126.7 (NO_2C**C**H), 142.3 N_3C), 146.1 (NO_2C), 160.3 (COO), 168.7 (CH_2**C**O).
IR (Nujol) [$\tilde{\nu}$/cm^{-1}]: 2117 (s), 1815 (s), 1737 (s), 1573 (s), 1307 (s). FD-MS [m/z]: 305.2 (65%, M^+).

7.5.5 (5-Azido-2-nitrobenzoyl)-allylamine

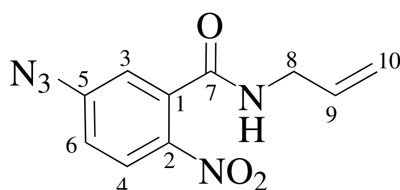

10 [247.21]

To a solution of N-hydroxylsuccinimidyl-5-azido-2-nitrobenzoate (1 g, 3.28 mmol) in dry THF (50 ml) and chloroform (20 ml) was stirred at 0 °C under argon atmosphere. Allylamine (3 g, 12 mmol, 4 eq.) was then added in acetonitrile (20 ml) and the resulting mixture was stirred for 26 h in the dark. The solvent was removed *in vacuo* and the crude compound was purified by silica gel column chromatography (diethylether/EtOH/toluene 10:3:7) to give the product as a yellow powder in a 96% yield.
^{1}H NMR (250 MHz, $_6$-DMSO) δ [ppm]: 3.86 (m, 2 H, 8-CH_2), 5.10 (dd, 1 H, ^3J = 17.2 Hz and ^2J = 1.9 Hz, CH**H**H$_{cis}$), 5.24 (dd, 1 H, ^3J = 10.4 Hz and ^2J = 1.9 Hz, CHH**H**$_{trans}$), 5.89 (dm, 1 H, $^3J_{trans}$ = 17.1 Hz and $^3J_{cis}$ = 10.4 Hz, C**H**HH), 7.19 (d, 1 H, J = 2.5 Hz, H_{ar}), 7.30 (dd, 1 H, J = 8.7 Hz and 2.5 Hz, H_{ar}), 8.05 (d, 1 H, J = 8.7 Hz, H_{ar}), 8.76 (t, 1 H, J = 5.4 Hz, NH).
^{13}C NMR (63 MHz, d_6-DMSO) δ [ppm]: 39.6 (CH_2), 115.9 (10-**C**H_2), 119.7 (CH_{ar}), 120.52 (CH_{ar}), 126.6 (CH_{ar}), 134.6 (**C**HCH_2), 135.3 (1-**C**$_{ar}$CO), 154.4 (2-**C**$_{ar}NO_2$), 157.1 (5-**C**$_{ar}N_3$), 165.0 (CO).
IR (KBr) [$\tilde{\nu}$/cm^{-1}]: 3295 (s), 2132 (s), 1664 (s), 1580 (s), 1519 (s). FD-MS [m/z]: 246.9 (30%, M^+).

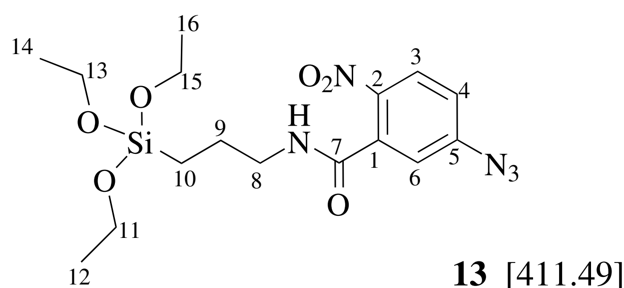

13 [411.49]

7.5.6 (5-Azido-2-nitrobenzyl)triethoxysilylpropylamide (ANTSP)

Into a round bottom flask that had been passivated with hexamethyldisilazane (HMDS) under vacuum the night before was added at room temperature a solution of N-hydroxylsuccinimidyl-5-azido-2-nitrobenzoate (1.5 g, 4.92 mmol) in dry chloroform (15 ml) and aminopropyltriethoxysilane (1.1 g, 4.96 mmol, 1 eq.) in acetonitrile (4 ml). The mixture was allowed to stir for 22 h, always monitored by TLC. The solvent was removed *in vacuo* and the excess APTS was removed with a vacuum pump (freeze drying) to give a viscous red-yellow compound. The crude product was chromatographed (passivated silica column, chloroform/ethyl acetate (49:1)) to afford 1.72 g (48%) of the title compound as a yellow solid.
^{1}H NMR (250 MHz, $CDCl_3$) δ [ppm]: 0.72 (t, 2 H, J = 8.0 Hz, $SiCH_2$), 1.18 (t, 9H, J = 7.0 Hz, $OCH_2C\mathbf{H}_3$), 1.78 (m, 2 H, $SiCH_2C\mathbf{H}_2$), 3.47 (m, 2H, $SiCH_2CH_2C\mathbf{H}_2$), 3.79 (q, 6H, J = 7.0 Hz, $OC\mathbf{H}_2CH_3$), 6.38 (t, 1 H, **J** = 4.0 Hz, NH), 7.11 (d, 1 H, J = 2.5 Hz, H_{ar}), 7.15 (dd, 1 H, J = 8.8 Hz and 2.5 Hz, H_{ar}), 8.11 (d, 1 H, J = 8.8 Hz, H_{ar}).
^{13}C NMR (63 MHz, $CDCl_3$) δ [ppm]: 8.0 ($SiCH_2$), 18.1 ($OCH_2\mathbf{C}H_3$), 23.2 ($SiCH_2\mathbf{C}H_2$), 42.7 ($SiCH_2CH_2\mathbf{C}H_2$), 58.3 ($O\mathbf{C}H_2CH_3$), 119.6 (CH_{ar}), 119.9 (CH_{ar}), 126.5 (CH_{ar}), 129.3 (1-C_{ar}), 145.8 (NO_2C_{ar}), 146.4 (N_3C_{ar}), 164.8 (CONH).
IR (KBr) [$\tilde{\nu}$/cm^{-1}]: 3253 (m), 2124 (s), 1713 (s), 1666 (m), 1581 (s), 1213 (s) FD-MS [m/z]: 412.6 (100%, M^+).

7.5.7 α-(Benzotriazol-1-yl-)arylethyl ether

Method A: (**38** [253.30])

A solution of benzaldehyde (3 g, 0.028 mol), benzotriazole (4.04 g, 0.034 mol, 1.2 eq.), abs. ethanol (2.5 g, 0.056 mol, 2 eq.), triethylorthoformate (0.084 mol, 3 eq.) and a catalytic amount of sulfuric acid in THF (50 ml) was allowed to stir at room temperature for 3 h. After refluxing for further 2.5 h the solution was allowed to cool down to room temperature and extracted with diethyl ether (100 ml) and washed with Na_2CO_3 (2x 200 ml) and H_2O (1x 200 ml). The solvent was removed *in vacuo* to yield a crude yellow oil, which was purified on a

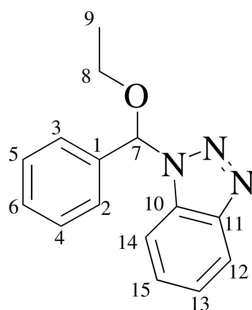

silica column using Hex/EtOAc (14:1). The desired product was obtained as a viscous oil in a 43% yield, which solidified upon refrigeration at +4 °C.
FD-MS [m/z]: 253.4 (60% M^+).

Method B: (**38a** [253.30])

A solution of benzaldehyde diethyl acetal (3.98 g, 22.1 mmol) and benzotriazole (1.98 g, 16.7 mmol, 1.5 eq.) in toluene (50 ml) was heated under reflux for 4 h and monitored by TLC. The solution was allowed to cool down, extracted with diethyl ether (200 ml) and washed with sat. Na_2CO_3 (2x 250 ml), H_2O (1x 250 ml), and dried over $MgSO_4$. The solvent was removed in vacuo and the crude residue was purified with flash column chromatography on silica (EtOAc/Hex = 1:6) to yield 81% of the title compound as a colourless semi-crystalline wax.
^{1}H NMR (250 MHz, $CDCl_3$) δ [ppm]: 1.26 (t, 3 H, J = 7.0 Hz, CH_3), 3.41-3.54 (m, 1 H, 8-CH**H**), 3.68-3.85 (m, 1 H, 8-C**H**H), 7.20 (s, 1 H, 7-CH), 7.29-7.36 (m, 6 H, H_{ar}), 7.40-7.47 (m, 2 H, H_{ar}), 8.03-8.09 (m, 1 H, H_{ar}).
^{13}C NMR (63 MHz, d_6-DMSO) δ [ppm]: 15.0 (CH_3), 64.79 (CH_2), 88.9 (7-C), 111.6 (14-C_{ar}), 119.9 (12-C_{ar}), 124.8 (13-C_{ar}), 126.3 (2-C_{ar}, 3-C_{ar}), 128.2 (6-C_{ar}), 128.2 (4-C_{ar}, 5-C_{ar}), 129.3 (15-C_{ar}), 131.6 (10-C), 137.1 (1-C), 146.3 (11-C).
IR (Nujol) [$\tilde{\nu}$/cm^{-1}]: 2853 (s), 2723 (w), 2285 (m). FD-MS [m/z]: 253.4 (100%, M^+).

7.5.8 3',5'-Dimethoxybenzoin

A solution of α-(Benzotriazol-1-yl)-arylethyl ether (3.24 g, 12.8 mmol) in dry THF (50 ml) was cooled to -78 °C. n-Butyl lithium (8.8 ml (1.6 M in Hex), 14.1 mmol, 1.1 eq.) was added slowly over 2 min under anhydrous conditions and allowed to stir for 40 s. As soon as n-BuLi had been added the original yellow solution turned turquoise green indicating an instant deprotonation of the methine group due to the strong activation of the benzotriazole moiety and formation of the anion. A solution of 3,5-dimethoxybenzaldehyde (2.67 g, 16.13 mmol, l.26 eq.) in cold THF (5 ml) was then added slowly and stirred for another 2 min. Thereupon the colour of the solution turned orange. The lithium ion was captured with water (30 ml) at

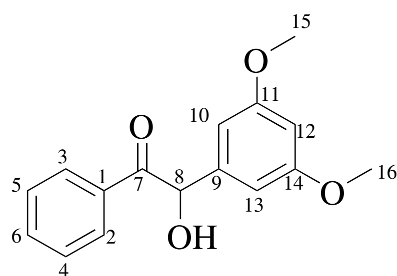

39 [272.30]

the same temperature. Diluted HCl (8 ml conc. HCl and 20 ml H_2O) was immediately added to hydrolyse the ketone, as indicated by a colour change to orange-red. The mixture was allowed to warm up and then stir at room temperature for 1 h. It was extracted with diethyl ether (100 ml) and washed with sat. Na_2CO_3 (2x 200 ml) and H_2O (2x 200 ml), and dried over $MgSO_4$. Removing the solvent *in vacuo* afforded a dark red viscous compound, which was purified with column chromatography on silica (Hex/EtOAc/CH_2Cl_2 = 15:3:1) to yield 56% of the title compound as an yellow-orange oil that solidified upon standing.

^{1}H NMR (250 MHz, $CDCl_3$) δ [ppm]: 3.74 (s, 6 H, OCH_3), 5.85 (s, 1 H, CH), 6.35 (t, 1 H, J = 2.2 Hz, H_{ar}), 6.46 (d, 2 H, J = 2.2 Hz, H_{ar}), 7.41 (tt, 2 H, J = 7.4 Hz, H_{ar}), 7.55 (tt, 1 H, J = 1.6 Hz and 7.4 Hz, H_{ar}), 7.91 (d, 2 H, J = 7.3 Hz, H_{ar}).

^{13}C NMR (63 MHz, $CDCl_3$) δ [ppm]: 27.5 (OCH_3), 78.4 (CH), 102.4 (12-CH), 107.8 (13-CH, 14-CH), 130.6 (4-CH, 5-CH), 131.1 (3-CH, 2-CH), 131.7 (1-C), 135.9 (9-C), 143.0 (6-CH), 164.0 (11-CH, 14-CH), 200.7 (7-CO)

IR (Nujol) [$\tilde{\nu}$/cm^{-1}]: 3520 (m), 2924 (s), 1709 (s). FD-MS [m/z]: 272.6 (100%, M^+).

7.5.9 But-4-enoic acid-1-(3,5-dimethoxy-phenyl)-2-oxo-2-phenylethyl ester

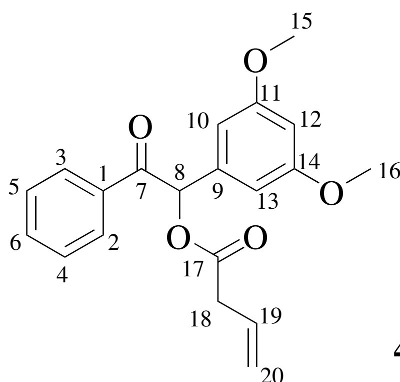

40 [340.37]

A solution of dimethoxybenzoin (0.5 g, 1.83 mmol), butenoic acid (0.63, 7.32 mmol, 4 eq.) and DMAP (0.11 g, 0.915 mmol, 0.5 eq.) in dry dichloromethane was stirred under argon

atmosphere. Diisopropylcarbodiimide (0.92 g, 7.32 mmol) was added with a syringe to the flask and the mixture was allowed to stir overnight. The precipitated urea was filtered off and the solvent was removed *in vacuo* to yield a crude, red coloured viscous compound. After purification with a flash chromatography column on silica (Hex/EtOAc/CH_2Cl_2 15:3:1), the product was obtained as a yellow semi-crystalline wax in a 64% yield.
^{1}H NMR (250 MHz, $CDCl_3$) δ [ppm]: 3.27 (t, 2 H, J = 6.9 Hz, CH_2), 3.76 (s, 6 H, OCH_3), 5.18-5.25 (dm, 1 H, ^3J = 20.4 Hz, CH**H**H_{cis}), 5.21-5.25 (m, 1 H, $^3J_{cis}$ = 11.9 Hz, CHH**H**$_{trans}$), 5.88-5.94 and 5.97-6.04 (dm, 1 H, $^3J_{trans}$ = 20.4 Hz and $^3J_{cis}$ = 11.9 Hz, C**H**HH_{trans}), 6.41 (t, 1 H, J = 2.2 Hz, H_{ar}), 6.90 (d, 1 H, J = 2.2 Hz, H_{ar}), 6.76 (s, 1 H, 8-CH), 7.40 (tt, 2 H, J = 1.6 Hz and 6.8 Hz, H_{ar}), 7.52 (tt, 2 H, J = 1.6 Hz and 6.8 Hz, H_{ar}), 7.93 (dd, 2 H, J = 1.6 Hz and 6.8 Hz, H_{ar}).
^{13}C NMR (63 MHz, $CDCl_3$) δ [ppm]: 36.7 (10-CH_2), 53.5 (2 C, OCH_3), 79.3 (8-CH), 99.3 (16-C), 104.7 (14-CH, 17-CH), 117.1 (12-C, $CHCH_2$), 126.7 (13-C), 126.9, 127.8 (4 CH, phenyl), 129.2 (1-CH), 131.6 (6-C), 133.5 (11-C, CH**C**H_2), 159.1 (2 C, **C**OCH_3), 169.3 (OCO), 193.4(CO).
IR (Nujol) [$\tilde{\nu}$/cm^{-1}]: 2853 (s), 1742 (s), 1698 (s), 1652 (m). FD-MS [m/z]: 340.4 (100%, M^+), 254.4 (35% photoproduct).

7.5.10 Undec-10-enoic acid-1-(3,5-dimethoxy-phenyl)-2-oxo-2- phenylethyl ester

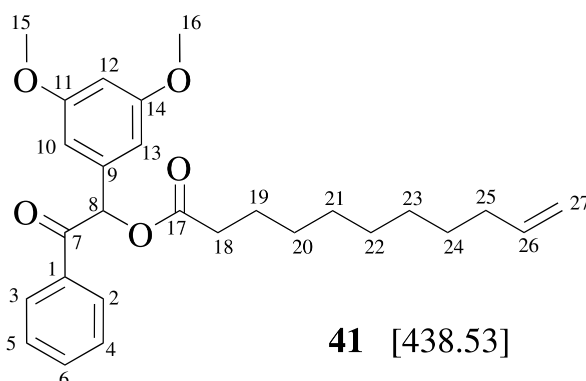

To a solution of 3’, 5’-dimethoxybenzoin (2.45 g, 9 mmol), triethylamine (2.07 g, 20.5 mmol, 2.3 eq.) and DMAP (1.3 mol, 0.14 eq.) in dry dichloromethane (50 ml) was added slowly under anhydrous conditions undecenoyl chloride (2.35 g, 11.6 mmol, 1.3 eq.). The solution was allowed to stir at room temperature for 17 h and then extracted with ethylacetate (2x 150 ml). The organic layers were combined and washed successively with 10% HCl (2x 200 ml), 10% Na_2CO_3 (1x 200 ml) and H_2O (2x 200 ml), and then dried over $MgSO_4$. The solvent was removed in vacuo, followed by column chromatography on silica (Hex/EtOAc/CH_2Cl_2 = 15:3:1) and then (CH_2Cl_2/EtOAc = 96:4) to give 67% of the title compound as light yellow

semi-crystalline wax.
^{1}H NMR (250 MHz, $CDCl_3$) δ [ppm]: 1.23-1.38 (m, 10 H, alkyl chain CH_2), 1.62-1.71 (m, 2 H, 19-C**H**$_2$), 1.99-2.06 (m, 2 H, 25-C**H**$_2$), 2.37-2.56 (m, 2 H, 18-CH_2), 3.76 (s, 6 H, OCH_3), 4.90-4.91 and 5.01-5.02 (dm, 1 H, ^3J = 33.03 Hz, CH**H**H_{cis}), 4.93-4.96 (m, 1 H, ^2J = 6.4 Hz, CHH**H**$_{trans}$), 5.74-5.80 and 5.82-5.88 (dm, 1 H, ^3J = 27.14 Hz, C**H**HH), 6.41 (t, 1 H, J = 2.3 Hz, H_{ar}), 6.59 (d, 1 H, J = 2.3 Hz, H_{ar}), 6.75 (s, 1 H, 8-CH), 7.40 (tt, 2H, J = 1.3 Hz and 7.4 Hz, H_{ar}), 7.52 (tt, 2 H, J = 1.3 Hz and 7.4 Hz, H_{ar}), 7.94 (dt, 1 H, J = 1.3 Hz and 7.4 Hz, H_{ar}).
^{13}C NMR (75.5 MHz, $CDCl_3$) δ [ppm]: 24.8 (19-CH_2), 28.9, 29.05, 29.2, 29.3, 30.3 (5 CH_2, alkyl chain), 33.8 (**C**H_2CO), 34.0 (CH_2CH**C**H_2), 55.4 (OCH_3), 77.2 (8-C), 106.6 (13-C_{ar}, 10-C_{ar}), 114.1 (**C**H_2CH), 125.5 (9-C), 128.6, 128.8 (4 CH, phenyl), 133.4 (6-CH), 134.70 (9-C), 135.7 (**C**$_{ar}$CO), 139.2 (26-**C**H), 161.2 (2 C, **C**OCH_3), 173.28 (OCO), 193.7 (CO).
IR (Nujol) [$\tilde{\nu}$/cm^{-1}]: 2854 (s), 1730 (s), 1694 (s), 1640 (m). FD-MS [m/z]: 438.5 (100%, M^+), 877.5 (11%, dimer).

7.5.11 12,12,12-Triethoxsilyl-dodecanoicacid-1-(3,5-dimethoxy-phenyl)-2-oxo-2-phenyl ethyl ester

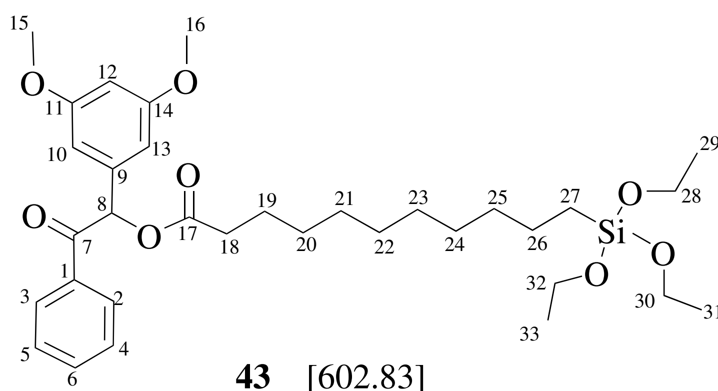

43 [602.83]

A solution of undec-10-enoic acid-1-(3,5-dimethoxy-phenyl)-2-oxo-2-phenylethyl ester (0.30 g, 0,68 mmol) in triethoxysilane (1.12 g, 6.8 mmol, 10 eq.) was heated under anhydrous conditions to 70 °C. 5 drops of H_2PtCl_6 (1.64% in i-PrOH) were added and the solution was allowed to stir for 4.5 h. Excess $HSi(OEt)_3$ was removed under vacuum and the crude product was purified on a passivated silica column (CH_2Cl_2/EtOH = 100:1) to afford 68% of the desired product as a pale yellow crystalline wax. The resulting silane was visible on a TLC plate as a characteristic large smudged spot.
^{1}H NMR (250 MHz, $CDCl_3$) δ [ppm]: 0.63 (t, 2 H, J = 8.1 Hz, $SiCH_2$), 1.22 (t, 9 H, J = 6.7 Hz, OCH_2C**H**$_3$), 1.18-1.39 (m, 14 H, alkyl chain CH_2), 1.67 (m, 2H, 19-C**H**$_2$), 2.46 (m, 2 H, 18-C**H**$_2$), 3.76 (s, 6 H, OCH_3), 3.81 (q, 6 H, J = 7.0 Hz, OC**H**$_2CH_3$), 6.41 (t, 1 H, J = 2.2 Hz,

H_{ar}), 6.59 (d, 2 H, J = 2.2 Hz, H_{ar}), 6.75 (s, 1 H, 8-CH), 7.42 (t, 2 H, J = 7.4 Hz, H_{ar}), 7.52 (tt, 2 H, J = 1.6 Hz and 7.4 Hz, H_{ar}), 7.94 (d, 1 H, J = 7.2 Hz, H_{ar}).
^{13}C NMR (75.5 MHz, $CDCl_3$) δ [ppm]: 10.4 ($SiCH_2$), 18.3 ($OCH_2\mathbf{C}H_3$), 22.8 ($SiCH_2\mathbf{C}H_2$), 24.8 (19-CH_2), 29.10-29.50 (5 CH_2, alkyl chain), 33.2 ($\mathbf{C}H_2CO$), 34.0 ($SiCH_2CH_2\mathbf{C}H_2$), 55.4 (OCH_3), 58.3 ($O\mathbf{C}H_2CH_3$), 78.8 (8-C), 101.2 (12-C_{ar}), 106.6 (10-C_{ar}, 13-C_{ar}), 128.61-128.79 (4 CH, CH_{ar}), 133.4 (9-C), 134.7 (1-C_{ar}), 135.7 (6-C_{ar}), 161.2 (2 C, $\mathbf{C}OCH_3$), 173.3 (OCO), 193.8 (CO).
IR (Nujol) [$\tilde{\nu}$/cm^{-1}]: 2854 (s), 1741 (s), 1700 (s). FD-MS [m/z]: 602.7 (100%, M^+), 1204.5 (11%, dimer).

7.5.11.1 Passivation of a Silica Gel Column

HMDS was added to the slurry before packing the column as 2% solution in the eluent (CH_2Cl_2/EtOH, 25:1). The slurry was allowed to stir for 10 min in order to partly convert the most reactive hydroxyl groups of the silica gel into hydrophobic methyl groups. After packing, the column was completely washed with pure eluent in order to remove any excess HMDS, before adding the crude compound for separation.

7.6 Laser Irradiation

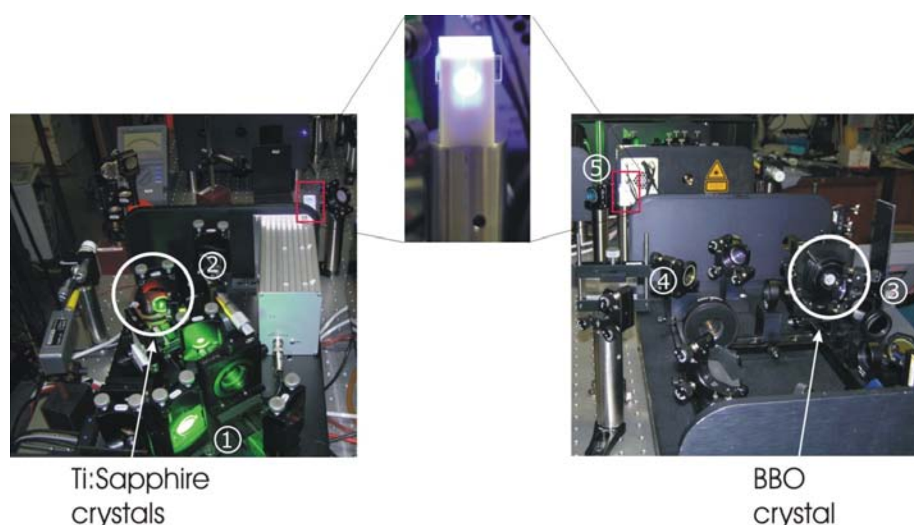

Figure 7.1: *Laser setup: (1) light from Nd:Yag laser passes through Ti:Sapphire crystal (2) and upon passing through BBO crystal (3) the frequency is doubled. The now blue light then passes through a UV lens for broadening (4) and irradiates the wafers in the Teflon holder (5)*

The Titanium:Sapphire laser (Ti:Sa) was provided by the LARISSA group of the University of Mainz. The Ti:Sap laser was pumped by a high-energy, 10 kHz, frequency-doubled Nd:Yag laser. The emitted light of the Ti:Sap laser, which ranges from 720 nm to 920 nm, then passed through a Beta-Barium-Borat (BBO) crystal for frequency doubling. The thus generated wavelengths of λ = 411 nm and 420 nm were then used for irradiation of the quartz and silicon wafers.

The quartz and Silicon wafers were irradiated using a home-build Teflon holder into which the wafers could be inserted vertically to guarantee a nearly perfect horizontal irradiation (Fig. 7.1). The Teflon holder was placed roughly 50 cm away from the outcoming laser beam and with the use of lenses the beam was broadened from 1 mm^2 to ca. 1 cm^2.
For tripling of the fundamental frequency, the red laser light of the Ti:Sa laser was first doubled in a BBO crystal and then split into its red and blue components. The polarisation of the blue beam was rotated with half a wave plate and then both beams were combined in a second BBO crystal for frequency mixing in order to generate the 3rd harmonic. The resulting frequency was 253nm with an irradiance of $5 mW\cdot cm^{-2}$.

Chapter 8

Summary

The aim of this thesis was to investigate novel techniques to create complex hierarchical chemical patterns on silica surfaces with micro to nanometer sized features. These surfaces were used for a site-selective assembly of colloidal particles and oligonucleotides. To do so, functionalised alkoxysilanes (commercial and synthesised ones) were deposited onto planar silica surfaces. The functional groups can form reversible attractive interactions with the complementary surface layers of the opposing objects that need to be assembled. These interactions determine the final location and density of the objects onto the surface.

In **Chapter 4**, colloidal adsorption experiments were presented on photolithographically patterned silica surfaces that were then modified with commercial silanes. Hydrophobic and hydrophilic particles were used for the assembly experiments. As expected, the hydrophobic silica particles absorbed mainly onto the hydrophobic regions of a substrate when deposited from a suspension in hydrophobic solvent (toluene). Deposition from a more polar and protic solvent (ethanol) showed an affinity of the same particles for the hydrophilic regions on a substrate, due to dewetting of the solvent from the hydrophobic regions and pinning at the hydrophilic regions.

Charge dependent colloidal adsorption experiments were carried out with COOH functionalised colloids on charged/uncharged and polar/nonpolar patterned substrates by changing the pH of the adsorption experiment. At low pH no selectivity in the assembly of the particles onto the surfaces was observed; whereas, a selectivity contrast was obtained at high pHs in all cases, apart from when using the completely uncharged particles. Experiments performed with uncharged particles were not affected by the pH, as expected.
The particle density of the assembly is also affected by the pH: the higher inter-particle repulsion at pH 9 (carboxylic acid groups are in their ionised carboxylate form) leads to lower particles density than at pH 4 (carboxylic acid groups are protonated). Moreover, it could

also be demonstrated that lower charged particles lead to higher particle densities due to less inter-particle repulsion.

In the second part of this thesis, the concept of novel, “smart” alkoxysilanes was introduced that allows parallel surface activation and patterning in a one-step irradiation process. These novel species bear a photoreactive head-group in a protected form. Surface layers made from these molecules can be irradiated through a mask to remove the protecting group from selected regions and thus generate lateral chemical patterns of active and inert regions on the substrate

In **Chapter 5** the synthesis of an azide-reactive alkoxysilane was successfully accomplished. Silanisation conditions were carefully optimised as to guarantee a smooth surface layer, without formation of micellar clusters. ^{1}H NMR and DLS experiments corroborated the absence of clusters when using neither water nor NaOH as catalysts during hydrolysis, but only the organic solvent itself.
Upon irradiation of the azide layer, the resulting nitrene may undergo a variety of reactions depending on the irradiation conditions. Contact angle measurements demonstrated that the irradiated surfaces were more hydrophilic than the non-irradiated azide layer and therefore the formation of an amine upon irradiation was postulated. Successful photoactivation could be demonstrated using condensation patterns, which showed a change in wettability on the wafer surface upon irradiation. Colloidal deposition with COOH functionalised particles further underlined the formation of more hydrophilic species.

Orthogonal photoreactive silanes were described in **Chapter 6**. The advantage of orthogonal photosensitive silanes is the possibility of having a coexistence of chemical functionalities homogeneously distributed in the same layer, by using appropriate protecting groups. For this purpose, a 3’,5’-dimethoxybenzoin protected carboxylic acid silane was successfully synthesised and the kinetics of its hydrolysis and condensation in solution were analysed in order to optimise the silanisation conditions. This compound was used together with a nitroveratryl protected amino silane to obtain bicomponent surface layers. The optimum conditions for an orthogonal deprotection of surfaces modified with this two groups were determined.

A 2-step deprotection process through a mask generated a complex pattern on the substrate by activating two different chemistries at different sites. This was demonstrated by colloidal adsorption and fluorescence labelling of the resulting substrates. Moreover, two different single stranded oligodeoxynucleotides were immobilised onto the two different activated areas and then hybrid captured with their respective complementary, fluorescent labelled strand. Selective hybridisation could be shown, although non-selective adsorption issues need to be resolved, making this technique attractive for possible DNA microarrays.

Advantages for using this technique are the number of discrete sites in the array that could be doubled, since each site possesses two different functionalities. These can be selectively activated in two different steps and used for the immobilisation of two different oligonucleotides.

Bibliography

[Adams 89] S. R. Adams, J. P. Y. Kao, R. Y. Tsien. Biologically Useful Chelators That Take Up Ca^{2+} upon Illumination. *J. Am. Chem. Soc.* **111**, 7957–7968 (1989).

[Aizenberg 00] J. Aizenberg, P. V. Braun, P. Wiltzius. Patterned Colloidal Deposition Controlled by Electrostatic and Capillary Forces. *Phys. Rev. Lett.* **84**, 2997–3000 (2000).

[Albericio 00] F. Albericio. Orthogonal Protecting groups for N^{α}-Amino and C-Terminal Carboxyl functions in Solid-Phase Peptide Synthesis. *Biopolymers* **55**, 123–139 (2000).

[Atkins 98] P. W. Atkins. Physical Chemistry. Oxford University Press, Oxford (1998).

[Bayley 84] H. Bayley, J. V. Staros. Photoaffinity labelling and related techniques. In E. F. V. Scriven (eds.), Azides and Nitrenes, pp. 95–204. Academic Press, Inc., New York (1984).

[Becker 91] H.G.O Becker. Einführung in die Photochemie. Deutscher Verlag d. Wissenschaften, Berlin (1991).

[Behrens 01] S. H. Behrens, D. G. Grier. The charge of glass and silica surfaces. *J. Chem. Phys.* **115**, 6716–6721 (2001).

[Blackley 75] D. C. Blackley. Emulsion Polymerisation - Theory and Practice. Applied Science Publisher Ltd., London (1975).

[Blanc 02] A. Blanc, Ch. G. Bochet. Wavelenth-Controlled Orthogonal Photolysis of Protecting Groups. *J. Org. Chem.* **67**, 5567–5577 (2002).

[Bloomberg 93] G. B. Bloomberg, D. Askin, A. R. Gargaro, M. J. A. Tanner. Synthesis of a branched cyclic peptide using a strategy employing Fmoc chemistry and two additional orthogonal protecting groups. *Tetrahedron Lett.* **34**, 4709–4712 (1993).

[Bochet 00] Ch. G. Bochet. Wavelength-Selective Cleavage of Photolabile Protecting Groups. *Tetrahedron Lett.* **41**, 6341–6346 (2000).

[Bochet 02] Ch. G. Bochet. Photolabile Protecting Groups and Linkers. *J. Chem. Soc., Perkin Trans. 1* **67**, 125–162 (2002).

[Brandow 99] S. L. Brandow, M.-S. Chen, M. R. Aggarwal, C. S. Dulcey, J. M. Calvert, W. J. Dressick. Fabrication of patterned amine reactivity templates using 4-chloromethylphenylsiloxane self-assembled monolayer films. *Langmuir* **15**, 5429–5432 (1999).

[Burmeister 99] F. Burmeister, W. Badowsky, T. Braun, W. Wieperich, J. Boneberg, P. Leiderer. Colloidal monolayer lithography - a flexible approach for nanostructuring of surfaces. *Appl. Surf. Sci.* **144**, 461–466 (1999).

[Cameron 91] J. F. Cameron, J. M. J. Frechet. Photogeneration of Organic bases from *o*-Nitrophenyl-Derived Carbamates. *J. Am. Chem. Soc.* **113**, 4303–4313 (1991).

[Chamberlin 66] J. W. Chamberlin. Use of the 3,5-Dimethoxybenzyloxycarbonyl Group as a Photosensitive N-Protecting Group. *J. Org. Chem.* **31**, 1658–1660 (1966).

[Chen 00] K. M Chen, X. Jiang, L. C. Kimerling, P. T. Hammond. Selective Self-Organization of Colloids on Patterned Polyelectrolyte Templates. *Langmuir* **16**, 7825–7834 (2000).

[Collins 97] E. A. Collins. Measurement of Particle Size and Particle Size Distribution. In P. A. Lovell, M. S. El-Asser (eds.), Emulsion Polymerisation and Emulsion Polymers, pp. 386–436. John Whiley and Sons Ltd., Chichester, England (1997).

[Corey 65] E. J. Corey, D. Seebach. Carbanions of 1,3-Dithianes. Reagents for C-C Bond Formation by Nucleophilic Displacement and Carbonyl Addition. *Angew. Chem. Int. Ed. Engl.* **4**, 1075–1077 (1965).

[Craighead 00] H. G. Craighead. Nanoelectromechanical Systems. *Science* **290**, 1532–1535 (2000).

[Creighton 83] T. E. Creighton. Proteins: Structures and Molecular Proper. Freeman, New York (1983).

[Davidson 01] M. W. Davidson, M. Abramowitz. *Optical Microscopy*. Internet article, http://microscopy.fsu.edu, National High Magnetic Field Laboratory, The Florida State University (2001).

[del Campo a] A. del Campo. *privat communications*.

[del Campo b] A. del Campo, D. Boos, R. Müller-Speiel, V. Maus, U. Jonas, H. W. Spiess. Novel photolabile protected silanes for chemical patterning. *manuscript in preparation*.

[del Campo c] A. del Campo, D. Boos, H. W. Spiess, U. Jonas. Surface modification with novel orthogonal photosensitive silanes for sequential chemical lithography. *manuscript in preparation*.

[Denkov 92] N. D. Denkov, 0. D. Velev, P. A. Kralchevsky, I. B. Ivanov, H. Yoshimura, K. Nagayama. Mechanism of Formation of Two-Dimensional Crystals from Latex Particles on Substrates. *Langmuir* **8**, 3183–3190 (1992).

[DePuy 77] Ch. H. DePuy, O. L. Chapman. Molekül-Reaktionen und Photochemie. Verlag Chemie, Weinheim, New York (1977).

[Dulcey 91] C. S. Dulcey, Jr. J. H. Georger, V. Krauthamer, D. Stenger, T. L. Fare, J. M. Calvert. Deep UV Photochemistry of Chemisorbed Monolayers: Patterned Coplanar Molecular Assemblies. *Science* **252**, 551–554 (1991).

[Dutta 03] J. Dutta, H. Hofmann. Self-Organization of Colloidal Nanoparticles. *Enzyc. Nanosci. Nanotechn.*pp. 1–23 (2003).

[Egen 02] A. Egen, R. Zentel. Tuning the Properties of Photonic Films from Polymer Beads by Chemistry. *Chem. Mater.* **14**, 2176–2183 (2002).

[Egen 04a] A. Egen, L. Braun, R. Zentel, K. Tännert, P. Frese, O. Reis, M. Wulf. Artificial Opals as Effect Pigments in Clear Coatings. *Macromol. Mater. Eng.* **289**, 158–163 (2004).

[Egen 04b] A. Egen, R. Zentel. Surfactant Free Emulsion Polymerization of various methacrylates: Towards Monodisperse Colloids for Polymer Opals. *Macromol. Chem. Phys.* **205**, 1476–1488 (2004).

[Elender 96] G. Elender, M. Kuener, E. Sackmann. Functionalization of Si/SiO_2 and glass surfaces with ultrathin dextran films and depostion of lipid bilayers. *Biosensensors and Bioelectronics* **11**, 565–577 (1996).

[Evers 02] M. Evers, H. J. Schope, T. Palberg, N. Dingenouts, M. Ballauf. Residual order in amorphous dry films of polymer films: indication of an influence of particle interaction. *J. Non-Cryst. Solids* **307**, 579–583 (2002).

[Fadeev 99] A. Y. Fadeev, T. J. McCarthy. Trialkylsilane Monolayers Covalently Attached to Silicon Surfaces: Wettability Studies Indicating that Molecular Topography Contributes to Contact Angle Hysteresis. *Langmuir* **15**, 3759–3766 (1999).

[Feynman 60] R. P. Feynman. *There's plenty of room at the bottom*. Internet article, http://www.zyvex.com/nanotech/feynman.html, Californian Institute of Technology (1960).

[Fitch 71] R. M. Fitch, C. H. Tsai. Particle Nucleation in Polymer Colloids. Plenum Press, New York (1971).

[Fodor 91] S. P. A. Fodor, J. L. Read, M. C. Pirrung, L. Stryer, A. T. Lu, D. Solas. Light Directed, Spatially Addressable Parallel chemical Synthesis. *Science* **251**, 767–773 (1991).

[Fustin 03] S. C. A. Fustin, G. Glasser, H. W. Spiess, U. Jonas. Site-Selective Growth of Colloidal Crystals with Photonic Properties on Chemically Patterned Surfaces. *Adv. Mater.* **15**, 1025–1028 (2003).

[Gilbert 95] R. G. Gilbert. Emulsion Polymerization - a Mechanistic Approach. Academic Press, London (1995).

[Hattori 01] H. Hattori. Anti-Reflection Surface with Particle Coating Deposited by Electrostatic Attraction. *Adv. Mater.* **13**, 51–54 (2001).

[Iler 66] R. K. J. Iler. *J. Colloid Interface Sci.* **21**, 569–594 (1966).

[Im 02] S. H. Im, Y. T. Lim, D. J. Suh, O. O. Park. Three dimensional self-assembly of colloids at a water-air interface: a novel technique for the fabrication of photonic bandgap crystals. *Adv. Mater.* **14**, 1367–1369 (2002).

[Ishida 84] H. Ishida, J. D. Miller. Substrate Effects of the Chemisorbed and Physisorbed Layers of Methacryl Silane Modified Particulate Minerals. *Macromolecules* **17**, 1659–1666 (1984).

[Israelachvili 85] J. N. Israelachvili. Intermolecular and Surface Forces. Academic Press, London (1985).

[Johnson 96] C. A. Johnson, A. M. Lenhoff. Adsorption of Charged Latex Particles on Mica Studied by Atomic Force Microscopy. *J. Colloid Interface Sci.* **179**, 587–599 (1996).

[Jonas 02a] U. Jonas, A. del Campo, Ch. Krüger, G. Glasser, D. Boos. Colloidal Assemblies on Patterned Silane Layers. *Proc. Nat. Acad. Science* **99**, 5034–5039 (2002).

[Jonas 02b] U. Jonas, Ch. Krüger. The Effect of Polar, Nonpolar, and Electrostatic Interactions and Wetting Behaviour on the Particle Assembly at Patterned Surfaces. *J. Supramol. Chem.* **2**, 255–270 (2002).

[Kallury 94] K. M. R. Kallury, P. M. McDonalds, M. Thompson. Effect of Surface Water and Base Catalysis on the Silanization of Silica by (Aminopropyl)alkoxysilanes Studied by X-ray Photoelectron Spectroscopy and ^{13}C Cross-Polarization/Magic Angle Spinning Nuclear Magnetic Resonance. *Langmuir* **10**, 492–499 (1994).

[Kampes 99] A. Kampes, B. Tieke. Self-assembly of carboxylated latex particles at charged surfaces: influences of preparation conditions on the state of order of the monolayers. *Mater. Sci. Eng. C* **8-9**, 195–204 (1999).

[Katritzky 95] A. R. Katritzky, H. Lang, Z. Wang, Z. Zhang, H. Song. Benzotriazole-Mediated Conversions of Aromatic and Heteroaromatic Aldehydes to Functionalized Ketones. *J. Org. Chem.* **60**, 7619–7624 (1995).

[Kotzyba-Hilbe 95] F. Kotzyba-Hilbert, I. Kapfer, M. Goeldner. Neue Entwicklungen bei der Photoaffinitätsmarkierung. *Angew. Chem.* **107**, 1391–1408 (1995).

[Kralchevsky 01] P. A. Kralchevsky, N. D. Denkov. Capillary forces and structuring in layers of colloid particles. *Curr. Opin. Coll. Interf. Sci.* **6**, 383–401 (2001).

[Krüger 01] Ch. Krüger. *Kolloidale Organisation auf lithographisch hergestellten Silanschichten: Neue Möglichkeiten der Strukturbildung auf Oberflächen*. Dissertation, Universität, Mainz (2001).

[Lahiri 99] J. Lahiri, L. Isaacs, J. Tien, G. M. Whitesides. A Strategy for the Generation of Surfaces Presenting Ligands for Studies of Binding Based on an Active Ester as a Common Reactive Intermediate: A Surface Plasmon Resonance Study. *Anal. Chem.* **71**, 777–790 (1999).

[Lee 02] I. Lee, H. Zheng, M. F. Rubner, P. T. Hammond. Controlled Cluster Size in Patterned Particle Arrays via Directed Adsorption on Confined Surfaces. *Adv. Mater.* **14**, 572–577 (2002).

[Lehman 73] P. A. Lehman, R. S. Berry. Flash Photolytic Decomposition of Aryl Azides. Measurement of an Intramolecular Closure Rate. *J. Am. Chem. Soc.* **95**, 8614–8620 (1973).

[Lewis 75] F. D. Lewis, R. T. Lauterbach, H. G. Heine, W. Hartmann, H. Rudolph. Photochemical .alpha. cleavage of benzoin derivatives. Polar transition states for free-radical formation. *J. Am. Chem. Soc.* **97**, 1519–1525 (1975).

[Lewis 77] R. V. Lewis, M. F. Roberts, E. A. Dennis, W. S. Allison. Photoactivated Heterobifunctional Cross-Linking Reagents Which Demonstrate the Aggregation State of Phospholipase A_2. *Biochemistry* **16**, 5650–5654 (1977).

[Li 00] Y. Li, C. W. Park. Effective medium approximation and deposition of colloidal particles in fibrous and granular media. *Adv. Coll. Interf. Sci.* **87**, 1–74 (2000).

[Lipson 96] M. Lipson, N. J. Turro. Picosecond investigation of the effect of solvent on the photochemistry of benzoin. *J. Photochem. Photobiol. A. Chem.* **99**, 93–96 (1996).

[Machida 99] M. Machida, K. Norimoto, T. Watanabe, K. Hashimoto, A. Fujishima. The effect of SiO_2 addition in super-hydrophilic property of TiO_2 photocatalyst. *J. Mat. Sci.* **34**, 2569–2574 (1999).

[McGall 96] G. H. McGall, A. D. Barone, M. Diggelmann, S. P. A. Fodor, E. Gentalen, N. Ngo. The Efficiency of Light-Directed Synthesis of DNA Arrays on Glass Substrates. *Colloids Surfaces A: Physicochem. Eng. Aspects* **109**, 363–374 (1996).

[Moore 65] G. E. Moore. Cramming more components onto integrated circuits. *Electronics* **38**(8) (1965).

[Nagayama 97] K. Nagayama. Two-dimensional self-assembly of colloids in liquid thin films. *J. Am. Chem. Soc.* **119**, 5081–5090 (1997).

[Nakagawa 00] M. Nakagawa, S.-K. Oh, K. Ichimura. Photopatterning and Visualization of Adsorbed Monolayers of Bis(1-benzyl-4-pyridinio)ethylene Moieties. *Adv. Mater.* **12**, 403–407 (2000).

[Park 98] S. H. Park, Y. Xia. Macroporous Membranes with Highly Ordered and Three-Dimensionally Interconnected Spherical Pores. *Adv. Mater.* **10**, 1045–1048 (1998).

[Patchornik 70] A. Patchornik, B. Amit, R. B. Woodward. Photosensitive Protecting Groups. *J. Am. Chem. Soc.* **92**, 6333–6335 (1970).

[Pillai 80] V. N. R. Pillai. Photoremovable Protecting Groups in Organic Synthesis. *Synthesis* **1**, 1–26 (1980).

[Reiser 70] A. Reiser, L. J. Leyson. A Correlation between Negative Charge on Nitrogen and the Reactivity of Aromatic Nitrenes . *J. Am. Chem. Soc.* **92**, 7487 (1970).

[Reiser 71] A. Reiser, H. M. Wagner. The chemistry of the azido group. p. 444. Interscience, New York (1971).

[Riedel 90] E. Riedel. Anorganische Chemie. Walter de Gruyter, Berlin, New York (1990).

[Ritzen 00] A. Ritzen, B. Basu, S. K. Chattopadhyay, F. Dossa, T. Frejd. Synthesis of optically active arylene bis-alanine derivatives carrying orthogonal protecting groups. *Tetrahedron: Asymmetry* **9**, 503–512 (2000).

[Rochat 00] S. Rochat, C. Minardi, J. Y. de Saint Laumer, A. Herrmann. Controlled Release of Perfumery Aldehydes and Ketones by Norrish Type-II Photofragmentation of -Keto Esters in Undegassed Solution . *Helv. Chim. Acta* **83**, 1645–1671 (2000).

[Sambrook 01] J. Sambrook, D. W. Russel. Molecular Cloning, A Laboratory Manual, 3rd Ed. Cold Springer Harbor Laboratory Press, New York (2001).

[Sanger 86] W. Sanger. Principles of Nucleic Acid Structures. Springer-Verlag, New York (1986).

[Serizawa 98] T. Serizawa, H. Takeshita, M. Akashi. Electrostatic Adsorption of Polystyrene Nanospheres onto the Surface of an Ultrathin Polymer Film Prepared by Using an Alternate Adsorption Technique. *Langmuir* **14**, 4088–4094 (1998).

[Sheehan 64] J. C. Sheehan, R. M. Wilson. Photolysis of Desyl Compounds. A New Photolytic Cyclization. *J. Am. Chem. Soc.* **86**, 5277–5281 (1964).

[Sheehan 71] J. C. Sheehan, R. M. Wilson, A. W. Oxford. The Photolysis of Methoxy-Substituted Benzoin Esters. A Photosensitive Protecting Group for Carboxylic Acids. *J. Am. Chem. Soc.* **93**, 7222–7228 (1971).

[Sims 74] P. J. Sims, A. S. Waggoner, C.-H. Wang, J. F. Hoffman. Studies on the mechanism by which cyanine dyes measure membrane potential in red blood cells and phosphatidylcholine vesicles. *Biochemistry* **13**, 3315–3330 (1974).

[Skoog 96] D. A. Skoog, J. J. Leary. Instrumentelle Analytik. Springer-Verlag, Berlin, Heidelberg (1996).

[Smirnov 82] V. A. Smirnov, S. B. Brichkin. Spectral and Photochemical Properties of Aromatic Nitrenes. *Chem. Phys. Lett.* **87**, 548–551 (1982).

[Smith 84] P. A. S. Smith. Aryl and Heteroaryl Azides and Nitrenes. In E. F. V. Scriven (eds.), Azides and Nitrenes, pp. 95–204. Academic Press, Inc., New York (1984).

[Stenger 92] D. Stenger, J. H. Georger, C. S. Dulcey, J. J. Hickman, A. S. Rudolph, T. B. Nielsen, S. M. McCort, J. M. Calvert. Coplanar molecular assemblies of amino and perfluorinated alkylsilanes: characterization and geometric definition of mammalian cell adhesion and growth. *J. Am. Chem. Soc.* **114**, 8435–8442 (1992).

[Sticks 01] G. Sticks, G. M. Whitesides, J. C. Love, M. L. Roukes. Spektrum der Wissenschaft, Spezial: Nanotechnologie, pp. 6–39. Scientific American, Heidelberg (2001).

[Stowell 96] M. H. B. Stowell, R. S. Rock, D. C. Rees, S. I. Chan. Efficient Synthesis of Photolabile Alkoxy Benzoin Protecing Groups. *Tetrahedron Lett.* **37**, 307–310 (1996).

[Sundberg 74] R. J. Sundberg, R. W. Heintzelman. Reactivity of Aryl Nitrenes. Competition between Carbazole Formation and Internal Bond Reorganization in Biphenylnitrenes. *J. Org. Chem.* **39**, 2546–2552 (1974).

[Suppan 94] P. Suppan. Chemistry and Light. The Royal Society of Chemistry, Cambridge, UK (1994).

[Swenton 70] J. S. Swenton, T. J. Ikeler, B. W. Williams. The Photochemistry of Singlet and Triplet Azide Excited States. *J. Am. Chem. Soc.* **92**, 3103–3109 (1970).

[Tarlov 93] M. J. Tarlov, D. R. F. Burgess, G. Gillen. UV Photopatterning of Alkanethiolate Monolayers Self-Assembled on Gold and Silver. *J. Am. Chem. Soc.* **115**, 5305–5306 (1993).

[Tieke 01] B. Tieke, K.-F. Fulda, A. Kampes. Mono- and Multilayers of Spherical Polymer Particles Prepared by Langmuir-Blodgett and Self-Assembly Techniques. In M. Rosoff (eds.), Nano-Surface Chemistry, pp. 213–242. Marcel Dekker, New York (2001).

[Tsui 76] F. P. Tsui, Y. H. Chang, T. M. Vogel, G. Zon. Thermal α-Deoxysilylation of *N*, *o*-Bis(Trimethylsilyl)-*N*-phenylhydroxylamine. *J. Org. Chem.* **41**, 3381–3388 (1976).

[Ulman 91] A. Ulman. An Introduction to Ultrathin Organic Films from Langmuir-Blodgett to Self-Assembly. Academic Press, London, UK (1991).

[Velev 99] O. D. Velev, E. W. Kaler. In Situ Assembly of Colloidal Particles into Miniaturized Biosensors. *Langmuir* **15**, 3693–3699 (1999).

[Vossmeyer 97] T. Vossmeyer, E. DeIonno, J. R. Heath. Light-Directed Assembly of Nanoparticles. *Angew. Chem. Int. Ed. Engl.* **36**, 1080–1084 (1997).

[Vossmeyer 98] T. Vossmeyer, S. Jia, E. DeIonno, M. R. Diehl, S. H. Kim, X. Peng, A. P. Alivisatos, J. R. Heath. Combinatorial Approaches Toward Patterning Nanocrystals. *J. Appl. Phy.* **84**, 3664–3670 (1998).

[Wade 00] J. D. Wade. In S. A. Kates, F. Albericio (eds.), Solid Phase Synthesis, A Practical Guide, pp. 103–128. Marcel Dekker, New York (2000).

[Waggoner 89] A. S. Waggoner, R. DeBiasio, P. Conrad, G. R. Bright, L. Ernst, K. Ryan, M. Nederlof, D. Taylor. Multiple spectral parameter imaging. *Methods in Cell Biology* **30**, 449–478 (1989).

[Wang 97] R. Wang, A. Fujishima, M. Chikuni, A. Kitamura, M. Shimohigohi, T. Watanabe. Light-Induced Amphiphilic Surfaces. *Nature* **388**, 431–432 (1997).

[Whitesides 02] G. M. Whitesides, B. Grzybowski. Self-Assembly at all Scales. *Science* **295**, 2418–2421 (2002).

[Wilhelm 98] S. Wilhelm, B. Gröber, M. Gluch, H. Heinz. *Confocal Laser Scanning Microscopy: Principles*. Internet article, www.zeiss.de, Carl Zeiss Jena (1998).

[Winnik 97] M. A. Winnik. The Formation and Properties of Latex Films. In P. A. Lovell, M. S. El-Asser (eds.), Emulsion Polymerisation and Emulsion Polymers, pp. 467–518. John Whiley and Sons Ltd, Chichester, England (1997).

[Wit 98] P. J. Wit, H. J. Busscher. Site Selectivity in the Deposition and Redeposition of Polystyrene Particles to Glass. *J. Colloid Interface Sci.* **208**, 351–352 (1998).

[Xia 98] Y. Xia, G. M. Whitesides. Soft Lithography. *Angew. Chem. Int. Ed. Engl.* **37**, 550–575 (1998).

[Xia 99] Y. Xia, J. A. Rogers, K. E. Paul, G. M. Whitesides. Unconventional Methods for Fabricating and Patterning Nanostructures. *Chem. Rev.* **99**, 1823–1848 (1999).

[Xia 00] Y. Xia, B. Gates, Y. Yin, Y. Lu. Monodispersed Colloidal Spheres: Old Materials with New Applications. *Adv. Mater.* **12**, 693–713 (2000).

[Xu 99] J. Xu, P. Lei, C. Wu). Formation of highly monodispersed emulsifier-free cationic poly(methylstyrene) latex particles . *J. Polym. Sci. Part A: Polym. Chem.* **37**, 2069–2074 (1999).

[Yablonovitch 93] E. Yablonovitch. Photonic band-gap structures. *J. Opt. Soc. Am. B* **10**, 283–296 (1993).

[Yin 01] Y. Yin, Y. Lu, B. Gates, Y. Xia. Template-Assisted Self-Assembly: A Practical Route to Complex Aggregates of Monodispersed Colloids with Well-Defined Sizes, Shapes, and Structures. *J. Am. Chem. Soc.* **123**, 8718–8729 (2001).

[Zheng 02a] H. Zheng, I. Lee, M. F. Rubner, P. T. Hammond. Two Component Particle Arrays on Patterned Polyelectrolyte Multilayer Templates. *Adv. Mater.* **14**, 569–572 (2002).

[Zheng 02b] H. Zheng, M. F. Rubner, P. T. Hammond. Particle Assembly on Patterned "Plus/Minus" Polyelectrolyte Surfaces via Polymer-on-Polymer Stamping. *Langmuir* **18**, 4505–4510 (2002).

[Zhu 00] T. Zhu, G.-J. Boons. A new set of orthogonal protecting groups for oligosaccharide synthesis on a polymeric support. *Tetrahedron: Asymmetry* **11**, 199–205 (2000).

Acknowledgements

An dieser Stelle möchte ich mich herzlich bei all denen bedanken, die zum Gelingen dieser Arbeit tatkräftig beigetragen haben:

- *Prof. Dr. H. W. S.* für die Möglichkeit, meine Doktorarbeit in seinem Arbeitskreis durchzuführen, für sein Interesse und seine Unterstützung.
- *Dr. U. J.*, meinem Projektleiter für die Betreuung, die anregenden Gespräche und die Freiheit, mit der er mich an der dieser Dissertation arbeiten ließ.
- *Dr. A. del C. B.* (die "gute Seele") für ihre Unterstützung, ihre Ideen, ihre Betreuung und die schöne Zeit in Italien.
- *Prof. Dr. I. B.*, for the opportunity to stay within his working group at the University of Urbino, Italy (lovely place that Urbino!).
- *PD Dr. K. W.* für die Bereitstellung des Ti:Sa Lasers und seiner LARISSA Gruppe (besonders *Ch. G.*, *K. B.*, *Thomas Kessel* und *K. F.*) für die Hilfe mit den Bestrahlungen.
- *Prof. Dr. R. Z.* und *M. E.* für die großzügige Bereitstellung der PS-Cellulose Partikel.
- *Dr. A. K.* (das rheinhessische Urgestein) für die Hilfe mit Organik Problemen, seine Hilfe beim Zusammenschreiben der Arbeit und für die leckeren Teesorten, die er unserem Büro zur Verfügung stellte.
- *Dr. R. B.* für die AFM Messungen und seine Hilfe jeglicher Art mit AFM Fragen.
- *G. G.* für die SEM Messungen.
- *A. B.* für die LSM Messungen und das viele Infomaterial.
- *B. M.* für die DLS Messungen.
- *P. K.* für die NMR Messungen ihre Hilfe bei der Benutzung der AMX 300 Konsole
- der *Max-Planck Gesellschaft* für ihre finanzielle Unterstüzung.
- *A.-S. D.* für die AFM Messungen in Belgien.
- den Mitgliedern der 'Eidgenössischen Bastelkammer' (*M. H.*, *F. K.* und *H. R.*) für die Hilfe in allen Lebenslagen und mit dem PC (mit euch würde ich auf jeden Gipfel hochklettern).

- dem EDV Team um *V. M.* (dem besten “Bergabstiegs”partner), *T. R.* und *A. S.* für die schnelle Hilfe mit dem Computer.
- *C. K.* und *B. D.-S.* für die aufmunternden Worte und Hilfe mit jeglicher Art von bürokratischen Unwegsamkeiten.
- *S. S.* (the best lab partner in the world) für ihre Hilfe und Unterstützung (keiner versteht meine Welt der Chemie so gut wie du!) und meinen reslichen Bürokollegen *A. H.* und *Ch. D.* von 1.106 für die gute Laune, die leckeren Nascheinheiten und die super Atmospäre .
- Der Laborcrew (ehemalige und aktuelle), besonders *M. D.* für die Massenspektren und *U. P.* für die Hilfe mit den Emulsionen, den *Kreuznacher “Gässjer”* für die partriotischen Augenblicke am 3. August Wochenende jeden Jahres, und *Ch.-A. F.* für die Unterstützung bei den Kolloidexperimenten.
- *S. B.* für das Autoklavieren meiner Pufferlösungen.
- *C. C.* für die Weisheiten über *flash column chromatography* und das Korrekturlesen.
- *S. H.* for his proof reading and friendship (I hope you liked the gummibears!).
- allen ehemaligen und jetzigen Mitgliedern des Arbeitskreises, die ich nicht namentlich genannt habe.
- *meiner Familie* und *T. D.* für die Liebe, die bedingungslose Unterstützung und Hilfe im Hintergrund.